Università degli Studi di Padova

Facoltà di Ingegneria

Corso di Laurea Magistrale in Bioingegneria

In silico evaluation of multivariated methods to assess functional connectivity from EEG data

Relatore: Prof.ssa Gianna Maria Toffolo

Correlatore: Ing. Elisa Sartori

Laureanda: Federica Bassano

15 Ottobre 2013

Ai miei genitori

"Ogni viaggio, per quanto vicino o lontano ci possa portare,

inizia sempre con un semplice, umile passo." (A.K.)

Contents

Introduzione

Negli ultimi vent'anni gli studi funzionali sul cervello umano hanno avuto un ampio sviluppo sia grazie ai progressi tecnologici che hanno messo a disposizione apparecchiature sempre più sensibili e sofisticate, sia grazie all'impiego di tecniche di indagine non invasive (Risonanza Magnetica funzionale (fMRI), Tomografia ad Emissione di Positroni (PET), Magnetoencefalografia (MEG), Elettroencefalografia (EEG)) che permette di ricavare immagini e segnali dell'attività cerebrale a partire da sue misure emodinamiche, metaboliche, elettromagnetiche o elettriche. Le prime ricerche condotte puntavano a studiare quell'aspetto dell'organizzazione delle strutture cerebrali che comunemente viene indicato con il nome di *segregazione funzionale.* Tali studi, infatti, avevano l'obiettivo di riuscire ad individuare e isolare le regioni funzionalmente specializzate nello svolgimento di determinati compiti cognitivi o attività sensoriali. Più recentemente, soprattutto negli ultimi dieci anni, l'interesse si è focalizzato sullo studio della cosiddetta *integrazione funzionale*, cioè la rilevazione e la comprensione dei legami e dei meccanismi che permettono a gruppi di neuroni di interagire e integrarsi tra di loro. A tal proposito sono state sviluppate diverse tecniche e metodiche per lo studio dell'attività cerebrale che si sono rivelate fondamentali per la comprensione dei complessi meccanismi che regolano il funzionamento del cervello umano. Tali metodiche hanno dimostrato che le diverse regioni neuronali del cervello non operano in isolamento ma interagiscono tra loro formando una complessa rete di connessioni. Lo studio di queste relazioni/connessioni esistenti tra le diverse regioni corticali è generalmente indicato come *studio della connettività*. La definizione di connettività può essere classificata in tre categorie principali:

- *connettività anatomica*: è strettamente associata alla presenza di connessioni assoniche tra i vari neuroni;
- *connettività funzionale*: è definita come la correlazione temporale tra eventi neurofisiologici appartenenti a diverse regioni neurali;

- *connettività effettiva*: è definita come l'influenza che una regione neurale esercita attraverso una relazione causa-effetto su un'altra regione.

In letteratura sono presenti due principali approcci per lo studio della connettività: uno è di tipo esplorativo, basato esclusivamente sui dati da cui estrarre informazioni sia sulla topologia sia sulla forza, l'altro, invece, prevede la conoscenza a priori di un modello di rete per ottenere informazioni circa l'intensità degli accoppiamenti. Al primo approccio appartengono i metodi basati sui modelli autoregressivi multivariati (MVAR), da cui derivano una serie di indici quali Directed Transfer Function (DTF), Partial Directed Coherence (PDC) e i coefficienti di causalità di Granger; al secondo approccio, invece, appartiene il metodo detto Structural Equation Modeling (SEM). L'obiettivo di questa tesi si è focalizzato sulla validazione e implementazione di questi metodi. Essi sono stati ampiamente esaminati in letteratura per quantificare la loro capacità di rilevare le connessioni cerebrali, ma gli studi di simulazione proposti sono basati su modelli di generazione dei dati in silico che semplificano molto la reale complessità del cervello ([7]) e che si basano sui modelli autoregressivi stessi. Perciò, per superare questo problema, è stata sviluppata una simulazione con un approccio innovativo basato sull'utilizzo di un Neural Mass Model ([9]). L'obiettivo consiste nel generare dati simulati completamente indipendenti dalle equazioni lineari dei metodi che poi si vanno a testare e, al contempo, in grado di simulare la complessità delle reti neurali. Brevemente, la simulazione consiste nelle seguenti fasi:

- vengono simulati diversi set di dati in silico utilizzando il modello neurale di massa con diversi modelli di topologia, livelli di non linearità e intensità di connessioni;
- per ogni set dei suddetti parametri vengono generate 100 realizzazioni di segnali di 2 secondi;
- le reti stimate a partire dai parametri di connettività calcolati con i metodi considerati vengono confrontate con le reti vere.

Questa tesi riporta per esteso l'analisi di 3 reti ed è la prosecuzione e il completamento di un lavoro precedente ([19]) in cui è stata ampiamente analizzata un'altra tipologia di rete della quale, in questa sede, vengono riportati i risultati. L'obiettivo principale di questo studio di simulazione è innanzitutto quello di confrontare, per ogni determinata situazione di analisi, le prestazioni dei vari indici di stima della connettività sottolineando per ognuno i pregi e i limiti al fine di fornire una procedura robusta da usare per l'analisi della connettività del cervello umano, in grado di classificare i diversi stati del cervello in supporto sia della ricerca in ambito cognitivo sia dell'attività clinica.

Questa tesi si sviluppa in cinque capitoli di seguito brevemente riassunti. Nel **Capitolo 1** si definiscono sia i modelli multivariati autoregressivi e gli indici derivati per stimare la connettività in termini di causalità di Granger e nel dominio della frequenza, sia il metodo SEM. Inoltre in questo capitolo vengono descritti i metodi impiegati per la valutazione della significatività statistica dei vari stimatori. Nel **Capitolo 2** si descrive il modello (Neural Mass Model) utilizzato per la generazione dei dati simulati analizzati in questa tesi e si presentano le caratteristiche principali delle reti di simulazione considerate e dei dataset simulati. Nel **Capitolo 3** vengono riportati i valori dei parametri adottati nelle equazioni del Neural Mass Model per la generazione dei dati in silico e vengono mostrati alcuni esempi di segnali simulati. Nel **Capitolo 4** si presentano i principali risultati ottenuti dallo studio della connettività corticale per ogni rete per tutti i dataset. Infine, nel **Capitolo 5** si discutono i risultati presentati nel capitolo 4 evidenziando pregi, difetti, vantaggi, svantaggi e limiti dei vari metodi in modo da definire globalmente le loro prestazioni. L'Appendice, infine, riporta i risultati per ogni esperimento individuale condotto per ogni rete.

Introduction

In the recent years the functional studies about the human brain had a large development both due to technological advances, which have offered more and more sensitive and sophisticated instruments, both due to use of non-invasive techniques (the functional Magnetic Resonance Imaging (fMRI), the Positron Emission Tomography (PET), the Magnetoencephalography (MEG), the Electroencephalography (EEG)) which allows to get images and signals of the cerebral activity starting from hemodynamic, metabolic, electromagnetic or electrical measures. The earlier researches aimed to study the so called *functional segregation*. Indeed, these studies aimed to identify and isolate regions functionally specialized in the performance of some cognitive tasks or sensory activities. Recently, especially in the last decade, interest has focused on the study of so called *functional integration*, that is the detection and understanding of the linkages and mechanisms which allow groups of neurons to interact and integrate with each other. Different techniques and methods have been developed for the study of cerebral activity and have proved to be fundamental for the understanding of the complicated mechanisms which control the functioning of the human brain. These methods have shown that different neural regions do not operate alone but they interact establishing structure-function relationships in human brain. In literature such relationships have been defined in terms of structural, functional and effective connectivity.

- The *structural connectivity* refers to a pattern of anatomical links among brain regions. The analysis aims to characterize the architecture of complex networks underlying the cerebral functional organization.

- *Functional connectivity* and *effective connectivity* aim at identifying the presence and the strength of connections in terms of statistically significant dependency. The former is defined as the temporal correlation between neurophysiological events occurring in distributed neuronal groups and areas. The latter describes the causal influence that one neural system exerts over another either directly or indirectly in terms of temporal precedence and physical control ([1],[2]). Functional and effective connectivity can be estimated exploiting both Functional Magnetic Resonance Imaging (fMRI) and electrophysiological signals, such as Electroencephalography (EEG) and Magnetoencephalography (MEG), with different advantages and drawbacks. fMRI provides high spatial resolution (mm) but poor temporal precision (s) while EEG/MEG has more limited spatial resolution (cm) and higher temporal precision (ms). Since functional and effective connectivity are largely estimated over time, EEG and MEG are more suitable for calculating such connectivity.

In literature several methods have been developed to characterize brain connectivity in terms of network topology, connections strength and causality, following two main approaches: the *data-driven*, where topology, causality and strength are all inferred from data, and the *neural model-based*, where the model topology is postulated from a priori knowledge and only the connections strength is estimated from the data. The first approach consists of methods based on multivariated autoregressive models (MVAR) from which some indices are quantified such Directed Transfer Function (DTF), Partial Directed Coherence (PDC) and Granger causality coefficients; the second approach consists of a method called Structural Equation Modeling (SEM). The objective of this work focused on validation and implementation of these methods. They have been examined in literature to quantify their ability in revealing cerebral connections ([7],[8],[4]) but based on simulation studies not able to provide a comprehensive analysis because they use *in silico* data generated by self-referential linear methods which do not reproduce the complexity of the brain. Thus, to overcome this issue, an innovative simulation approach has been developed in this work, based on a nonlinear neural mass model ([9]) totally independent of SEM and MVAR linear equations and able to address the complexity of neural networks. This no-self referential approach was exploited to generate in silico network data to be used as a benchmark, to quantitatively compare obtained results with true connections.

Briefly, the simulation consists of the following stages:

- different in silico datasets are simulated using the neural mass model with different topology, level of non-linearity, and connections strength;
- 100 realizations of 2 second signals are generated for each dataset of these parameters;
- networks estimated from the connectivity parameters, calculated with the methods considered, are compared with the real networks.

This work reports a complete analysis of three networks and it is the continuation and completion of a previous work ([19]) where another type of network has been extensively analyzed the results of which are included here for completeness.
The main objective of this work was to understand limits and advantages of MVAR indices and SEM by exploiting the simulation study. Thus, it mainly serves as a proof-of-concept for connectivity measures under ideal conditions. Our purpose was to derive from simulation results some practical procedures in order to classify different brain states to support both cognitive research and clinical activity.

This thesis consists of five chapters below briefly summarized.
Chapter 1 describes the considered connectivity measures, such are those based on Multivariate Autoregressive models and the Structural Equation Modelling. It explains how the connecting parameters of MVAR and SEM models are identified on EEG data and describes procedures commonly exploited to analyze connectivity. Besides, it describes the procedure used to evaluate the statistical significance of each index results, such are the F-test for Granger causality index and the null distribution threshold using surrogate data for MVAR frequency indices. **Chapter 2** reports an overview about the principal models used to generate *in silico* data, namely the neural mass models, and describes the neural mass model exploited in this work. Finally, it characterizes network models adopted to simulate data and lists the procedure followed to generate *in silico* datasets. **Chapter 3** reports parameter values adopted in NMM equations for the generation of in silico data and are shown examples of simulated signals of different network models. **Chapter 4** illustrates the main results obtained with the simulation study for all networks for all datasets, in terms of both topology and strength estimates. Finally, **Chapter 5** discusses the results showed in the Chapter 4 and underlines strengths, weaknesses, advantages, disadvantages and limits of

different methods so as to define their overall performance. The Appendix reports results for each individual experiment performed for each network.

Chapter 1

Multivariate methods for connectivity analysis

In literature several methods have been developed to characterize brain connectivity in terms of network topology, connections strength and causality, following two main approaches: the neural model based approach, where the model topology is postulated from a priori knowledge and only connection strength is estimated from the data, and the data driven approach, where topology, causality and strength are all inferred from the data. The most prevalent data driven methods are those based on Granger causality principles, while those based on neural model are the Dinamic Causal Modeling (DCM) and the Structural Equation Modeling (SEM). Granger causality and SEM have been largely applied but, however, some criticisms have been arisen in literature concerning their assumptions ([6]). Both methods are based on multivariate linear regression models but they differ as regards the way they address temporal information. Granger causality is computed by using Multivariate Autoregressive Models, where correlations among measurements at different time lags are used to quantify coupling. SEM models instantaneous interactions among variables and ignores the influence that previous states have on current responses.

This chapter explains how the connecting parameters of MVAR and SEM models are identified on EEG data and describes procedures commonly exploited to analyze connectivity.

1.1 MVAR model identification

A multivariate autoregressive model is a discrete-time, linear and time invariant model and it is described by difference equations. The MVAR model with N variables is expressed as:

$$\boldsymbol{y}(n) = -\sum_{k=1}^{p} \boldsymbol{A}(k)\boldsymbol{y}(n-k) + \boldsymbol{e}(n) \tag{1.1}$$

where $\boldsymbol{y}(n) = [y_1(n), y_2(n) \ldots . y_N(n)]^{\mathrm{T}}$ is the data vector of dimension N containing the n-samples of the N time series, p is the model order, $\boldsymbol{A}(k)$, k =1…p, are the N x N matrices containing model coefficients, $\boldsymbol{e}(n) = [e_1(n), e_2(n) \ldots . e_N(n)]^{\mathrm{T}}$ is the vector containing the n-samples of the prediction errors, i.e. it is a multivariate white noise process with diagonal covariance matrix $\sum_e = \mathrm{diag}[\sigma_1^2, \sigma_2^2, \ldots, \sigma_{\mathrm{N}}^2]$. Assuming that the order p is known, identifying the model means to define numerical values for the model coefficients and for the covariance matrix. The model coefficients and the covariance matrix are identified on time series data by applying the correlation approach known as the multichannel Yule-Walker method which minimizes the mean square prediction error to find the optimum MVAR parameters set.

Considering the autocorrelation definition

$$\boldsymbol{R}_y(k) = E\{\boldsymbol{y}(n)\boldsymbol{y}(n-k)^T\}, \tag{1.2}$$

we can obtain the following set of equations, knows as multivariate Yule-Walker equations

$$\boldsymbol{R}_y(k) = -\sum_{i=1}^{p} \boldsymbol{A}(i)\boldsymbol{R}_y(k-i) + \Sigma_e \delta(k), \tag{1.3}$$

where $\delta(k)$ is Kronecker delta function ($\delta(k) = 1$ when $k = 0$, otherwise $\delta(k) = 0$).

Therefore, let $\mathbf{s}$ be a set of N time series:

$$\mathbf{s}(n) = [\mathbf{s}_1(n), \mathbf{s}_2(n), \ldots, \mathbf{s}_N(n)], \; n=1, \ldots, \mathrm{L} \tag{1.4}$$

where L is the number of data points applied in the estimation.

Using the sample correlation $\hat{R}_s(k)$ and the set of equations (1.3) with (p+1) matrix equations and (p+1) unknown matrix parameters, the MVAR coefficient matrices ($\boldsymbol{A}(k)$, Σ_e) can be solved using the Levinson – Durbin recursion extended to the multivariate Yule – Walker. We have previously assumed the model order as known but, generally, even the model order must be inferred from data. To this purpose, several MVAR models are calculated while varying p, and the best order is the one minimizing a parsimony criterion. We considered the Akaike Information Criterion (AIC) given by

$$AIC(p) = L\ log(det\Sigma_e)+2pN^2 \tag{1.5}$$

For reliable parameter identification, the number of parameters must be significantly smaller than the number of data points available, i.e. $pN^2 << NL$.

1.2 Granger causality index

The origin of causality concept in time series analysis arose in statistical field, when Wiener (1956) ([10]) recognized the role of temporal ordering in the inference of cause-effect relationship between two simultaneously measured time series. Coupling is defined in terms of ability of one time series to better predict a second time series by incorporating knowledge of the first one. Later, in 1969, Granger ([3]) defined a mathematical formulation of the causality concept introduced from Wiener. He formalized this notion for linear regression models of stochastic processes specifying that a decrease in prediction error variance of the second time series, once the knowledge of the first one was incorporated, implies a driver-response relationship between them. Different implementations of this concept were applied to study the feedback relation between input and output variables and to multivariate autoregressive processes introducing the concept of conditional causality ([11],[12]). In the 1990s neurobiological applications rapidly spread, growing interest in studying the effect that one part of the nervous system has on another, either in the absence of identifiable behavioral events or in the context of task performances ([13]).

The original bivariate Granger definition is generalized to interactions among sets of interdependent variables taking into account the data variance. According to Granger definition, a cause-effect relationship exists between two time series $y_i(n)$ and $y_j(n)$, with i ≠ j, if the variance of the prediction error of y_j(n) estimated with a MVAR model including all the N time series of $\mathbf{y}$(n), called the complete model, is lower than the one estimated with a MVAR model including all the N time series of $\mathbf{y}$(n) but y_i(n), called the restricted model.

Hence, the Granger causality from $y_i(n)$ to $y_j(n)$ respect to all the other inputs is measured as:

$$GC_{(y_i \to y_j | y)} = \ln \frac{\tilde{\sigma}_j}{\sigma_j} \tag{1.6}$$

where $\tilde{\sigma}_j$ and σ_j are the variance of prediction error for restricted and complete regression model, respectively.

As an example, let us consider three jointly distributed, stationary multivariate stochastic processes $\mathbf{y}_1$, $\mathbf{y}_2$ and $\mathbf{y}_3$. To measure the causality from $\mathbf{y}_2$ to $\mathbf{y}_1$ given $\mathbf{y}_3$, the complete MVAR model is the following:

(1.7)

$$y_1(n) = -\sum_{k=1}^{p} a_{1,1}(k) y_1(n-k) - \sum_{k=1}^{p} a_{1,2}(k) y_2(n-k) - \sum_{k=1}^{p} a_{1,3}(k) y_3(n-k) + e_1(n)$$

$$y_2(n) = -\sum_{k=1}^{p} a_{2,1}(k) y_1(n-k) - \sum_{k=1}^{p} a_{2,2}(k) y_2(n-k) - \sum_{k=1}^{p} a_{2,3}(k) y_3(n-k) + e_2(n)$$

$$y_3(n) = -\sum_{k=1}^{p} a_{3,1}(k) y_1(n-k) - \sum_{k=1}^{p} a_{3,2}(k) y_2(n-k) - \sum_{k=1}^{p} a_{3,3}(k) y_3(n-k) + e_3(n)$$

with covariance matrix $\Sigma = \begin{bmatrix} \sigma_1^2 & \sigma_{12}^2 & \sigma_{13}^2 \\ \sigma_{21}^2 & \sigma_2^2 & \sigma_{23}^2 \\ \sigma_{31}^2 & \sigma_{32}^2 & \sigma_3^2 \end{bmatrix}$.

The restricted MVAR model, instead, is described by the following equations:

(1.8)

$$y_1(n) = -\sum_{k=1}^{p} \tilde{a}_{1,1}(k) y_1(n-k) - \sum_{k=1}^{p} \tilde{a}_{1,3}(k) y_3(n-k) + \tilde{e}_1(n)$$

$$y_3(n) = -\sum_{k=1}^{p} \tilde{a}_{3,1}(k) y_1(n-k) - \sum_{k=1}^{p} \tilde{a}_{3,3}(k) y_3(n-k) + \tilde{e}_3(n)$$

with covariance matrix $\tilde{\Sigma} = \begin{bmatrix} \rho_1^2 & \rho_{13}^2 \\ \rho_{31}^2 & \rho_3^2 \end{bmatrix}$.

The Granger causality $\mathbf{y}_2 \rightarrow \mathbf{y}_1$, defined in equation (1.6), is expressed from the elements of $\tilde{\Sigma}$ and Σ as follows:

$$GC_{(y_2 \rightarrow y_1 | y_3)} = \ln \frac{\rho_1^2}{\sigma_1^2}$$

This index is positive when the prediction error of $\mathbf{y}_1$ estimated in the complete model is lower than the one estimated in the restricted model, whilst is close to zero when $\mathbf{y}_2$ does not improve the regression.

In general we can conclude that Granger causality index is always defined as a non negative index and it is zero when there is no link between the analyzed signals. Whereas a significantly non-zero value indicates that there is a connection/causality between the two analyzed signals.

1.2.1 Statistical significance: F-test for Granger causality

Statistical significance can be determined via F-statistic which is an application to regression problems of classical F-test:

$$F_{(y_i \rightarrow y_j | y)} = \frac{explained\ variance}{unexplained\ variance} = \frac{\frac{\tilde{\sigma}_j - \sigma_j}{p}}{\frac{\sigma_j}{(L - 2p - 1)}} \quad (1.9)$$

where $explained\ variance$ is associated to the difference of the Residuals Sum of Squares of restricted and unrestricted models and the $unexplained\ variance$ is the Residuals Sum of Squares of unrestricted model, corrected for numerator and denominator degrees of freedom. $\widetilde{\sigma_j}$ and σ_j are the Residuals Sum of Squares of restricted and complete models respectively; p and $(L-2p-1)$ are the degrees of freedom of numerator and denominator. A significant F-statistic is interpreted as evidence that the complete model provides a better prediction and better estimates of the parameters compared to what does the restricted one ([13]). In fact, model with more parameters will always be able to fit the data at least as well as the model with fewer parameters.

In order to determine whether the unrestricted model gives a significantly better fit to data, the F calculated from the data should be greater than the critical value of the F-distribution for some desired false rejection probability.

1.3 Frequency indices

The spectral representation of a MVAR model gives useful tools for the analysis of stochastic processes, based on MVAR model transformation into Z domain. In fact, considering the MVAR model equation (1.1) and moving the autoregressive part to the left side of the equality the following occurs:

$$\boldsymbol{y}(n)+\sum_{k=1}^{p}\boldsymbol{A}(k)\boldsymbol{y}(n-k)=\boldsymbol{e}(n) \tag{1.10}$$

Going to transformation into Z domain:

$$\mathbf{Y}(z)=\mathbf{H}(z)\mathbf{E}(z) \tag{1.11}$$

where $\mathbf{H}(z)$ is the system transfer matrix

$$\mathbf{H}(z)=(\mathbf{I}+\sum_{k=1}^{p}\mathbf{A}(k)z^{-k})^{-1} \tag{1.12}$$

and $\mathbf{E}(z)$ is the prediction error Z-transform.

The N x N frequency response matrix can be expressed as:

$$\mathbf{H}(f) = \mathbf{H}(z)|_{z = e^{i2\pi fT}} \tag{1.13}$$

where *T* is the sampling period, while the cross-spectral matrix can be derived as follows:

$$\mathbf{S}(f) = \mathbf{H}(f)\Sigma_e\mathbf{H}(f)^H \tag{1.14}$$

where $(*)^H$ stands for the Hermitian transpose and $\Sigma_e = diag(\sigma_i^2)$ prediction error covariance matrix.

The most traditional function proposed to detect cooperative neuronal activity in a couple of electro-physiological signals, $y_i(n)$ and $y_j(n)$, is coherence which is defined as follows:

$$Coh_{ij}(f) = \frac{S_{ij}(f)}{\sqrt{S_{ii}(f)\,S_{jj}(f)}} \tag{1.15}$$

where $S_{ij}(f)$ and $S_{ii}(f)$, $S_{jj}(f)$ are the cross and the auto – spectra respectively, evaluated from the cross-spectral matrix (1.14) and varying in the range 0-1. High values of coherence between two EEG signals are interpreted as evidence for ongoing cooperation and long-range synchronization. Although coherence is a consolidated index to describe the linear coupling between two processes, it provides a symmetrical information, i.e. $Coh_{ij}(f)$=$Coh_{ji}(f)$, and hence cannot distinguish the direction of the relation. To overcome this problem, several measures have been suggested ([14]) and the most applied are Directed Transfer Function ([15]) and Partial Directed Coherence ([16]).

Directed Transfer Function (DTF)

Let us consider the equation (1.15) representing the coherence definition between two signals $y_i(n)$ and $y_j(n)$ and rewritten as follows:

$$Coh_{ij}(f) = \sum_{n=1}^{N} \frac{\sigma_n H_{in}(f)}{\sqrt{S_{ii}(f)}} \frac{\sigma_n H_{jn}^*(f)}{\sqrt{S_{jj}(f)}} \tag{1.16}$$

The first factor contains the generalized version of DTF index; thus, DTF index is defined as:

$$\begin{aligned} \gamma_{j\to i}(f) &= \frac{\sigma_j H_{ij}(f)}{\sum_{n=1}^{N} \sqrt{\sigma_n^2 |H_{in}|^2(f)}} \\ &= \frac{\sigma_j H_{ij}(f)}{\sqrt{\sigma_n^2 H_{i:}(f) H_{i:}^H(f)}} \end{aligned} \tag{1.17}$$

with $H_{i:}(f)$ being the *i-th* row of $H(f)$.

Unlike the coherence, DTF index is able to identify dependency direction, since it exclusively depends on the frequency response, which is a non-symmetrical matrix, $H_{ij}(f) \neq H_{ji}(f)$. It expresses the influence of y_j on y_i as the ratio between the inflow from *j* to *i* to all the inflows to *i*. Since DTF is normalized, it varies in the interval [0, 1], where 0 means no significant connections and positive values describe the presence of connection. DTF index represents a robust and reliable estimation method because it is able to distinguish the direction of the relation between two signals, but it is not able to distinguish between direct and indirect connections.

Partial Directed Coherence (PDC)

Unlike DTF, PDC relies on the inverse of the frequency response matrix, written as follows:

$$\mathbf{H}_{inv}(f) = \mathbf{H}(f)^{-1} = \bar{\mathbf{A}}(f) \tag{1.18}$$

where $\bar{\mathbf{A}}(f)$ is expressed as

$$\bar{A}_{ij}(f) = \sum_{k=1}^{p} \bar{a}_{ij}(k) e^{-j2\pi fk} \tag{1.19}$$

directly based on the MVAR model coefficients, and is defined as follows:

$$\pi_{j\to i}(f) = \frac{\bar{A}_{ij}(f)}{\sum_{n=1}^{N} \sqrt{\sigma_n^2 |\bar{A}_{nj}(f)|^2}} \tag{1.20}$$

$$= \frac{\bar{A}_{ij}(f)}{\sqrt{\bar{A}_{:j}^H(f)\bar{A}_{:j}(f)}}$$

with $\bar{A}_{:j}(f)$ being the j-th column of $\bar{\mathbf{A}}(f)$.

PDC describes the influence of y_j on y_i as the ratio between the outflow from y_j to y_i to all the outflows from the source y_j. As for coherence and DTF, also PDC varies in the interval [0, 1], where 0 means no significant connections and a positive value at a specific frequency f indicates the presence of connection at that frequency. Unlike DTF, PDC clearly reflects the interdependencies within a system providing representation of direct causalities. In other words PDC is able to identify direct connections.

Comparison between DTF and PDC

It is interesting to note that, even if both DTF and PDC operate in frequency domain, they assume different meanings. As we have said previously, DTF and PDC differ in the ability of distinguishing direct and indirect dependencies: DTF shows not only direct but also cascade flows, whereas PDC shows only direct flows. In order to understand better this concept, let us consider, as before, three stochastic processes $\mathbf{y}_1$, $\mathbf{y}_2$ and $\mathbf{y}_3$ described by the MVAR model of equation (1.7) with frequency response rewritten as follows:

$$\boldsymbol{H}(f) = \frac{1}{\det(\bar{\mathbf{A}}(f))}\begin{bmatrix} \bar{A}_{22}\bar{A}_{33} - \bar{A}_{23}\bar{A}_{32} & -(\bar{A}_{12}\bar{A}_{33} - \bar{A}_{13}\bar{A}_{32}) & \bar{A}_{12}\bar{A}_{23} - \bar{A}_{13}\bar{A}_{22} \\ -(\bar{A}_{12}\bar{A}_{33} - \bar{A}_{13}\bar{A}_{32}) & \bar{A}_{11}\bar{A}_{33} - \bar{A}_{13}\bar{A}_{31} & -(\bar{A}_{11}\bar{A}_{23} - \bar{A}_{13}\bar{A}_{21}) \\ \bar{A}_{21}\bar{A}_{32} - \bar{A}_{22}\bar{A}_{31} & -(\bar{A}_{11}\bar{A}_{32} - \bar{A}_{12}\bar{A}_{31}) & \bar{A}_{11}\bar{A}_{22} - \bar{A}_{12}\bar{A}_{21} \end{bmatrix} \tag{1.21}$$

Coupling between variables *i* and *j* described with DTF, equation (1.17), results in a linear combination of the elements of the $\bar{\mathbf{A}}(f)$ matrix (1.18), whilst PDC, equation (1.20), considers the single $\bar{A}_{ij}(f)$ element. If there is absence of direct connection between *i* and *j*, then $\bar{a}_{ij}(k)$=0 for each *k* and, hence, PDC equals zero. Differently DTF reveals some connections in any case due to alternative indirect paths linking those two variables. For example, let us consider the element in position (1,2) of matrix $\boldsymbol{H}(f)$ (1.21). Even if we suppose that $\bar{A}_{12}$ is equal zero, the element (1,2) is not null because the other term $\bar{A}_{13}\bar{A}_{32}$ provides the information about link 1→2 throughout indirect connection. Therefore, DTF can be treated as a global index which describes interaction between *i* and *j* throughout both direct and indirect connections, while PDC only reveals direct ones.

Moreover, another difference between two indices concerns the interpretation in terms of spectral density. DTF can be interpreted in terms of spectral density as the power spectrum of y_i coming from y_j normalized to all the contributions to y_i at frequency f. Unlike DTF, PDC has not a direct correspondence with the power spectrum. It depends on the inverse of the frequency response matrix (equation (1.13)) which does not reflect spectral information.

DTF and PDC magnitude is usually evaluated at the peak frequency and the more these functions rise the more connection strength increases. In order to quantitatively sum up their frequency information, global DTF and PDC indices can be derived by AUC (Area Under the Curve):

$$DTF_{tot} = \int_0^{f_{max}} \gamma_{j\to i}(f)\, df \quad , \quad PDC_{tot} = \int_0^{f_{max}} \pi_{j\to i}(f)\, df \tag{1.22}$$

In addition, to evaluate connection strength in classical EEG bands, AUC integrals are computed considering δ, θ, α, β and γ frequency intervals.

1.3.1 Statistical significance: Null hypothesis test for DTF and PDC

To examine the statistical significance of DTF and PDC a null hypothesis test is performed for each pair of signals. This statistical test is a modified version of the surrogate data strategy proposed in ([26]). Specifically, instead of shuffling the time series, the phase randomization is used in order to break time relationships. Consider i.e. DTF (but the same is also true for PDC). Its null distribution is determined using phase randomization, i.e. each data set is transformed in frequency domain via FFT, randomly shuffled in order to change phase information and then reported in time domain via iFFT. If we suppose to iterate this procedure 100 times, we obtain 100 realizations under the null hypothesis and for each realization a DTF profile is computed and its maximum value is selected, thus obtaining one-hundred distinct values. Hence the null distribution is estimated by pooling together the peak value reached in each surrogate realization, as shown in Fig. 1.1. This choice has two main reasons. First, it is cautious since considers high indices values avoiding as much as possible spurious connections. Second, it is a global value independent of the frequency structure of the data. Threshold at P<0.05 fixes γ_0 critical value at its 95th percentile. Hence, there exists a connection for a specific frequency f_0 between two signals if DTF (or PDC) function overcomes threshold line in correspondence to f_0.

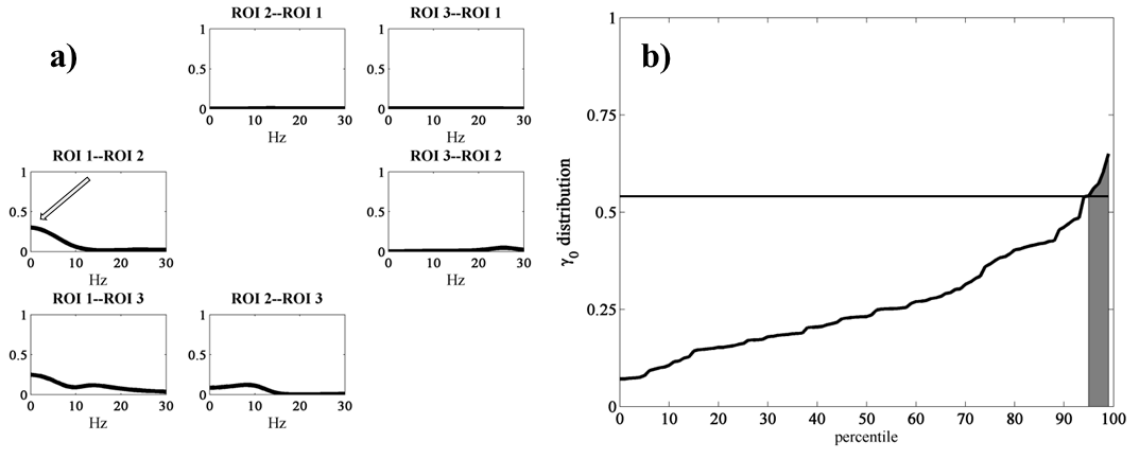

Fig. 1.1: *Representative example of null distribution resulting from 100 surrogate realizations for DTF. a) DTF functions among ROI 1, ROI 2 and ROI 3 when causal influence is absent: arrow indicates the peak value. b) DTF distribution by combining results from one hundred realizations.*

1.4 SEM (Structural Equation Modeling)

The analysis of brain imaging data has recently focused on the examination of the covariances of activity among neural regions during different behaviors. One of the main covariance-based methods is SEM (Structural Equation Modeling). SEM grew out of geneticist, social-science and economics fields from 1920s onwards and has been used in functional imaging since the early 1990s. It was firstly applied to animal autoradiographic data and then extended to human PET data to identify task-dependent differential activation of the dorsal and ventral visual pathways ([5],[17]). Since then, other researchers have used SEM to analyze fMRI and EEG data ([18],[7]).
SEM is a static multivariate regression model widely used to estimate connections within a defined network. It is based on the hypothesis that the topology of the network in terms of interconnections among interacting variables is a priori known and that inter variables coupling is linear time invariant. In fact, in this method, connections between brain areas are based on known neuroanatomy and the interregional covariances of activity are used to calculate path coefficients representing the magnitude of the influence of each directional path.
Considering as an example the following network

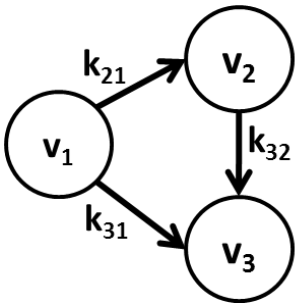

***Fig. 1.2**: An example of structural model with three regions and three connections. Each region is associated with variable, v_i , i = 1,2,3. Arrows indicate causal relationships that are assumed a priori and strength connections are defined by the scalar k_{ij} .*

these assumptions are translated in the following equations

$$v_2(t) = k_{21}v_1(t) + e_2(t)$$
$$v_3(t) = k_{31}v_1(t) + k_{32}v_2(t) + e_3(t) \quad (1.23)$$

where $v_n(t)$ is the model prediction for cortical activity associated with variable *n*, with *n*=1,2,3, k_{ij} is the path coefficient from variable *j* to variable *i* and $e_n(t)$ is a residual term with covariance Σ_e, interpreted as driving each variable stochastically and assumed to be uncorrelated with $v_n(t)$.
The path coefficients k_{ij} and the covariance matrix Σ_e are identified on time series data by minimizing the difference between the covariance matrix estimated from the data and the covariance matrix implied by the structural model in Fig. 1.2. Hence, in terms of neural systems, a measure of covariance represents the degree to which the activities of two or more regions are related.

Let **s** be a set of three time series:

$$\mathbf{s}(n) = [\mathbf{s}_1(n), \mathbf{s}_2(n), \mathbf{s}_3(n)], \ n=1, \dots, L. \tag{1.24}$$

The 3x3 covariance matrix estimated from the data is:

$$\boldsymbol{S} = \frac{\boldsymbol{s}^T \boldsymbol{s}}{L-1} \tag{1.25}$$

where L is the number of observations. Covariance matrix implied by the model, respect to equation (1.23), is calculated as:

$$\Sigma_v = (1-\mathbf{k})^{-T} \Sigma_e (1-\mathbf{k})^{-1} \tag{1.26}$$

where $\mathbf{k} = \begin{bmatrix} 0 & 0 & 0 \\ k_{21} & 0 & 0 \\ k_{31} & k_{32} & 0 \end{bmatrix}$.

The unknown parameters are estimated by minimizing a function of the observed (i.e. estimated from the data) and implied covariance matrices. The most widely used objective function for SEM is the maximum likelihood (ML) function:

$$F = ln|\Sigma_v| - tr\left(\boldsymbol{S}\Sigma_v^{-1}\right) - ln|\boldsymbol{S}| \tag{1.27}$$

The ML objective function of equation (1.27) is optimized by means of a fitting criterion which employs a Newton-type algorithm based on an analytic gradient. The starting values can be estimated using ordinary least square. Statistical inference takes into account two aspects: the goodness of the overall fit of the model and the difference between alternative models, called stacked-model approach. For example, the χ^2 statistic test can be used to infer statistical significance of the structural equation modeling.

Chapter 2

The neural mass model for data simulation

Modeling neurophisiological nervous system mechanisms rely upon simplifying assumptions and empirical priors. Recent years literature shows a rising interest in this issue and several approaches have been developed to model neural signals. The most feasible approach is based on mathematical tools, called *neural mass models* (NMM). They are designed to provide an easier description of electrical behavior of the brain areas than models mapping single neurons. Neural mass models obtain this simplification assuming that neighbor neurons, belonging to the same population, have a similar membrane potential. The main purpose of the neural mass models is to simulate different EEG signals when the connections between different brain areas change. This approach describes the processes generating EEG signals by arranging in series and in parallel simplified blocks which simulate the key mechanisms. A neural mass model of EEG is thus a surrogate of a cortical area. It usually comprises a small number of neural populations interacting each other and uses only one or two state variables to represent the mean activity of each single neural population. The dynamics of entire neural populations and of their synapses are described under the assumptions that neurons in the same population share similar inputs and synchronize their activity. Therefore by tuning the kinetics parameters of each population, this procedure is able to design specific signal rhythms and reproduce responses seen empirically.

One of the first proposed model is the Wilson-Cowan oscillator to study synchronization among neural oscillations ([30]). Subsequently, Lopes da Silva et al. proposed a simple model of two populations, by using a feedback loop incorporating excitatory and inhibitory neuron groups, to simulate the generation of the α rhythm in the thalamus ([31]). Freeman proposed a similar model to study dynamics in the olfactory cortex ([20]). These models have been subsequently improved by Jansen; his model includes the interaction between three neural populations with different synaptic kinetics (pyramidal neurons, excitatory interneurons, inhibitory interneurons) ([32]). The Jansen equations are still frequently used to build models of interconnected cortical areas, able to reproduce EEG dynamics in large regions of the brain, to study effective connectivity from EEG or fMRI data or to investigate how event related potentials depend on intrinsic connectivity ([33], [34],[35], [36]). An important improvement in the use of neural mass models has been provided by Wendling ([37]). Studying hippocampus dynamics during epilepsy, he proposed the addition of a fourth population to the Jansen's model to account for the presence of fast interneurons. This model allows to simulate the dynamics of real EEG signals measured with intracerebral electrodes in the hippocampus during epileptic seizures.

The majority of neural mass models of EEG responses have been designed to model alpha rhythms; recent studies have emphasized the necessitate to produce rhythms in different bands. Some of the literary works cited above show that the kinetic of inhibitory populations have a focal influence on signals generation in particular to generate a γ rhythm ([9]). Hence, in the last decade more attention has been drawn to simulate several rhythms coexisting in the same cortical area ([33], [38], [9]).

The model exploited to simulate our *in silico* data ([9]) aims to render the dynamics of the cerebral network as much realistic as possible. It has been developed by Ursino's team and consistent literature works prove its effectiveness in reproducing EEG signal behavior ([9], [16],[17],[18],[30],[31]). A new aspect in Ursino's model, not present in previous versions, consists in the inclusion of a self-loop among fast inhibitory interneurons. Two main objectives have been pursued by Ursino: (i) to enrich the model of a single cortical region with a new feedback loop, through which fast inhibitory interneurons can produce a γ rhythm per se (i.e. without the participation of the other neural populations), and (ii) to demonstrate that the modified model can easily produce EEGs PSD of a single cortical region characterized by several peaks.

2.1 The neural mass model

The model [9] simulates one cortical region and produces an intrinsic rhythm that can vary its frequency band by changing the synaptic kinetics parameters.

It consists of four neural populations representing pyramidal neurons, excitatory interneurons and inhibitory interneurons with slow and fast synaptic kinetics. Each populations represents a group of neurons of the same type which approximately share the same membrane potential and can be massed together. The dynamic of each group is described with a similar mathematical formalism consisting of three key blocks in cascade, as shown in Fig. 2.1: it represents general three blocks cascade to simulate the synapses junction and the information transmission.

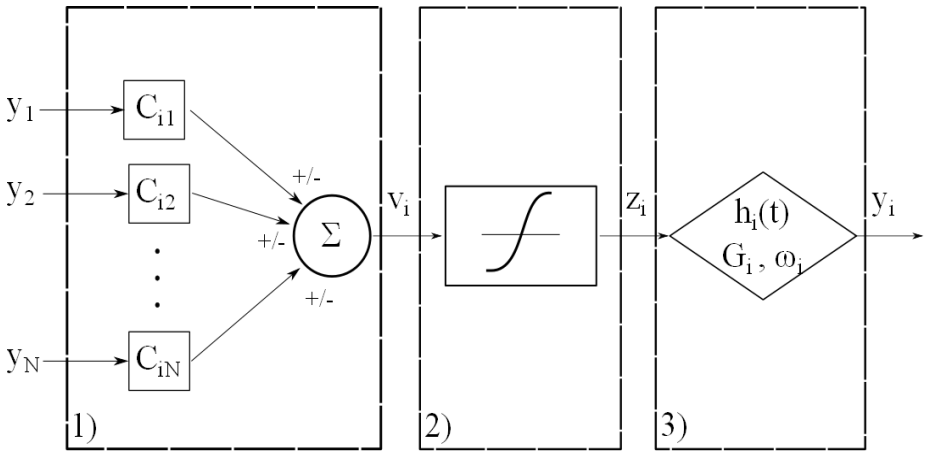

***Fig. 2.1**: Layout of the general model of a single population. Modified Fig. 1 of [9]*

Each block is characterized by an input-output relationship. The block 1) receives from other neural populations the so-called post-synaptic potentials y_i and combines them linearly by multiplying for a constant C_{ij}. It results in an average post-synaptic membrane potential v_i which subsequently is converted into an average density of spikes fired by the neurons, z_i, as represented in block 2). In order to account for the presence of inhibition (when potential is below a given threshold) and saturation (when potential is high), which are two non – linear mechanism, this conversion is simulated with a static sigmoidal relationship. Finally, the last block reproduces the synaptic kinetics with a second order system, with different parameter values each group. In the following, a quantity which belongs to a neural population will be denoted with subscript *p* (pyramidal), *e* (excitatory interneuron), *s* (slow inhibitory interneuron) and *f* (fast inhibitory interneuron). Hence, these previous concepts are summarized by the following equations:

$$\ddot{y}_i = G_i\,\omega_i\,z_i - 2\,\omega_i\,\dot{y}_i - \omega_i^2\,y_i$$

where

$$v_i = \sum_j C_{ij}\,y_j \qquad i = p, e, s, f \qquad (2.1)$$

$$z_i = \frac{2e_0}{1 + e^{-rv_i}} - e_0$$

where the subscript *j* refers to a presynaptic neural group, y_i is the post-synaptic potential change induced by a unitary synapse coming from other groups, C_{ij} represents the connectivity constant from the *j*th group to the *i*th one; parameters e_0 and *r*, assumed equal for all groups, set the maximal saturation and the slope of the sigmoidal relationship; G_i and ω_i represent the strength (i.e. the gain) and the reciprocal of the time constant (i.e. natural frequency) of the individual synapses. It is worth noting that, by giving different values to G_i and ω_i ($i = p, e, s, f$) one can mimic the impulse response of the different synapses. In the following, these impulse responses will be denoted with symbols $h_e(t)$, $h_s(t)$ and $h_f(t)$, assuming that excitatory interneurons have the same kinetics as pyramidal cells (i.e. $h_p(t) = h_e(t)$).

A particular attention should be drawn to the following scheme adopted for the fast inhibitory interneurons:

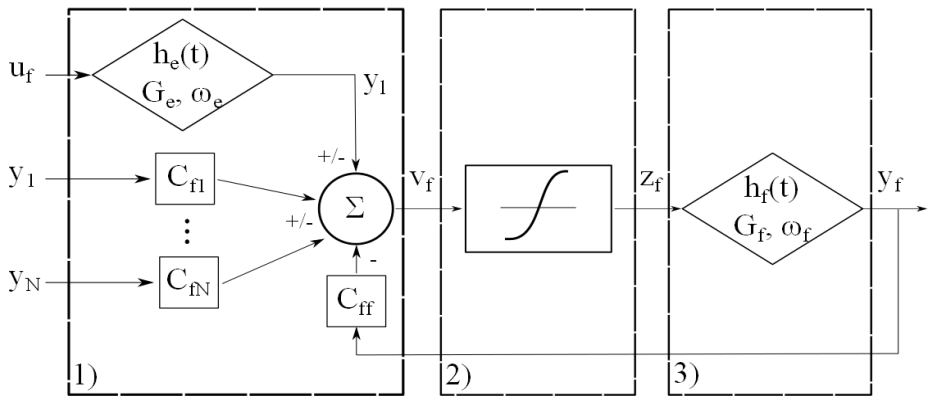

***Fig. 2.2**: Scheme of fast inhibitory interneurons. It consists of three blocks in cascade as for the general model in Fig. 2.1 but, in addition, the first block is powered by an external input $u_f(t)$ and by the feedback loop. Modified Fig. 2 of [9].*

This group synapses with itself and is powered by an external input. The rationale of this choice stands in previous work ([39]) which implements self loop to generate γ rhythms. The addition to this neural mass model of a feedback loop with fast inhibitory interneurons allows producing γ rhythm per se without the contribution of the other groups.

To model a whole cortical area, the four populations are connected via excitatory and inhibitory synapses, with impulse response $h_e(t)$, $h_s(t)$ or $h_f(t)$. Connecting these four groups we obtain the complete scheme of the neural mass model which is represented as follows:

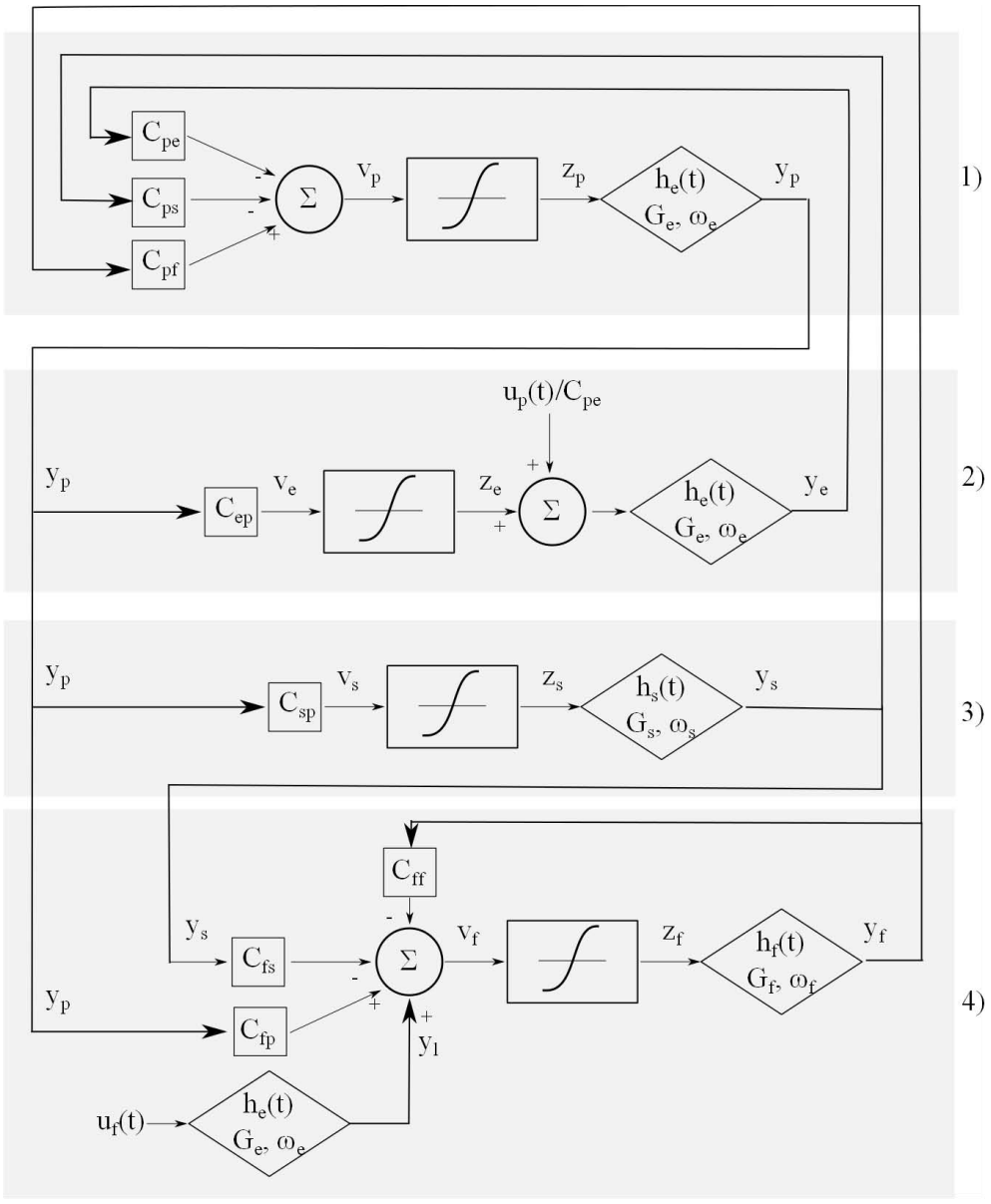

***Fig. 2.3**: Layout of the complete model for one region. Four neural groups, designed as shown in Fig. 2.1, communicating via excitatory and inhibitory synapses: 1) Pyramidal cells. 2) Excitatory interneurons. 3) Slow inhibitory interneurons. 4) Fast inhibitory interneurons. Modified Fig. 3 of [9].*

It consists of three general blocks cascade of Fig. 2.1 for the pyramidal cells, the excitatory interneurons and the slow inhibitory interneurons plus the scheme of Fig. 2.2 for the fast inhibitory interneurons. An important aspect of the model is the external inputs, targeting the excitatory and

the fast inhibitory interneurons. In a physiological context, these comprehend all external signals coming from the other cortical areas. In order to study connectivity between two cortical areas, a linear relationship is assumed between the averaged spike density of pyramidal neurons of the pre-synaptic area, z_p^k, and the input of the post-synaptic area, u_j^h, as follows:

$$u_j^h(t) = n_j^h(t) + N * W_j^{jk}\, z_p^k(t-\omega) \qquad j = p, f \tag{2.2}$$

where $n_j(t)$ represents Gaussian white noise, W_j is the weight factor and ω is the time delay. $N = 20$ tunes the input signal amplitude.

For brevity, in this work the model will be described with a condensed mathematical formalism to highlight the two different impulse responses, $h_{ex}(t)$ and $h_{in}(t)$, for excitatory and inhibitory inputs, respectively.

2.2 NMM parameters analysis

In order to generate electro-physiological signals, ranging in EEG band $0 - 30$ Hz, the NMM equations ([9]) have been studied by varying the kinetic parameters within the set (0, 5, 30, 55, 56, 80, 126, 130) and fixing the others (ω_e, ω_s, ω_f, G_e, G_s, G_f) to the values in Table 1 of ([9]).

To identify the optimal parameter set, several simulations have been performed to analyze both the system stability and its frequency response. To this purpose, the NMM equations, after been linearized, have been described as multi input-output (MIMO) system of linear differential equations with the state-space representation:

$$\begin{aligned} \dot{\mathbf{x}} &= \mathbf{A}\mathbf{x} + \mathbf{B}\mathbf{u} \\ \mathbf{v} &= \mathbf{C}\mathbf{x} + \mathbf{D}\mathbf{u} \end{aligned} \tag{2.3}$$

where **x** is a n by 1 vector representing the state, **u** and **v** are the input and the output, respectively. The matrices **A** (n by n), **B** (n by m), and **C** (r by n) determine the relationships between the state and input and output variables. In our case, there are ten first-order differential equations, two

inputs, $u_p(t)$ and $u_f(t)$, and four outputs $v_p(t), v_e(t), v_s(t), v_f(t)$. System matrices **A**, **B** and **C** are the following:

$$\mathbf{A}=\begin{bmatrix} 0 & 0 & 0 & 0 & 1 & 0 & 0 & 0 & 0 & 0 \\ 0 & 0 & 0 & 0 & 0 & 1 & 0 & 0 & 0 & 0 \\ 0 & 0 & 0 & 0 & 0 & 0 & 1 & 0 & 0 & 0 \\ 0 & 0 & 0 & 0 & 0 & 0 & 0 & 1 & 0 & 0 \\ -\omega_e^2 & k_1 C_{pe} & -k_1 C_{ps} & -k_1 C_{pf} & -2\omega_e & 0 & 0 & 0 & 0 & 0 \\ k_1 C_{pe} & -\omega_e^2 & 0 & 0 & 0 & -2\omega_e & 0 & 0 & 0 & 0 \\ k_2 C_{sp} & 0 & -\omega_s^2 & 0 & 0 & 0 & -2\omega_s & 0 & 0 & 0 \\ k_3 C_{fp} & 0 & -k_3 C_{fs} & -k_3 C_{ff} - \omega_f^2 & 0 & 0 & 0 & -2\omega_f & k_3 & 0 \\ 0 & 0 & 0 & 0 & 0 & 0 & 0 & 0 & 0 & 1 \\ 0 & 0 & 0 & 0 & 0 & 0 & 0 & 0 & -\omega_e^2 & -2\omega_e \end{bmatrix}$$

where $k_1 = G_e \omega_e \frac{e_0 r}{2}$, $k_2 = G_s \omega_s \frac{e_0 r}{2}$ and $k_3 = G_f \omega_f \frac{e_0 r}{2}$,

$$\mathbf{B} = \begin{bmatrix} 0 & 0 \\ 0 & 0 \\ 0 & 0 \\ 0 & 0 \\ 0 & 0 \\ \frac{G_e \omega_e}{C_{pe}} & 0 \\ 0 & 0 \\ 0 & 0 \\ 0 & 0 \\ 0 & G_e \omega_e \end{bmatrix}$$

$$\mathbf{C} = \begin{bmatrix} 0 & C_{pe} & -C_{ps} & -C_{pf} & 0 & 0 & 0 & 0 & 0 & 0 \\ C_{ep} & 0 & 0 & 0 & 0 & 0 & 0 & 0 & 0 & 0 \\ C_{sp} & 0 & 0 & 0 & 0 & 0 & 0 & 0 & 0 & 0 \\ C_{fp} & 0 & -C_{fs} & -C_{ff} & 0 & 0 & 0 & 0 & 1 & 0 \end{bmatrix}$$

To evaluate the system stability, work [19] has verified that all eigenvalues of **A** lie in the left-hand side, while to analyze the frequency response, in [19] the state-space representation was re-written into Laplace domain, as follows:

$$s\mathbf{X}(s) = \mathbf{A}\mathbf{X}(s) + \mathbf{B}\mathbf{U}(s)$$

$$(s\mathbf{I} - \mathbf{A})\mathbf{X}(s) = \mathbf{B}\mathbf{U}(s)$$

$$\mathbf{X}(s) = (s\mathbf{I} - \mathbf{A})^{-1}\,\mathbf{B}\mathbf{U}(s)$$

and

$$\mathbf{V}(s) = [\mathbf{C}(s\mathbf{I} - \mathbf{A})^{-1}\mathbf{B} + \mathbf{D}]\mathbf{U}(s) = \mathbf{H}(s)\mathbf{U}(s)$$

where $\mathbf{H}(s)$ is the *matrix transfer function* relating the output vector $\mathbf{V}(s)$ to the input vector $\mathbf{U}(s)$:

$$\mathbf{H}(s) = \frac{\mathbf{C}_{adj}\,(s\mathbf{I} - \mathbf{A})\mathbf{B} + det(s\mathbf{I} - \mathbf{A})\mathbf{D}}{det(s\mathbf{I} - \mathbf{A})}$$

In our case, $\mathbf{H}(s)$ is 4 by 2 matrix whose elements are the individual transfer functions relating a given component of the output $\mathbf{V}(s)$ to a component of the inputs $\mathbf{U}(s)$, as described in the following set of equations:

$$\begin{bmatrix} V_p(s) \\ V_e(s) \\ V_s(s) \\ V_f(s) \end{bmatrix} = \begin{bmatrix} H_{pp}(s) & H_{pf}(s) \\ H_{ep}(s) & H_{ef}(s) \\ H_{sp}(s) & H_{sf}(s) \\ H_{fp}(s) & H_{ff}(s) \end{bmatrix} \begin{bmatrix} U_p(s) \\ U_f(s) \end{bmatrix}.$$

Among the subsets of parameter values assuring the system stability, spectral analysis of the frequency response has been performed in order to find those generating signals with well-defined frequency peaks. The attention was focused on the transfer functions relating the inputs with $V_p(s)$, since $v_p(t)$ represents the cortical pyramidal cells signal. By evaluating their response magnitude:

$$\left|H_{pp}(\omega)\right|^2 \text{ and } \left|H_{pf}(\omega)\right|^2 \tag{2.4}$$

we choose those sets giving peak frequency around 5 Hz, 15 Hz and 30 Hz.
Since these two transfer functions refer to excitatory and inhibitory cells, respectively, to highlight their meaning they are called $H_{ex}(\omega)$ and $H_{in}(\omega)$ and, hence $h_{ex}(t)$ and $h_{in}(t)$ in time domain.

2.3 Simulated datasets

The NMM described above has been used to simulate a ROI cortical EEG, where the input is white noise $n(t)$ with zero mean and variance $\sigma^2 = 5$ for both impulse response $h_{ex}(t)$ and $h_{in}(t)$, while the output is $v_n(t)$, corresponding to the NMM $v_p(t)$, represented in condensed formalism in Fig. 2.4:

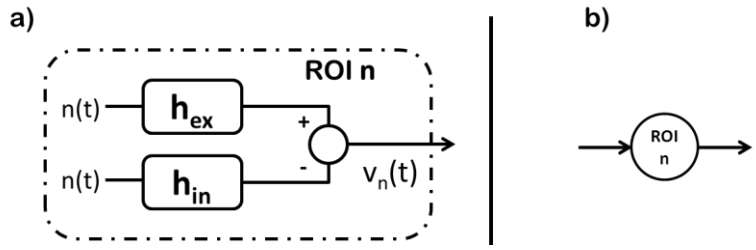

Fig. 2.4: *One ROI model. Each ROI is characterized by two impulse responses, $h_{ex}(t)$ and $h_{in}(t)$, for excitatory and inhibitory inputs, $n(t)$ which are assumed Gaussian with zero mean and variance $\sigma^2 = 5$. $v_n(t)$ corresponds to the pyramidal output $v_p(t)$ in the NMM (a). Picture in (b) shows the symbolism used for synthetic representations.*

By combining three populations - called ROI 1, ROI 2 and ROI 3, connected by weight parameters A, B, C and characterized by different synaptic kinetics - four different network models have been analyzed. The first one is a feed-forward network and it has been extensively analyzed in a previous work ([19]). This network is shown in Fig. 2.5a. The other three networks, instead, obtained by combining the same three ROIs, are analyzed in this work and they are: the open-loop network with two direct links, connecting ROI 1 to ROI 2 and ROI 2 to ROI 3 (Fig. 2.5b), the network with a feed-back link from ROI 2 to ROI 1 (Fig. 2.5c) and finally the cycle network (Fig. 2.5d).

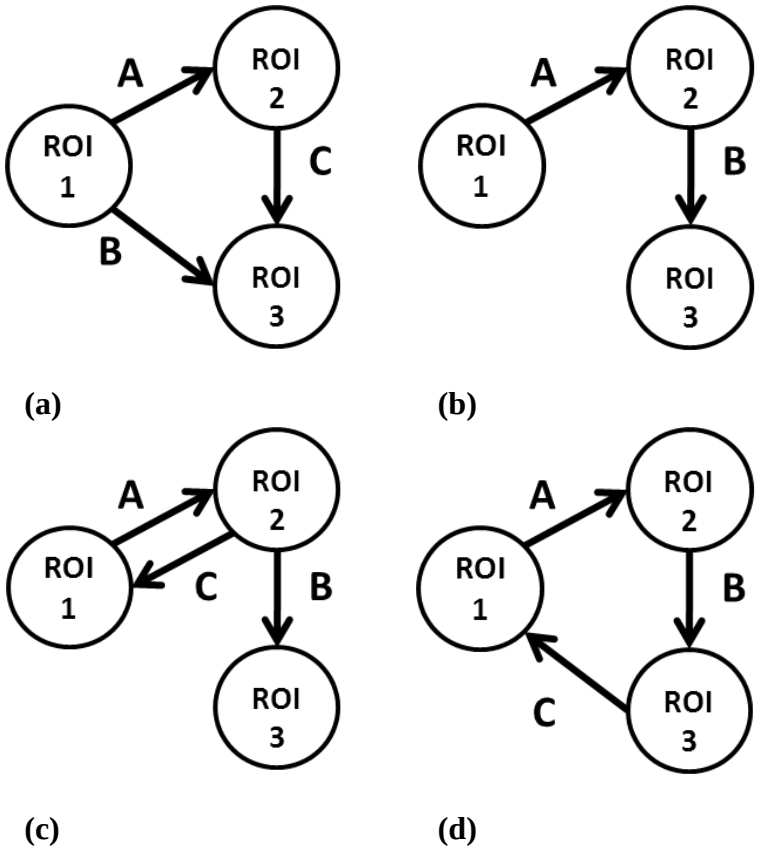

Fig. 2.5: *Neural network models used to simulate data. The connection intensity between coupled ROIs is described by weight parameters A, B and C. (a) feed-forward network, (b) open-loop network, (c) network with a feed-back link, (d) cycle network.*

For all these networks, three datasets have been generated with different degrees of non linearity defined as the slope *r* adopted in the sigmoid relationships of the model, assuming the following values:

- dataset 1 with $r = 0.36$;
- dataset 2 with $r = 0.56$;
- dataset 3 with $r = 0.66$.

For each dataset, weight parameters A, B and C have been fixed to simulate ten conditions as follows:

- basal condition : A=B=C=1;
- increasing A): A = 2, 3 and 4, while B = C = 1;
- increasing B): B = 2, 3 and 4, while A = C = 1;
- increasing C): C = 2, 3 and 4, while A = B = 1;

Summing up, for feed-forward network, network with feed-back link and cycle network thirty experiments have been simulated, while for open-loop network twenty-one experiments have been simulated. For each of them one hundred realizations of 2s have been generated for the three ROIs, with sampling frequency $F_s = 200$ Hz.

In Tables 2.1, 2.2, 2.3, 2.4 the network schemes and weight values assumed for each experiment are summarized.

The analysis is detailed for networks (b), (c) and (d) of Fig.2.5 while for network (a) only results are reported since the detailed analysis is in [19].

Networks	Weight values
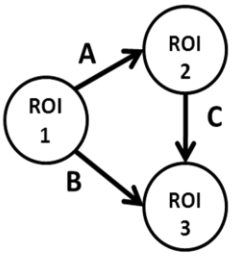	• A=B=C=1
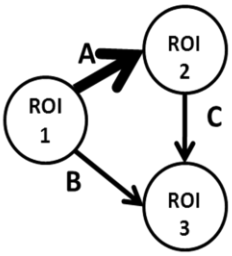	• A=2 B=C=1 • A=3 B=C=1 • A=4 B=C=1
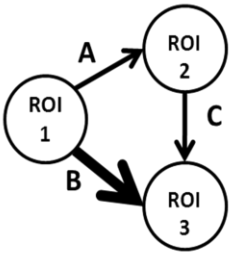	• B=2 A=C=1 • B=3 A=C=1 • B=4 A=C=1
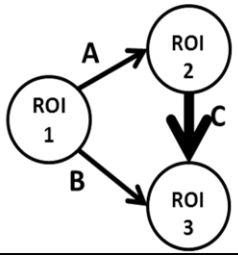	• C=2 A=B=1 • C=3 A=B=1 • C=4 A=B=1

***Table 2.1**: Feed-forward network schemes and weight values assumed for each experiment.*

Networks	Weight values
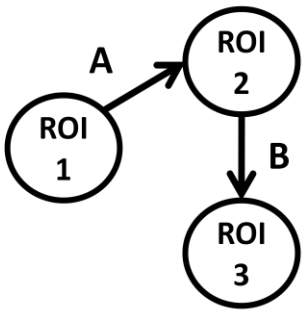	• A=B=1
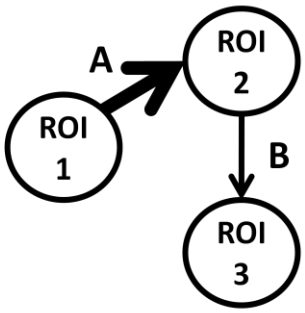	• A=2 B=1 • A=3 B=1 • A=4 B=1
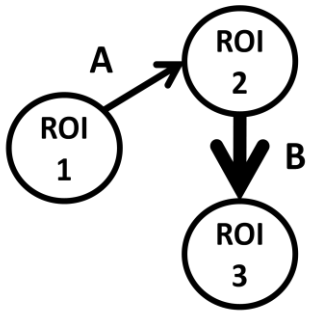	• B=2 A=1 • B=3 A=1 • B=4 A=1

***Table 2.2**: Open loop network schemes and weight values assumed for each experiment.*

Networks	Weight values
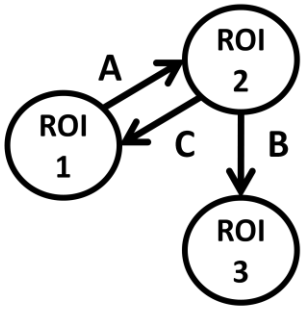	• A=B=C=1
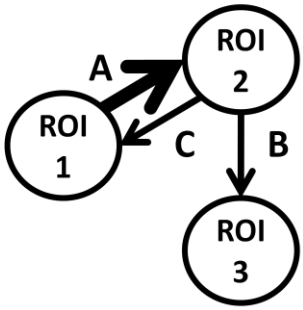	• A=2 B=C=1 • A=3 B=C=1 • A=4 B=C=1
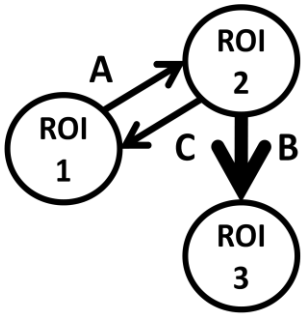	• B=2 A=C=1 • B=3 A=C=1 • B=4 A=C=1
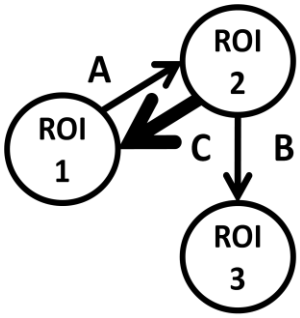	• C=2 A=B=1 • C=3 A=B=1 • C=4 A=B=1

***Table 2.3**: Network with feedback link schemes and weight values assumed for each experiment.*

Networks	Weight values
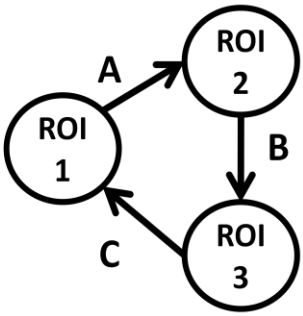	• A=B=C=1
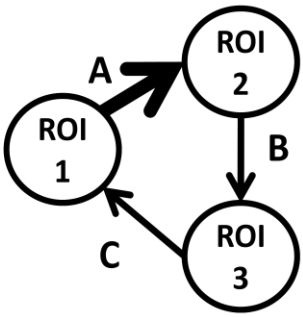	• A=2 B=C=1 • A=3 B=C=1 • A=4 B=C=1
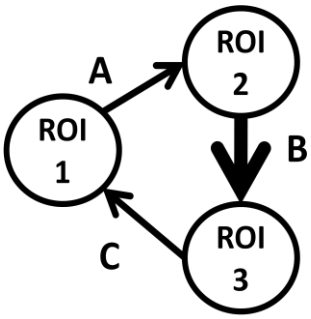	• B=2 A=C=1 • B=3 A=C=1 • B=4 A=C=1
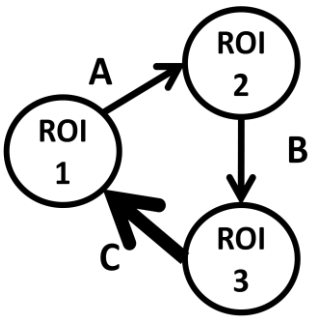	• C=2 A=B=1 • C=3 A=B=1 • C=4 A=B=1

***Table 2.4**: Cycle network schemes and weight values assumed for each experiment.*

Chapter 3

In silico experiments

In this chapter are reported parameter values (which are maintained the same for all analyzed networks) adopted in NMM equations for the generation of in silico data and are shown examples of simulated signals of different network models.

3.1 Simulation

3.1.1 NMM parameters

System stability analysis has been performed considering 7^7 different combinations of NMM parameter values. Among the subsets of parameter values assuring the system stability, we choose those sets giving peak frequency in low (around 5 Hz), medium (around 15 Hz) and high (around 30 Hz) frequency. Parameter values adopted in NMM equations are reported in Table 3.1:

a) Common parameters

Parameters	Symbols	Values
Average gain (mV)	G_e	5.17
	G_s	4.45
	G_f	57.1
Time Constant reciprocal (s^{-1})	w_e	75
	w_s	30
	w_f	75
Sigmoid saturation (s^{-1})	e_0	2.5
Time delay (ms)	ω	10
Input noise variance	σ^2	5

b) Region's parameters

Parameters	Symbols	ROI 1	ROI 2	ROI 3
Number of synaptic contacts	C_{ep}	55	5	130
	C_{pe}	5	5	5
	C_{sp}	5	5	105
	C_{ps}	55	55	130
	C_{fp}	56	56	80
	C_{fs}	5	5	126
	C_{pf}	0	5	30
	C_{ff}	5	5	30

Table 3.1*: Network models kinetics parameters. a) Common parameters are average gains, time constant reciprocals, sigmoid saturations and time delays. Values are the same of [21]. b) Regions' parameters are the synaptic contact numbers.*

3.1.2 Model predicted EEG signals

After identifying those parameter sets generating well-defined frequency peak in low, medium and high frequency, in silico EEG have been simulated using *ad hoc* Matlab code provided by Ursino's team. For each experiment described in 2.3, one hundred realizations 2s long of three joined time series have been generated with sampling frequency $F_s = 200$ Hz.

Examples of signals of the different network models are shown in Fig. 3.1, evidencing how the linking direction influences the frequency content.

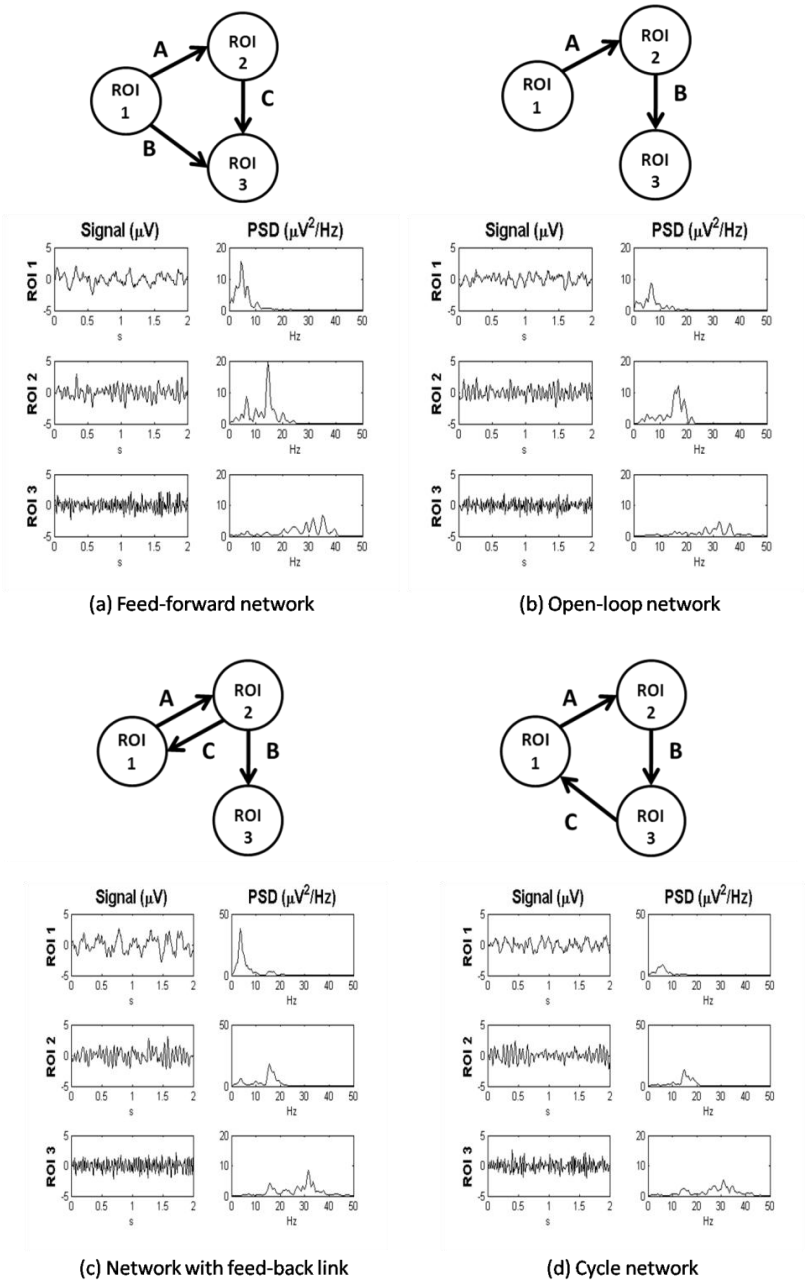

Fig. 3.1*: Model predicted EEG signals in time and frequency domain for each network model in basal condition, where all weights are equal to 1 and r=0.56.*

If we observe feed-forward and open-loop networks, Fig. 3.1 (a) and (b), we can see that ROI 2 clearly exhibits spectral contribute coming from ROI 1, while in ROI 3 there are not significant differences between the two network models, since its intrinsic gain is very low in the pass-band of ROI 1 and ROI 2 and, hence, frequency contents of inflowing ROIs are less evident. Differently, networks in Fig. 3.1 (c) and (d) produce an increasing in ROI 3 PSD, thanks to the synergic connection of the feed-back link.

The following figures show, for all networks, the model prediction in time and frequency domain in a representative realization characterized by different values of network sigmoid slope *r*. This parameter is very important because it influences frequency contents, since it directly modifies the intrinsic gain of each ROI. Figures show basal condition and experiments characterized by different values of A, B and C parameters.

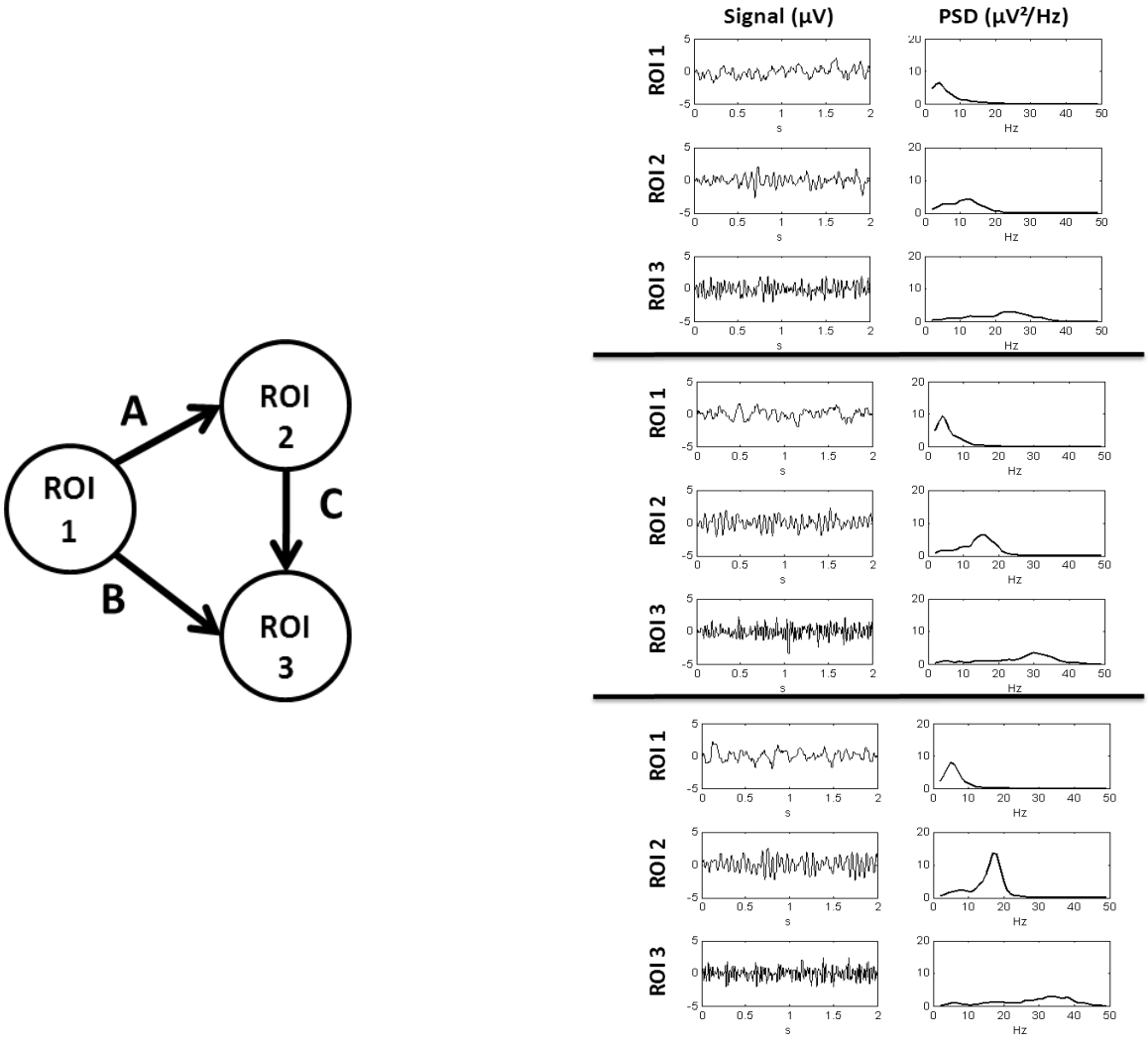

***Fig. 3.2**: Basal condition (A=B=C=1). Model predicted EEG signals in time and frequency domain in a representative realization for each dataset for feed-forward network. In the right side: upper panel r=0.36, middle panel r=0.56, lower panel r=0.66.*

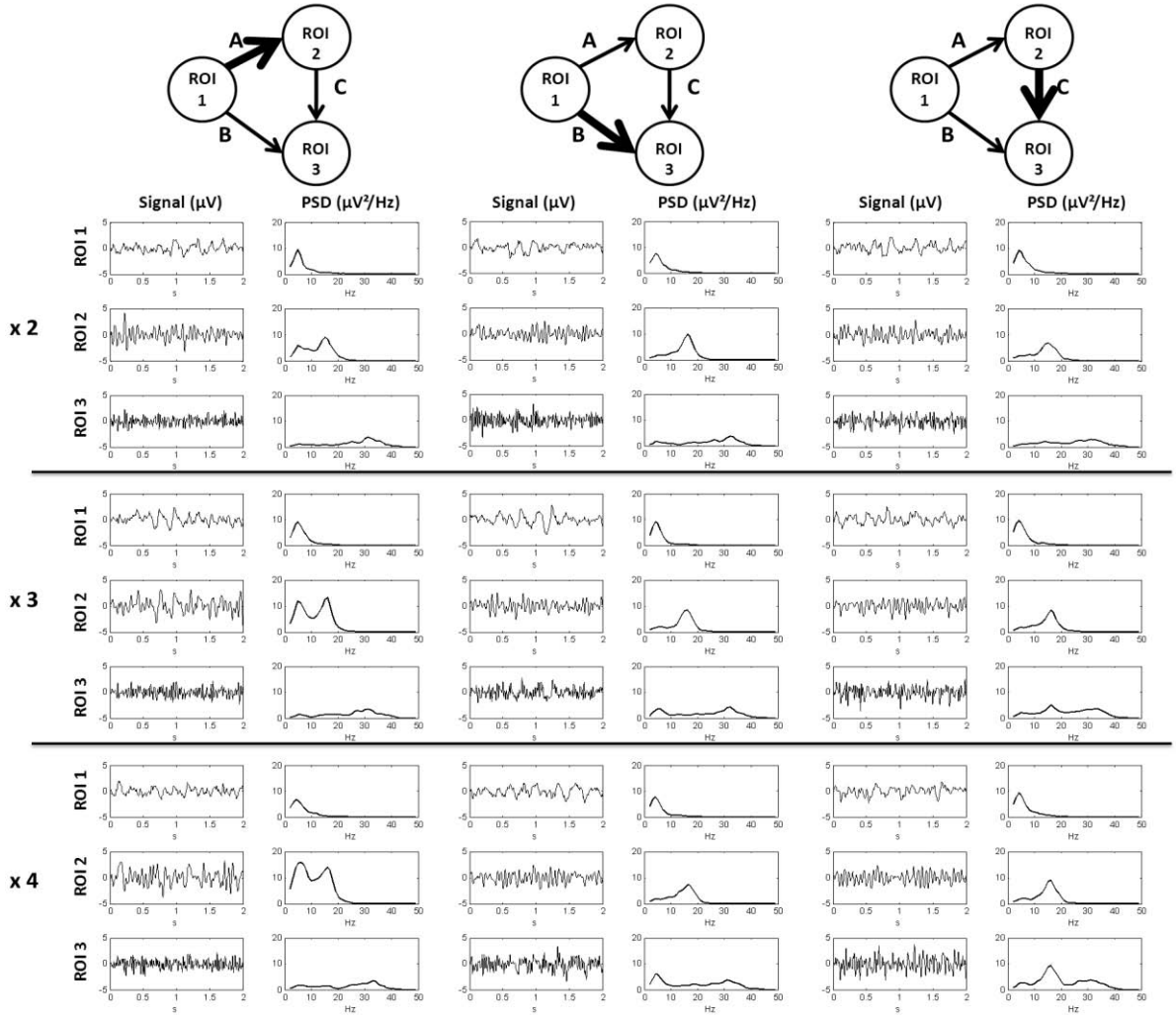

Fig. 3.3*: Model predicted EEG signals in time and frequency domain in a representative realization of experiments characterized by different values of A, B and C parameters of the network bold link (r=0.56 dataset).*

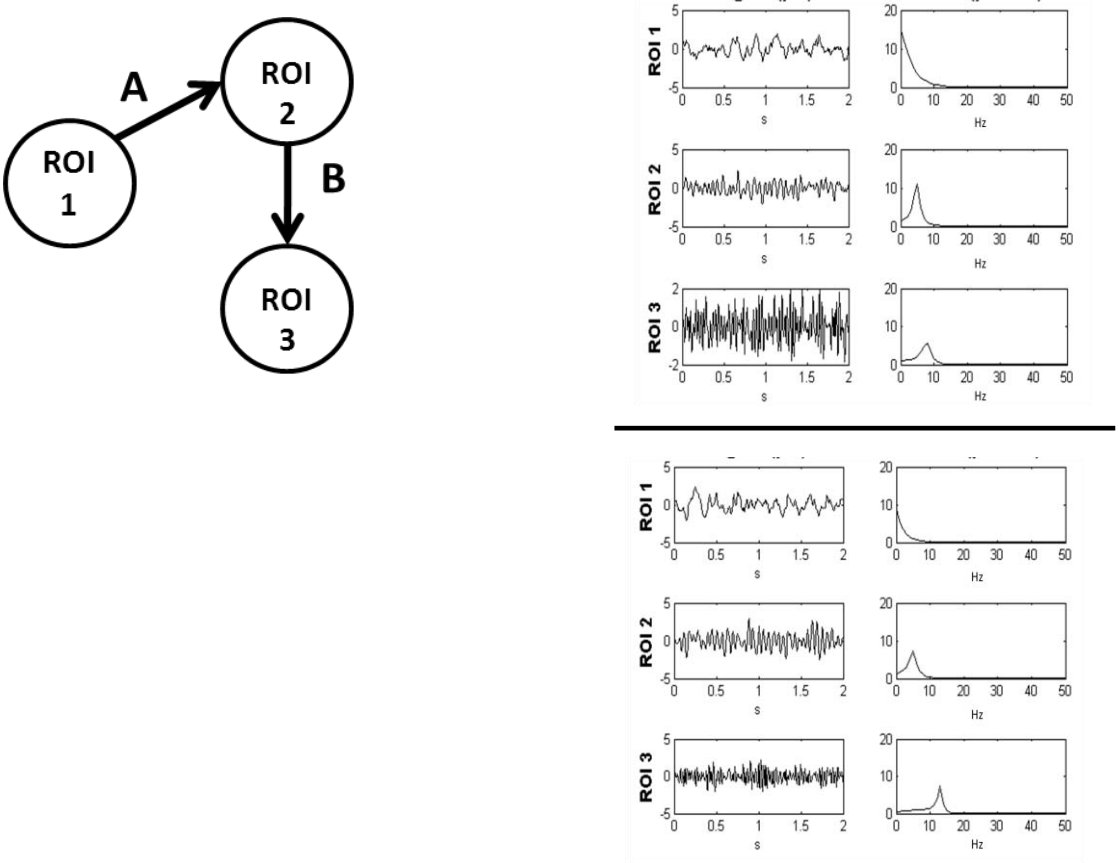

***Fig. 3.4**: Basal condition (A=B=1). Model predicted EEG signals in time and frequency domain in a representative realization for each dataset for open-loop network. In the right side: upper panel r=0.36, middle panel r=0.56, lower panel r=0.66.*

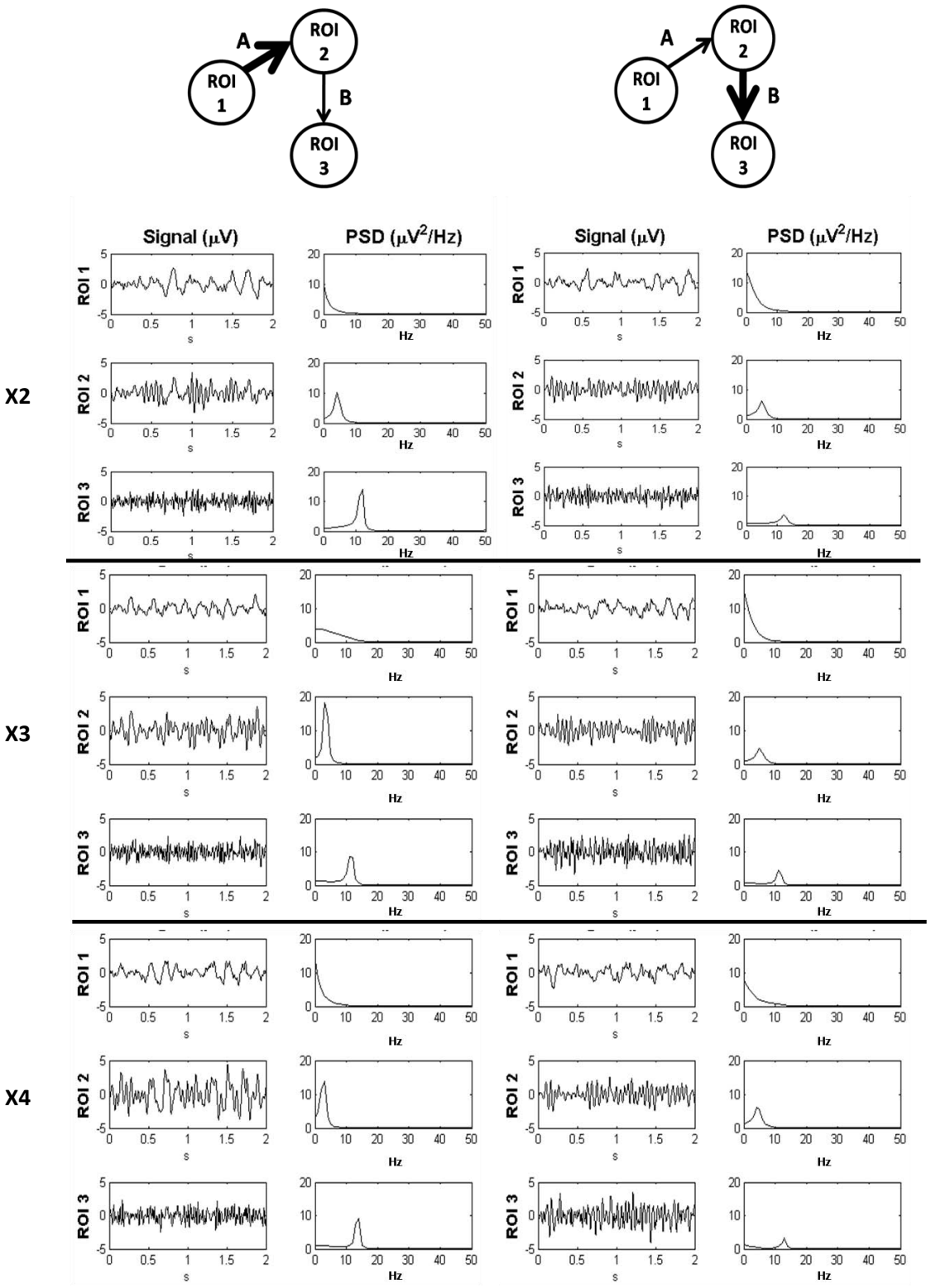

***Fig. 3.5**: Model predicted EEG signals in time and frequency domain in a representative realization of experiments characterized by different values of A and B parameters of the network bold link (r=0.56 dataset), for open-loop network.*

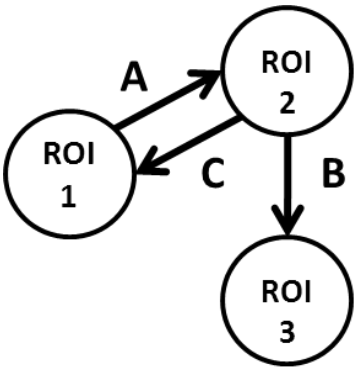

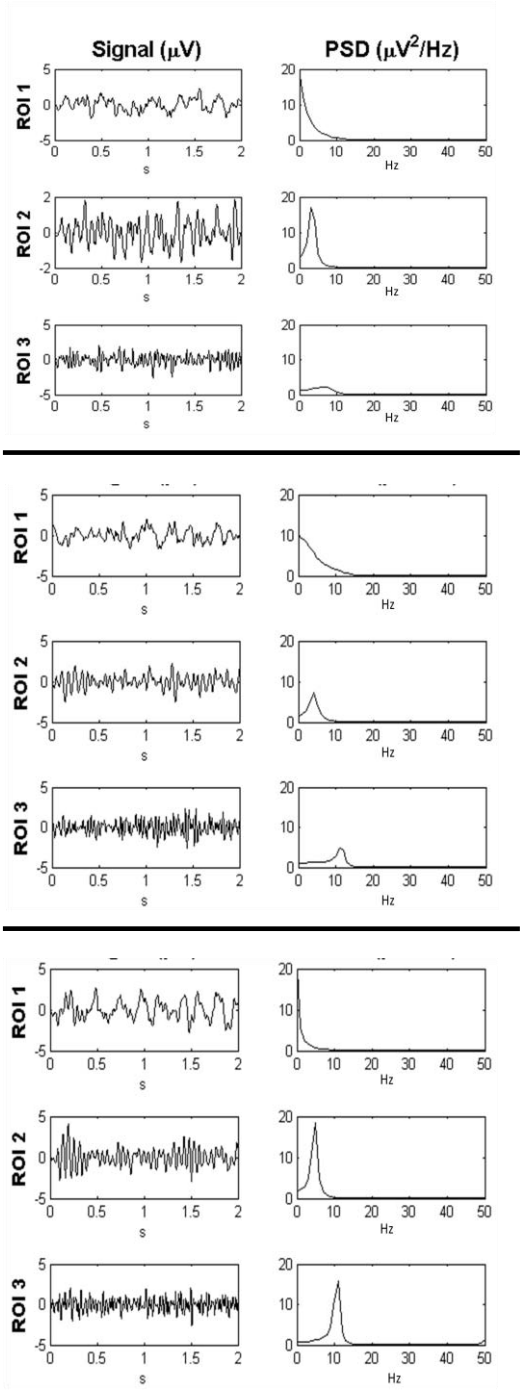

Fig. 3.6 *Basal condition (A=B=C=1). Model predicted EEG signals in time and frequency domain in a representative realization for each dataset for network with feed-back link. In the right side: upper panel r=0.36, middle panel r=0.56, lower panel r=0.66.*

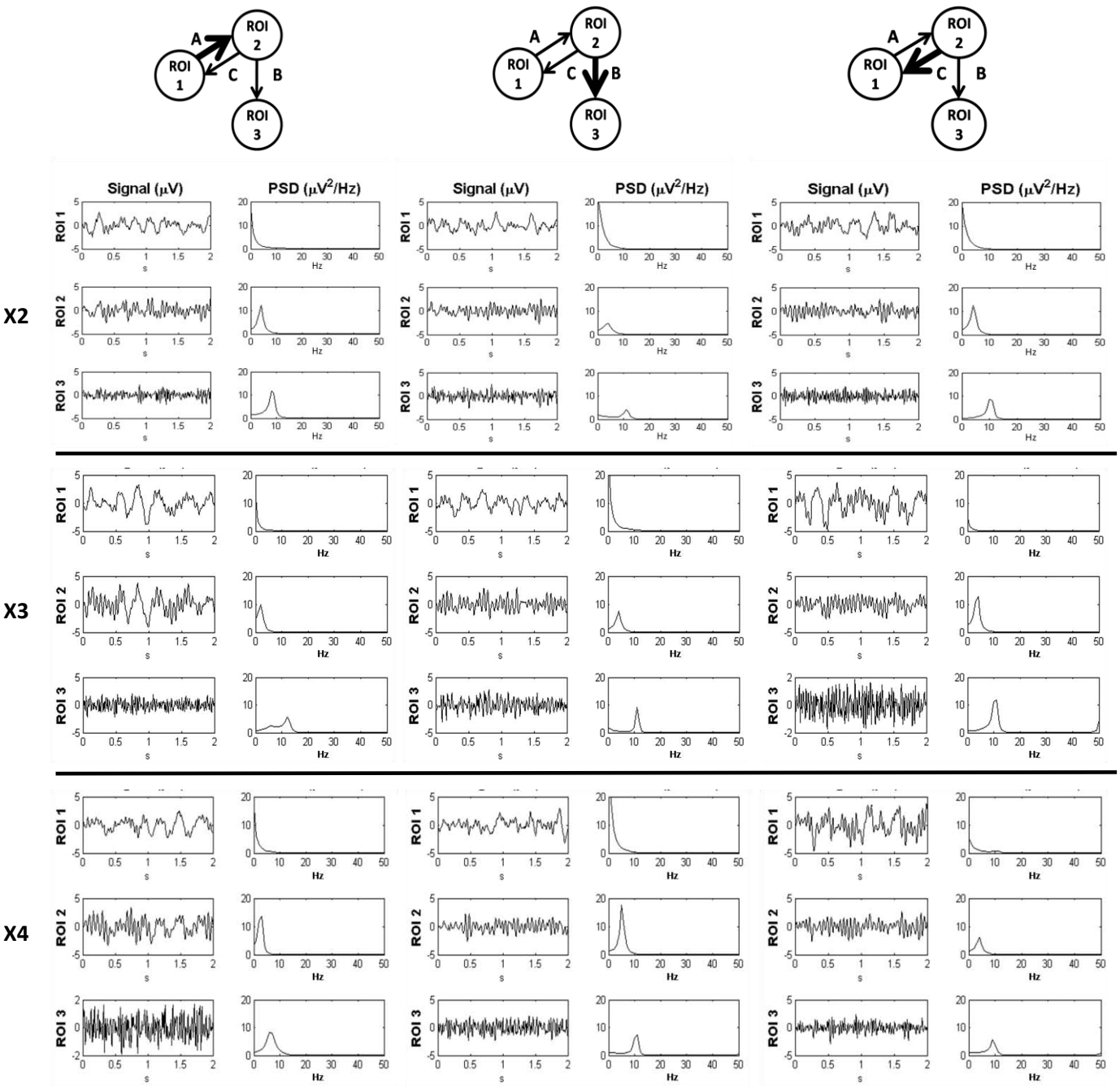

***Fig. 3.7**: Model predicted EEG signals in time and frequency domain in a representative realization of experiments characterized by different values of A, B and C parameters of the network bold link (r=0.56 dataset), for network with feed-back link.*

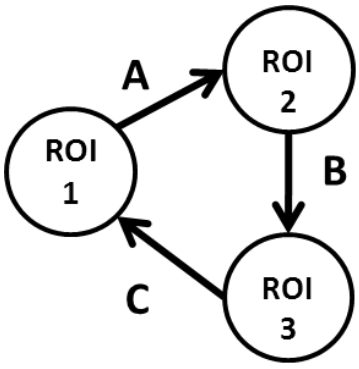

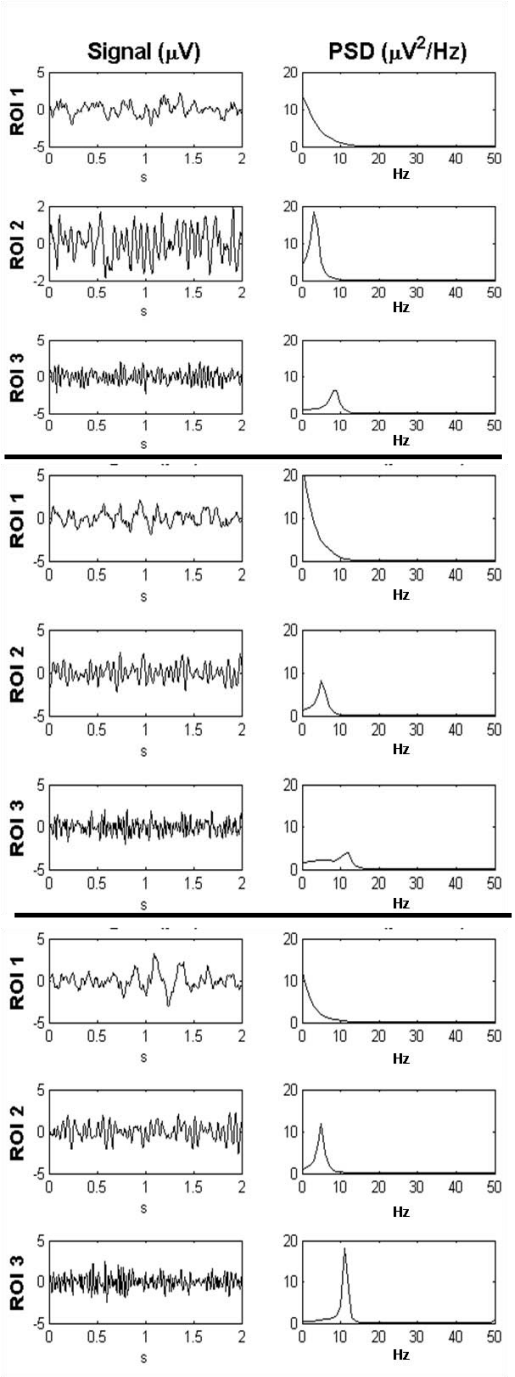

Fig. 3.8: *Basal condition (A=B=C=1). Model predicted EEG signals in time and frequency domain in a representative realization for each dataset for cycle network. In the right side: upper panel r=0.36, middle panel r=0.56, lower panel r=0.66.*

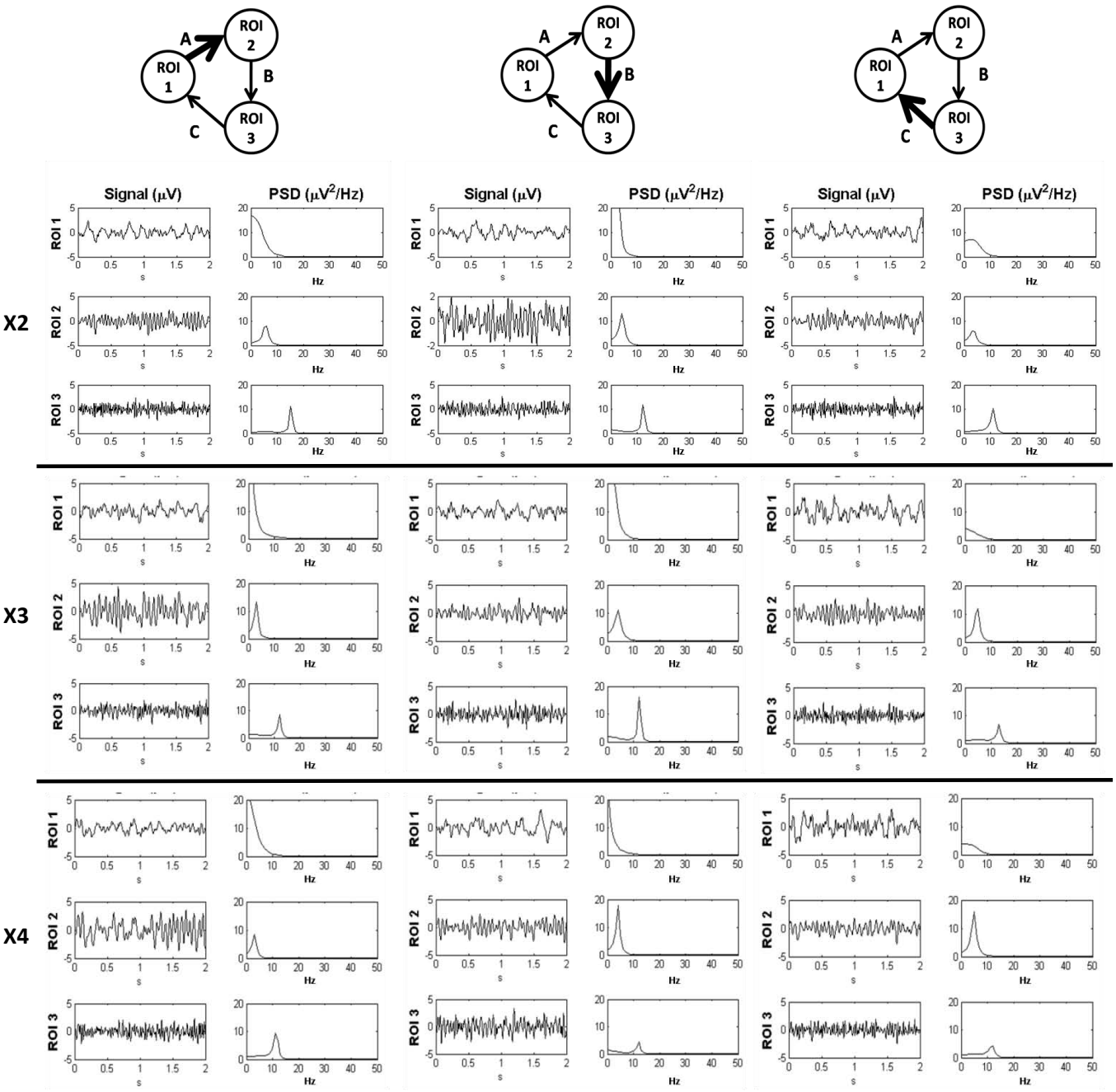

***Fig. 3.9**: Model predicted EEG signals in time and frequency domain in a representative realization of experiments characterized by different values of A, B and C parameters of the network bold link (r=0.56 dataset), for cycle network.*

Chapter 4

Assessment on in silico data: results

This chapter reports connectivity results obtained by means of MVAR and SEM methods for each considered network model.

4.1 Connectivity estimation

A multivariate model is fitted to each simulation data by means of the Matlab package ARFIT, based on stepwise least square algorithm ([22]), selecting the best order with Akaike's information criterion. Then, Granger causality estimation is achieved using the Matlab toolbox GCCA ([23]), with the ordinary-least-squares option, and frequency indices computation is performed by applying the Matlab toolbox implemented in ([24]). Estimation of SEM path coefficients is accomplished by analyzing data in R using its package "sem" ([25]). Obtained results are averaged over the one hundred realizations for each experiment.

4.1.1 Assessment of estimated indices

Topology analysis. Network topology is estimated by means of MVAR indices. GC, DTF and PDC are calculated initially for each realization and subsequently reported results are averaged over the one hundred realizations for each experiment. For each index, statistical tests are performed to evidence significant values.

Comparison with true network gives the amount of false negative and false positive results and statistical power of GC, DTF and PDC is described in terms of sensitivity and specificity, which are defined as follows:

$$Sensitivity = \frac{TP}{TP + FN}$$

$$Specificity = \frac{TN}{FP + TN}$$

where *TP* = true positives, *FN* = false negatives, *TN* = true negatives and *FP* = false positives.

Sensitivity relates to the ability of identifying true connections, while specificity refers to the test ability of identifying absence of connections.

Below, results will be expressed by means of the following scheme:

		Condition		
		True	False	
Outcome	Positive	TP	FP	Type I error (α)
	Negative	FN	TN	Type II error (β)
		Sensitivity	Specificity	

***Table 4.1**: Relationships between actual condition (true or false) and predicted outcomes (positive or negative). False positives (FP) and negatives (FN) provide type I (α) and type II (β) error rate, respectively. Ratio of true positives (TP) to combined TP and FN gives the sensitivity amount, while ratio of true negative (TN) to combined FP and TN furnishes the specificity.*

Strength analysis. Network strength connections are evaluated by considering the output scores of GC, equation (1.6), DTF and PDC AUC integrals, equation (1.22) and SEM path coefficients. Since estimates and true weights are measured with different scales, they are compared using linear regression to verify the existence of a linear relationship between them.

Following paragraphs report overall results throughout all experiments performed on the feed-forward network, on the open-loop network, on the network with feed-back link and on the cycle network, describing both topology and strength estimate.

4.1.2 Topology estimation

For each simulated dataset, consisting of 100 realizations, the number of identified connections, revealed by GC, DTF and PDC, is evaluated. Network topology is inferred by means of statistical test responses, such are F-test for GC and comparison with the null hypothesis threshold for DTF and PDC. For each set of 100 realizations is performed a total number of 3000 tests, since are executed 10 experiments for each considered dataset (there are three datasets).

In Tables 4.2, 4.3 and 4.4 are reported percentages of positive connections indentified between each pair of ROIs for three indices respectively, for feed-forward network. In Tables 4.5, 4.6 and 4.7 are reported percentages of positive connections indentified between each pair of ROIs for three indices respectively, for open-loop network. In Tables 4.8, 4.9 and 4.10 are reported percentages of positive connections indentified between each pair of ROIs for three indices respectively, for network with feed-back link. Finally, in Tables 4.11, 4.12 and 4.13 are reported percentages of positive connections indentified between each pair of ROIs for three indices respectively, for cycle network.

4.1.2.1 Feed-forward network

	Links	DATASET 1 A=B=C=1	DATASET 2 A=B=C=1	DATASET 3 A=B=C=1
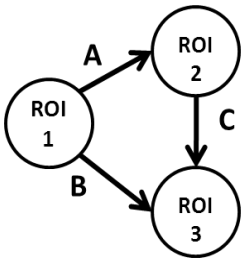	*ROI 1 -> ROI 2*	63	97	98
	ROI 1 -> ROI 3	46	88	98
	ROI 2 -> ROI 3	51	92	100
	ROI 2 -> ROI 1	3	4	5
	ROI 3 -> ROI 1	5	4	9
	ROI 3 -> ROI 2	3	3	1

	Links	DATASET 1			DATASET 2			DATASET 3		
		x2	x3	x4	x2	x3	x4	x2	x3	x4
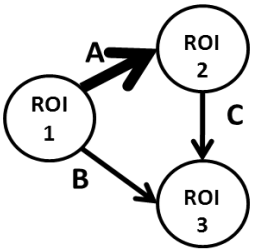	*ROI 1 -> ROI 2*	99	100	100	100	100	100	100	100	100
	ROI 1 -> ROI 3	33	40	14	72	57	51	90	72	67
	ROI 2 -> ROI 3	56	75	73	98	100	100	100	99	100
	ROI 2 -> ROI 1	4	2	4	7	6	9	4	8	12
	ROI 3 -> ROI 1	3	7	4	3	7	2	5	7	6
	ROI 3 -> ROI 2	7	6	1	3	4	9	2	10	10

	Links	DATASET 1			DATASET 2			DATASET 3		
		x2	x3	x4	x2	x3	x4	x2	x3	x4
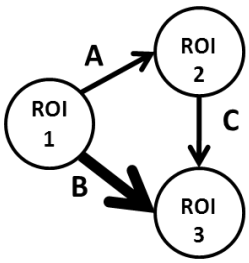	*ROI 1 -> ROI 2*	73	48	43	86	80	74	96	90	84
	ROI 1 -> ROI 3	98	99	100	100	100	100	100	100	100
	ROI 2 -> ROI 3	54	41	50	90	96	95	100	100	99
	ROI 2 -> ROI 1	2	6	3	5	6	4	6	4	2
	ROI 3 -> ROI 1	10	3	2	3	6	7	6	13	11
	ROI 3 -> ROI 2	6	5	3	3	5	10	6	2	1

	Links	DATASET 1			DATASET 2			DATASET 3		
		x2	x3	x4	x2	x3	x4	x2	x3	x4
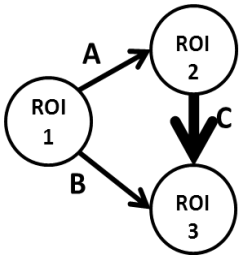	*ROI 1 -> ROI 2*	65	65	79	79	98	97	99	97	98
	ROI 1 -> ROI 3	41	39	46	84	78	85	93	93	96
	ROI 2 -> ROI 3	100	100	100	100	100	100	100	100	100
	ROI 2 -> ROI 1	1	6	6	2	4	4	3	5	6
	ROI 3 -> ROI 1	2	4	4	7	8	7	7	1	4
	ROI 3 -> ROI 2	1	3	7	4	3	6	5	12	5

***Table 4.2**: GC index: percentage of true and false positives in each experiment. Bold arrow in network model indicates the link with true strength multiplied by factors 2, 3 and 4.*

	Links	DATASET 1 A=B=C=1	DATASET 2 A=B=C=1	DATASET 3 A=B=C=1
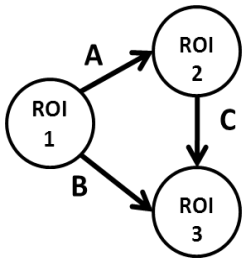	*ROI 1 -> ROI 2*	76	83	82
	ROI 1 -> ROI 3	85	98	97
	ROI 2 -> ROI 3	82	100	100
	ROI 2 -> ROI 1	14	7	6
	ROI 3 -> ROI 1	5	0	0
	ROI 3 -> ROI 2	3	0	0

	Links	DATASET 1			DATASET 2			DATASET 3		
		x2	x3	x4	x2	x3	x4	x2	x3	x4
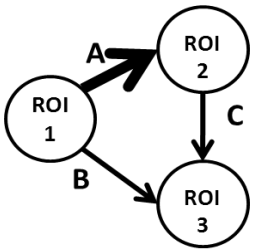	*ROI 1 -> ROI 2*	80	94	92	83	81	92	71	83	72
	ROI 1 -> ROI 3	53	82	58	89	76	80	80	86	76
	ROI 2 -> ROI 3	43	46	35	94	85	73	90	92	74
	ROI 2 -> ROI 1	6	3	3	9	6	3	4	3	5
	ROI 3 -> ROI 1	5	3	3	5	5	3	4	3	5
	ROI 3 -> ROI 2	5	3	3	5	5	3	4	3	5

	Links	DATASET 1			DATASET 2			DATASET 3		
		x2	x3	x4	x2	x3	x4	x2	x3	x4
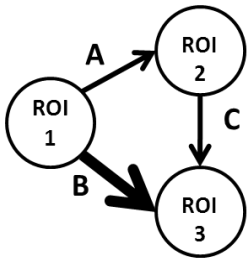	*ROI 1 -> ROI 2*	46	19	29	38	41	43	40	33	43
	ROI 1 -> ROI 3	93	97	99	96	100	99	100	99	100
	ROI 2 -> ROI 3	33	19	18	84	69	60	95	91	66
	ROI 2 -> ROI 1	9	5	6	9	9	9	5	5	3
	ROI 3 -> ROI 1	10	2	6	8	8	8	4	4	3
	ROI 3 -> ROI 2	9	2	5	8	8	8	4	4	3

	Links	DATASET 1			DATASET 2			DATASET 3		
		x2	x3	x4	x2	x3	x4	x2	x3	x4
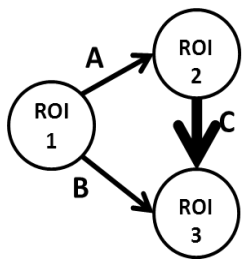	*ROI 1 -> ROI 2*	38	35	43	41	30	44	32	31	36
	ROI 1 -> ROI 3	55	50	58	72	46	60	68	54	57
	ROI 2 -> ROI 3	94	98	100	100	100	100	100	99	100
	ROI 2 -> ROI 1	8	7	3	7	5	6	10	5	5
	ROI 3 -> ROI 1	8	7	3	7	4	4	10	5	5
	ROI 3 -> ROI 2	8	8	3	7	4	4	10	5	5

Table 4.3: *DTF index (AUC): percentage of true and false positives in each experiment. Bold arrow in network model indicates the link with true strength multiplied by factors 2, 3 and 4.*

	Links	DATASET 1 A=B=C=1	DATASET 2 A=B=C=1	DATASET 3 A=B=C=1
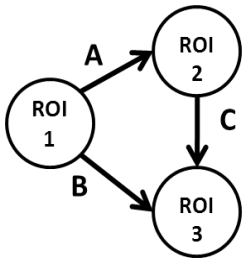	*ROI 1 -> ROI 2*	68	60	25
	ROI 1 -> ROI 3	72	86	84
	ROI 2 -> ROI 3	84	100	100
	ROI 2 -> ROI 1	7	0	0
	ROI 3 -> ROI 1	6	0	0
	ROI 3 -> ROI 2	3	0	0

	Links	DATASET 1			DATASET 2			DATASET 3		
		x2	x3	x4	x2	x3	x4	x2	x3	x4
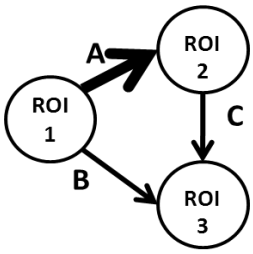	*ROI 1 -> ROI 2*	69	92	90	59	55	62	25	33	35
	ROI 1 -> ROI 3	11	8	4	18	8	3	16	8	6
	ROI 2 -> ROI 3	51	45	45	96	100	95	97	99	96
	ROI 2 -> ROI 1	5	3	3	5	5	3	4	3	5
	ROI 3 -> ROI 1	5	3	3	5	5	3	4	3	5
	ROI 3 -> ROI 2	5	3	3	5	5	3	4	3	5

	Links	DATASET 1			DATASET 2			DATASET 3		
		x2	x3	x4	x2	x3	x4	x2	x3	x4
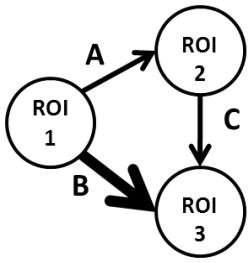	*ROI 1 -> ROI 2*	22	4	8	8	8	8	4	4	3
	ROI 1 -> ROI 3	82	96	98	93	99	99	94	98	100
	ROI 2 -> ROI 3	34	27	30	88	85	69	96	98	85
	ROI 2 -> ROI 1	9	5	6	8	8	8	4	4	3
	ROI 3 -> ROI 1	10	2	6	8	8	8	4	4	3
	ROI 3 -> ROI 2	9	2	5	8	8	8	4	4	3

	Links	DATASET 1			DATASET 2			DATASET 3		
		x2	x3	x4	x2	x3	x4	x2	x3	x4
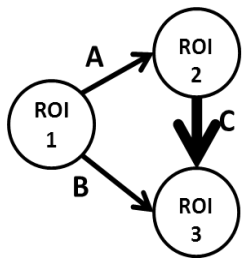	*ROI 1 -> ROI 2*	34	27	42	18	15	27	11	7	16
	ROI 1 -> ROI 3	24	22	14	34	15	13	28	11	19
	ROI 2 -> ROI 3	97	100	100	100	100	100	100	100	100
	ROI 2 -> ROI 1	8	7	3	7	4	4	10	5	5
	ROI 3 -> ROI 1	8	7	3	7	4	4	10	5	5
	ROI 3 -> ROI 2	8	8	3	7	4	4	10	5	5

***Table 4.4**: PDC index (AUC): percentage of true and false positives in each experiment. Bold arrow in network model indicates the link with true strength multiplied by factors 2, 3 and 4.*

4.1.2.2 Open-loop network

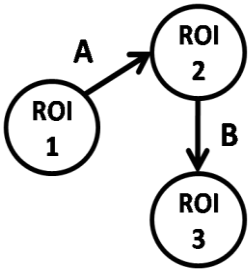

Links	DATASET 1 A=B=1	DATASET 2 A=B=1	DATASET 3 A=B=1
ROI 1 -> ROI 2	72	97	100
ROI 2 -> ROI 3	61	96	100
ROI 1 -> ROI 3	6	5	6
ROI 2 -> ROI 1	2	4	6
ROI 3 -> ROI 1	10	6	5
ROI 3 -> ROI 2	6	3	4

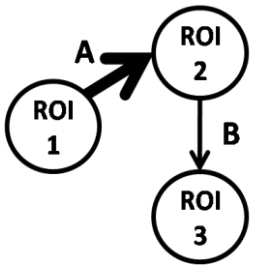

Links	DATASET 1			DATASET 2			DATASET 3		
	x2	x3	x4	x2	x3	x4	x2	x3	x4
ROI 1 -> ROI 2	100	100	100	100	100	100	100	100	100
ROI 2 -> ROI 3	67	68	83	98	98	100	100	100	100
ROI 1 -> ROI 3	4	2	3	3	8	2	7	5	3
ROI 2 -> ROI 1	9	3	1	6	7	5	6	13	9
ROI 3 -> ROI 1	5	2	1	8	0	7	8	5	6
ROI 3 -> ROI 2	4	3	2	4	5	5	2	1	6

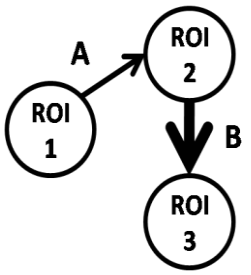

Links	DATASET 1			DATASET 2			DATASET 3		
	x2	x3	x4	x2	x3	x4	x2	x3	x4
ROI 1 -> ROI 2	68	82	67	97	95	97	99	100	99
ROI 2 -> ROI 3	100	100	100	100	100	100	100	100	100
ROI 1 -> ROI 3	1	8	6	1	5	4	4	5	7
ROI 2 -> ROI 1	6	5	1	0	4	5	2	4	6
ROI 3 -> ROI 1	5	3	3	3	6	5	6	6	8
ROI 3 -> ROI 2	2	5	5	4	7	8	5	9	8

***Table 4.5**: GC index: percentage of true and false positives in each experiment. Bold arrow in network model indicates the link with true strength multiplied by factors 2, 3 and 4.*

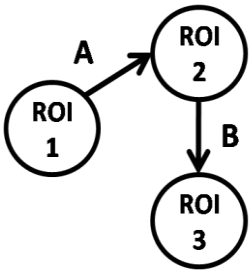

Links	DATASET 1 A=B=1	DATASET 2 A=B=1	DATASET 3 A=B=1
ROI 1 -> ROI 2	48	42	33
ROI 2 -> ROI 3	40	93	98
ROI 1 -> ROI 3	8	6	8
ROI 2 -> ROI 1	6	2	5
ROI 3 -> ROI 1	6	1	5
ROI 3 -> ROI 2	5	1	5

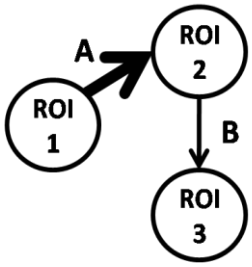

Links	DATASET 1			DATASET 2			DATASET 3		
	x2	x3	x4	x2	x3	x4	x2	x3	x4
ROI 1 -> ROI 2	85	87	94	86	89	89	74	85	76
ROI 2 -> ROI 3	43	41	34	91	81	69	91	76	59
ROI 1 -> ROI 3	6	14	17	25	26	39	29	42	31
ROI 2 -> ROI 1	3	3	5	7	8	9	7	7	4
ROI 3 -> ROI 1	2	3	4	6	6	9	7	6	4
ROI 3 -> ROI 2	2	3	4	6	6	9	7	6	4

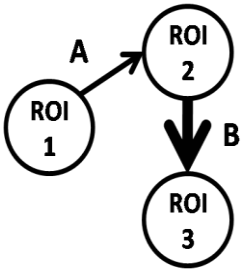

Links	DATASET 1			DATASET 2			DATASET 3		
	x2	x3	x4	x2	x3	x4	x2	x3	x4
ROI 1 -> ROI 2	29	43	40	43	48	34	29	26	40
ROI 2 -> ROI 3	94	99	100	100	100	100	99	98	100
ROI 1 -> ROI 3	9	20	14	12	22	20	15	15	30
ROI 2 -> ROI 1	2	3	3	5	6	6	6	4	9
ROI 3 -> ROI 1	2	4	4	5	6	6	6	3	9
ROI 3 -> ROI 2	3	3	3	5	6	6	6	3	9

Table 4.6: *DTF index (AUC): percentage of true and false positives in each experiment. Bold arrow in network model indicates the link with true strength multiplied by factors 2, 3 and 4.*

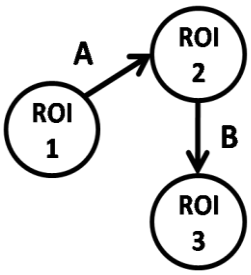

Links	DATASET 1 A=B=1	DATASET 2 A=B=1	DATASET 3 A=B=1
ROI 1 -> ROI 2	44	42	28
ROI 2 -> ROI 3	42	93	99
ROI 1 -> ROI 3	5	1	5
ROI 2 -> ROI 1	5	1	5
ROI 3 -> ROI 1	6	1	5
ROI 3 -> ROI 2	5	1	5

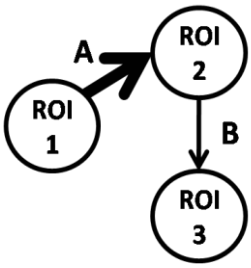

Links	DATASET 1			DATASET 2			DATASET 3		
	x2	x3	x4	x2	x3	x4	x2	x3	x4
ROI 1 -> ROI 2	84	88	94	86	88	89	73	84	70
ROI 2 -> ROI 3	47	53	49	98	98	92	98	100	100
ROI 1 -> ROI 3	2	3	4	6	6	9	7	6	4
ROI 2 -> ROI 1	4	3	4	6	6	9	7	6	4
ROI 3 -> ROI 1	2	3	4	6	6	9	7	6	4
ROI 3 -> ROI 2	2	3	4	6	6	9	7	6	4

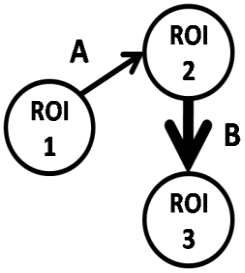

Links	DATASET 1			DATASET 2			DATASET 3		
	x2	x3	x4	x2	x3	x4	x2	x3	x4
ROI 1 -> ROI 2	29	44	42	42	47	34	28	26	37
ROI 2 -> ROI 3	96	99	100	100	100	100	100	100	100
ROI 1 -> ROI 3	2	5	3	5	6	6	6	3	9
ROI 2 -> ROI 1	2	3	3	5	6	6	6	3	9
ROI 3 -> ROI 1	2	4	4	5	6	6	6	3	9
ROI 3 -> ROI 2	3	3	4	5	6	6	6	3	9

***Table 4.7**: PDC index (AUC): percentage of true and false positives in each experiment. Bold arrow in network model indicates the link with true strength multiplied by factors 2, 3 and 4.*

4.1.2.3 Network with feed-back link

	Links	DATASET 1 A=B=1	DATASET 2 A=B=1	DATASET 3 A=B=1
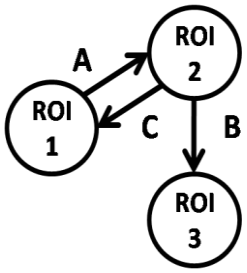	*ROI 1 -> ROI 2*	78	98	100
	ROI 2 -> ROI 3	52	98	100
	ROI 2 -> ROI 1	87	100	100
	ROI 1 -> ROI 3	2	4	2
	ROI 3 -> ROI 1	2	4	7
	ROI 3 -> ROI 2	7	2	4

	Links	DATASET 1			DATASET 2			DATASET 3		
		x2	x3	x4	x2	x3	x4	x2	x3	x4
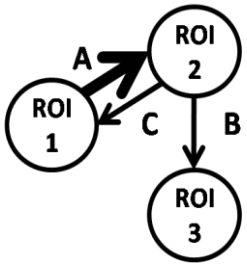	*ROI 1 -> ROI 2*	100	100	100	100	100	100	100	100	100
	ROI 2 -> ROI 3	73	65	67	98	98	100	99	100	96
	ROI 2 -> ROI 1	91	92	96	100	100	100	100	100	100
	ROI 1 -> ROI 3	5	4	5	4	11	14	6	22	48
	ROI 3 -> ROI 1	5	5	9	6	10	7	3	9	10
	ROI 3 -> ROI 2	6	0	3	5	5	7	4	9	6

	Links	DATASET 1			DATASET 2			DATASET 3		
		x2	x3	x4	x2	x3	x4	x2	x3	x4
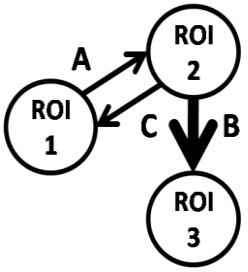	*ROI 1 -> ROI 2*	66	57	70	100	100	100	100	100	100
	ROI 2 -> ROI 3	100	100	100	100	100	100	100	100	100
	ROI 2 -> ROI 1	89	72	64	100	100	98	100	100	100
	ROI 1 -> ROI 3	4	5	6	9	5	10	9	15	13
	ROI 3 -> ROI 1	6	1	1	5	6	4	0	3	10
	ROI 3 -> ROI 2	4	3	2	4	2	1	6	2	10

	Links	DATASET 1			DATASET 2			DATASET 3		
		x2	x3	x4	x2	x3	x4	x2	x3	x4
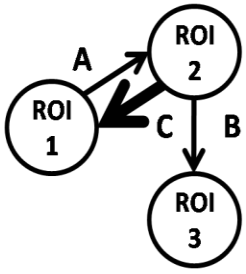	*ROI 1 -> ROI 2*	79	95	96	100	100	100	100	100	100
	ROI 2 -> ROI 3	41	34	37	89	80	53	96	88	67
	ROI 2 -> ROI 1	100	100	100	100	100	100	100	100	100
	ROI 1 -> ROI 3	0	8	3	4	5	2	5	10	8
	ROI 3 -> ROI 1	5	5	2	3	4	2	3	7	7
	ROI 3 -> ROI 2	2	5	6	4	2	5	3	5	4

***Table 4.8**: GC index: percentage of true and false positives in each experiment. Bold arrow in network model indicates the link with true strength multiplied by factors 2, 3 and 4.*

	Links	DATASET 1 A=B=1	DATASET 2 A=B=1	DATASET 3 A=B=1
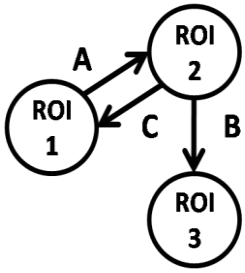	*ROI 1 -> ROI 2*	32	35	22
	ROI 2 -> ROI 3	44	90	94
	ROI 2 -> ROI 1	53	83	75
	ROI 1 -> ROI 3	4	16	7
	ROI 3 -> ROI 1	2	9	6
	ROI 3 -> ROI 2	2	9	6

	Links	DATASET 1			DATASET 2			DATASET 3		
		x2	x3	x4	x2	x3	x4	x2	x3	x4
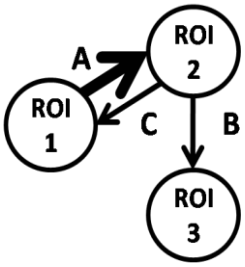	*ROI 1 -> ROI 2*	87	99	90	74	76	56	56	69	67
	ROI 2 -> ROI 3	45	33	32	75	36	11	46	8	7
	ROI 2 -> ROI 1	35	39	39	76	49	24	55	19	10
	ROI 1 -> ROI 3	12	17	28	16	18	9	12	8	7
	ROI 3 -> ROI 1	6	4	3	3	3	2	7	6	7
	ROI 3 -> ROI 2	6	4	3	3	3	2	7	6	7

	Links	DATASET 1			DATASET 2			DATASET 3		
		x2	x3	x4	x2	x3	x4	x2	x3	x4
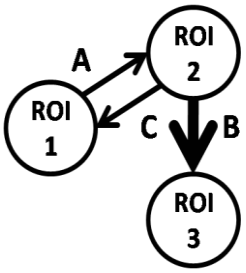	*ROI 1 -> ROI 2*	32	25	40	30	27	43	20	30	38
	ROI 2 -> ROI 3	92	100	100	100	100	100	96	98	99
	ROI 2 -> ROI 1	43	44	41	70	71	78	79	81	90
	ROI 1 -> ROI 3	7	6	13	8	11	17	4	8	18
	ROI 3 -> ROI 1	7	2	4	6	8	7	3	6	8
	ROI 3 -> ROI 2	6	2	4	6	8	7	3	6	8

	Links	DATASET 1			DATASET 2			DATASET 3		
		x2	x3	x4	x2	x3	x4	x2	x3	x4
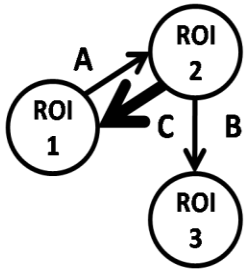	*ROI 1 -> ROI 2*	27	33	27	36	34	21	23	7	19
	ROI 2 -> ROI 3	28	14	14	81	69	35	69	46	21
	ROI 2 -> ROI 1	78	70	63	93	83	78	87	88	86
	ROI 1 -> ROI 3	6	4	7	9	6	7	7	5	10
	ROI 3 -> ROI 1	6	2	6	6	3	5	6	4	9
	ROI 3 -> ROI 2	7	2	7	6	3	5	6	4	9

Table 4.9: *DTF index (AUC): percentage of true and false positives in each experiment. Bold arrow in network model indicates the link with true strength multiplied by factors 2, 3 and 4.*

	Links	DATASET 1 A=B=1	DATASET 2 A=B=1	DATASET 3 A=B=1
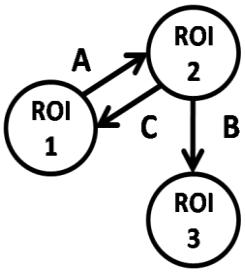	*ROI 1 -> ROI 2*	34	41	25
	ROI 2 -> ROI 3	33	62	38
	ROI 2 -> ROI 1	36	29	8
	ROI 1 -> ROI 3	3	9	6
	ROI 3 -> ROI 1	2	9	6
	ROI 3 -> ROI 2	2	9	6

	Links	DATASET 1			DATASET 2			DATASET 3		
		x2	x3	x4	x2	x3	x4	x2	x3	x4
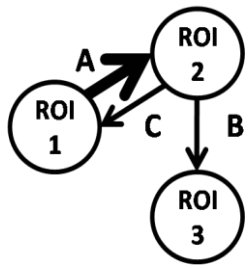	*ROI 1 -> ROI 2*	89	97	91	70	62	26	50	22	10
	ROI 2 -> ROI 3	36	32	22	48	29	14	27	13	7
	ROI 2 -> ROI 1	22	23	21	14	4	2	7	6	7
	ROI 1 -> ROI 3	6	4	3	3	3	2	7	6	7
	ROI 3 -> ROI 1	6	4	3	3	3	2	7	6	7
	ROI 3 -> ROI 2	6	4	3	3	3	2	7	6	7

	Links	DATASET 1			DATASET 2			DATASET 3		
		x2	x3	x4	x2	x3	x4	x2	x3	x4
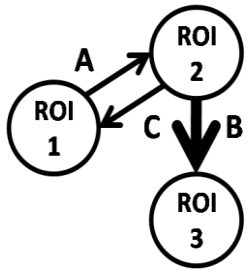	*ROI 1 -> ROI 2*	30	22	41	29	29	51	22	26	41
	ROI 2 -> ROI 3	89	100	100	96	100	100	84	100	99
	ROI 2 -> ROI 1	17	5	5	7	8	7	3	6	8
	ROI 1 -> ROI 3	6	2	4	6	8	7	3	6	8
	ROI 3 -> ROI 1	7	2	4	6	8	7	3	6	8
	ROI 3 -> ROI 2	6	2	4	6	8	7	3	6	8

	Links	DATASET 1			DATASET 2			DATASET 3		
		x2	x3	x4	x2	x3	x4	x2	x3	x4
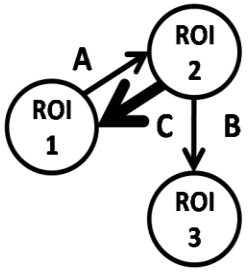	*ROI 1 -> ROI 2*	31	32	27	32	33	25	23	9	10
	ROI 2 -> ROI 3	10	8	6	13	8	5	9	4	9
	ROI 2 -> ROI 1	69	62	50	38	29	15	12	4	11
	ROI 1 -> ROI 3	6	2	6	6	3	5	6	4	9
	ROI 3 -> ROI 1	6	2	6	6	3	5	6	4	9
	ROI 3 -> ROI 2	7	2	6	6	3	5	6	4	9

Table 4.10: *PDC index (AUC): percentage of true and false positives in each experiment. Bold arrow in network model indicates the link with true strength multiplied by factors 2, 3 and 4.*

4.1.2.4 Cycle network

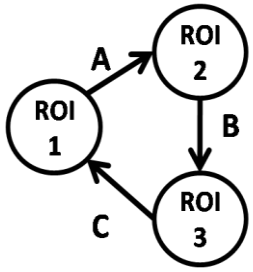

Links	DATASET 1 A=B=1	DATASET 2 A=B=1	DATASET 3 A=B=1
ROI 1 -> ROI 2	78	95	99
ROI 2 -> ROI 3	68	97	100
ROI 3 -> ROI 1	91	99	100
ROI 1 -> ROI 3	6	7	5
ROI 3 -> ROI 2	5	3	4
ROI 2 -> ROI 1	0	5	2

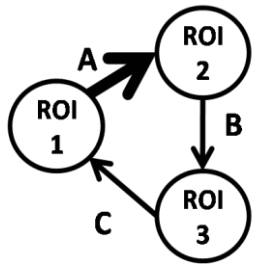

Links	DATASET 1			DATASET 2			DATASET 3		
	x2	x3	x4	x2	x3	x4	x2	x3	x4
ROI 1 -> ROI 2	100	100	100	100	100	100	100	100	100
ROI 2 -> ROI 3	77	77	73	97	98	100	100	100	100
ROI 3 -> ROI 1	86	95	91	99	100	100	100	100	100
ROI 1 -> ROI 3	6	7	5	6	2	6	6	8	16
ROI 3 -> ROI 2	3	4	4	6	6	3	2	3	7
ROI 2 -> ROI 1	7	4	5	7	3	4	5	13	23

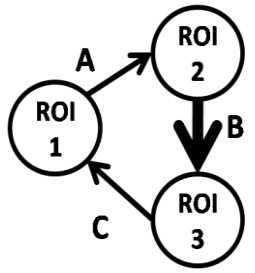

Links	DATASET 1			DATASET 2			DATASET 3		
	x2	x3	x4	x2	x3	x4	x2	x3	x4
ROI 1 -> ROI 2	62	73	69	97	97	99	100	100	100
ROI 2 -> ROI 3	100	100	100	100	100	100	100	100	100
ROI 3 -> ROI 1	89	93	94	100	100	100	100	100	100
ROI 1 -> ROI 3	7	5	3	7	8	10	7	14	16
ROI 3 -> ROI 2	3	1	3	5	7	4	5	3	11
ROI 2 -> ROI 1	3	2	5	5	5	6	4	9	5

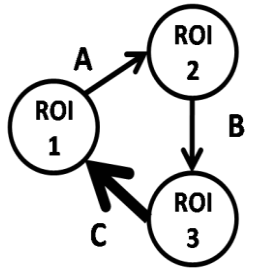

Links	DATASET 1			DATASET 2			DATASET 3		
	x2	x3	x4	x2	x3	x4	x2	x3	x4
ROI 1 -> ROI 2	87	84	97	99	99	100	100	100	100
ROI 2 -> ROI 3	67	64	68	99	99	100	100	100	100
ROI 3 -> ROI 1	100	100	100	100	100	100	100	100	100
ROI 1 -> ROI 3	16	21	32	8	9	7	6	15	21
ROI 3 -> ROI 2	6	7	5	2	1	4	4	3	9
ROI 2 -> ROI 1	3	6	3	3	7	6	7	10	16

Table 4.11*: GC index: percentage of true and false positives in each experiment. Bold arrow in network model indicates the link with true strength multiplied by factors 2, 3 and 4.*

	Links	DATASET 1 A=B=1	DATASET 2 A=B=1	DATASET 3 A=B=1
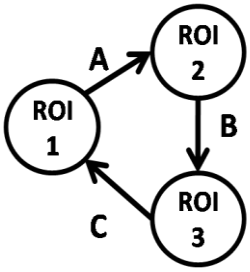	*ROI 1 -> ROI 2*	41	43	26
	ROI 2 -> ROI 3	48	93	92
	ROI 3 -> ROI 1	41	21	3
	ROI 1 -> ROI 3	3	10	3
	ROI 3 -> ROI 2	4	8	2
	ROI 2 -> ROI 1	3	8	2

	Links	DATASET 1			DATASET 2			DATASET 3		
		x2	x3	x4	x2	x3	x4	x2	x3	x4
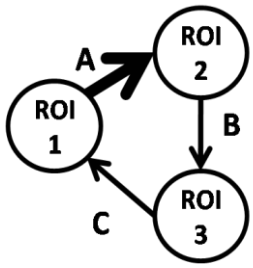	*ROI 1 -> ROI 2*	90	90	86	67	76	67	68	60	60
	ROI 2 -> ROI 3	43	40	28	85	67	54	84	56	37
	ROI 3 -> ROI 1	22	22	11	9	5	7	10	5	10
	ROI 1 -> ROI 3	9	10	11	13	17	22	17	23	25
	ROI 3 -> ROI 2	3	4	6	5	4	6	9	4	10
	ROI 2 -> ROI 1	3	3	6	6	4	6	9	4	10

	Links	DATASET 1			DATASET 2			DATASET 3		
		x2	x3	x4	x2	x3	x4	x2	x3	x4
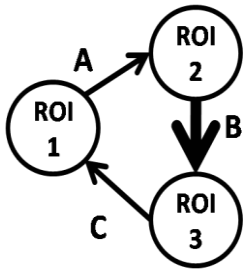	*ROI 1 -> ROI 2*	24	28	26	37	22	20	20	24	17
	ROI 2 -> ROI 3	93	97	100	98	99	100	99	99	100
	ROI 3 -> ROI 1	21	27	29	10	8	6	9	10	2
	ROI 1 -> ROI 3	4	6	6	13	6	7	10	11	7
	ROI 3 -> ROI 2	3	3	4	6	3	3	9	9	2
	ROI 2 -> ROI 1	8	11	23	10	23	59	10	32	69

	Links	DATASET 1			DATASET 2			DATASET 3		
		x2	x3	x4	x2	x3	x4	x2	x3	x4
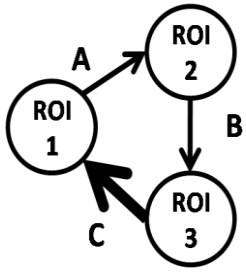	*ROI 1 -> ROI 2*	46	43	33	26	23	17	23	12	18
	ROI 2 -> ROI 3	35	34	22	80	71	55	83	82	65
	ROI 3 -> ROI 1	83	95	98	38	59	58	20	31	36
	ROI 1 -> ROI 3	9	13	14	2	5	2	5	5	6
	ROI 3 -> ROI 2	4	9	6	1	5	2	4	4	6
	ROI 2 -> ROI 1	4	8	6	4	6	4	6	8	12

Table 4.12: *DTF index (AUC): percentage of true and false positives in each experiment. Bold arrow in network model indicates the link with true strength multiplied by factors 2, 3 and 4.*

	Links	DATASET 1 A=B=1	DATASET 2 A=B=1	DATASET 3 A=B=1
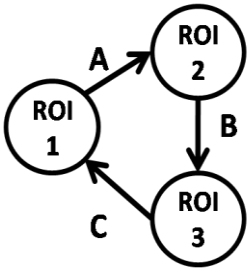	*ROI 1 -> ROI 2*	45	41	22
	ROI 2 -> ROI 3	51	93	96
	ROI 3 -> ROI 1	40	21	4
	ROI 1 -> ROI 3	4	9	2
	ROI 3 -> ROI 2	3	8	2
	ROI 2 -> ROI 1	3	8	2

	Links	DATASET 1			DATASET 2			DATASET 3		
		x2	x3	x4	x2	x3	x4	x2	x3	x4
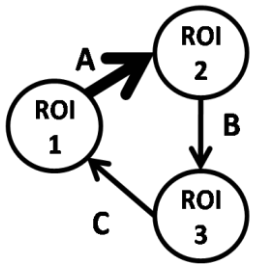	*ROI 1 -> ROI 2*	93	92	92	75	80	67	66	49	42
	ROI 2 -> ROI 3	52	48	47	92	93	95	99	98	95
	ROI 3 -> ROI 1	26	21	11	11	9	7	11	5	10
	ROI 1 -> ROI 3	3	3	6	5	4	6	9	4	10
	ROI 3 -> ROI 2	3	3	6	5	4	6	9	4	10
	ROI 2 -> ROI 1	3	3	7	5	4	6	9	4	10

	Links	DATASET 1			DATASET 2			DATASET 3		
		x2	x3	x4	x2	x3	x4	x2	x3	x4
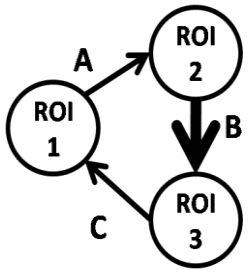	*ROI 1 -> ROI 2*	23	33	26	37	24	29	18	22	16
	ROI 2 -> ROI 3	92	100	100	99	99	100	100	100	100
	ROI 3 -> ROI 1	24	32	31	12	8	10	9	10	3
	ROI 1 -> ROI 3	3	3	4	6	3	3	9	9	2
	ROI 3 -> ROI 2	3	3	4	6	3	3	9	9	2
	ROI 2 -> ROI 1	3	3	4	6	3	3	9	9	2

	Links	DATASET 1			DATASET 2			DATASET 3		
		x2	x3	x4	x2	x3	x4	x2	x3	x4
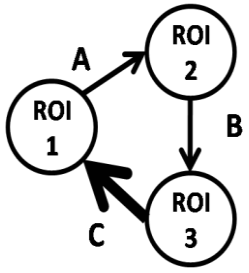	*ROI 1 -> ROI 2*	49	53	46	29	27	24	21	14	19
	ROI 2 -> ROI 3	44	35	25	86	86	77	91	96	91
	ROI 3 -> ROI 1	85	95	99	46	61	67	23	42	46
	ROI 1 -> ROI 3	9	11	13	1	5	2	4	5	6
	ROI 3 -> ROI 2	4	8	5	1	5	2	4	4	6
	ROI 2 -> ROI 1	4	8	5	1	5	2	4	4	6

Table 4.13: *PDC index (AUC): percentage of true and false positives in each experiment. Bold arrow in network model indicates the link with true strength multiplied by factors 2, 3 and 4.*

Observing the tables above, it is interesting to note that as regard GC index, in all networks percentage of identified connections is larger in links where the connection is true. This observation is true again as regard DTF and PDC indices for open-loop network, while for the other three networks sometimes it occurs that percentage of identified true connections is similar (or sometimes smaller) to percentage of identified false connections.

Another observation that can be done is the following: in each condition the strongest link clearly emerged, since it generally has the highest score. This is always true for GC index for all networks, while as regard DTF and PDC it does not always occur. Finally, for all networks and for all indices, a significant difference appears within experiments, where false negatives percentage relative to predominant links is smaller than false negatives percentage of those realizations characterized by equal connection strengths (for example in Table 4.2 we note that percentage of false negatives in basal condition for ROI 1 → ROI 2 is 37% while when A increases percentage of false negatives is 1% or 0%. This occurs also for the other significant connections).

Specificity and sensitivity are summarized in Tables 4.14, 4.15, 4.16 and 4.17. For all networks analyzed in this work, value of specificity is always greater than 90% for all indices, while value of sensitivity is greater than 90% only for GC index. Great value of specificity for each index respect to sensitivity suggests the methods are highly conservative. Globally, probability of error I is around 6% and there are high false negative rates for DTF and PDC indices.

(a) GC outcomes

	Positive Condition	Negative Condition		
Positive Outcomes	7574	456	**False Positive Rate (α)**	5%
Negative Outcomes	1426	8544	**False Negative Rate (β)**	16%
	Sensitivity	**Specificity**		
	84%	95%		

(b) DTF outcomes

	Positive Condition	Negative Condition		
Positive Outcomes	6354	476	**False Positive Rate (α)**	5%
Negative Outcomes	2646	8524	**False Negative Rate (β)**	29%
	Sensitivity	**Specificity**		
	71%	95%		

(c) PDC outcomes

	Positive Condition	Negative Condition		
Positive Outcomes	4819	443	**False Positive Rate (α)**	5%
Negative Outcomes	4181	8557	**False Negative Rate (β)**	46%
	Sensitivity	**Specificity**		
	54%	95%		

Table 4.14: *Statistical measures of the performances of GC (a), DTF (b) and PDC (c) throughout the experimental conditions, for feed-forward network.*

(a) GC outcomes

	Positive Condition	Negative Condition		
Positive Outcomes	3944	405	**False Positive Rate (α)**	5%
Negative Outcomes	256	7995	**False Negative Rate (β)**	6%
	Sensitivity	**Specificity**		
	94%	95%		

(b) DTF outcomes

	Positive Condition	Negative Condition		
Positive Outcomes	2926	724	**False Positive Rate (α)**	9%
Negative Outcomes	1274	7676	**False Negative Rate (β)**	30%
	Sensitivity	**Specificity**		
	70%	91%		

(c) PDC outcomes

	Positive Condition	Negative Condition		
Positive Outcomes	3063	413	**False Positive Rate (α)**	5%
Negative Outcomes	1137	7987	**False Negative Rate (β)**	27%
	Sensitivity	**Specificity**		
	73%	95%		

Table 4.15*: Statistical measures of the performances of GC (a), DTF (b) and PDC (c) throughout the experimental conditions, for open-loop network.*

(a) GC outcomes

	Positive Condition	Negative Condition		
Positive Outcomes	8259	527	**False Positive Rate (α)**	6%
Negative Outcomes	741	8473	**False Negative Rate (β)**	8%
	Sensitivity	**Specificity**		
	92%	94%		

(b) DTF outcomes

	Positive Condition	Negative Condition		
Positive Outcomes	4938	620	**False Positive Rate (α)**	7%
Negative Outcomes	4062	8380	**False Negative Rate (β)**	45%
	Sensitivity	**Specificity**		
	55%	93%		

(c) PDC outcomes

	Positive Condition	Negative Condition		
Positive Outcomes	2966	468	**False Positive Rate (α)**	5%
Negative Outcomes	6034	8532	**False Negative Rate (β)**	67%
	Sensitivity	**Specificity**		
	33%	95%		

***Table 4.16**: Statistical measures of the performances of GC (a), DTF (b) and PDC (c) throughout the experimental conditions, for network with feed-back link.*

(a) GC outcomes

	Positive Condition	Negative Condition		
Positive Outcomes	8556	608	**False Positive Rate (α)**	7%
Negative Outcomes	444	8392	**False Negative Rate (β)**	5%
	Sensitivity	**Specificity**		
	95%	93%		

(b) DTF outcomes

	Positive Condition	Negative Condition		
Positive Outcomes	4178	809	**False Positive Rate (α)**	9%
Negative Outcomes	4822	8191	**False Negative Rate (β)**	53%
	Sensitivity	**Specificity**		
	46%	91%		

(c) PDC outcomes

	Positive Condition	Negative Condition		
Positive Outcomes	4633	452	**False Positive Rate (α)**	5%
Negative Outcomes	4367	8548	**False Negative Rate (β)**	48%
	Sensitivity	**Specificity**		
	51%	95%		

***Table 4.17**: Statistical measures of the performances of GC (a), DTF (b) and PDC (c) throughout the experimental conditions, for cycle network.*

4.1.3 Strength estimation

Below, for all experiments by each index are reported estimates of strength connections for all networks analyzed in this work. As regard GC and SEM index, estimates of strength connections are obtained calculating average of strength estimates, while as regard DTF and PDC index estimates of strength connections are obtained via AUC of the main function in the frequency domain. Concerning this, in Figs. 4.1, 4.2 and 4.3, are shown, as an example, DTF and PDC index as function of frequency for three networks; in this figures, for simplicity, are considered only basal condition (A=B=C=1) and the experiments with A=C=1 and B=2.

Since estimates and true weights are measured with different scales, estimates are analyzed in terms of their correlation with true value, so as to assess the ability of each index to reproduce strength proportionality within networks.

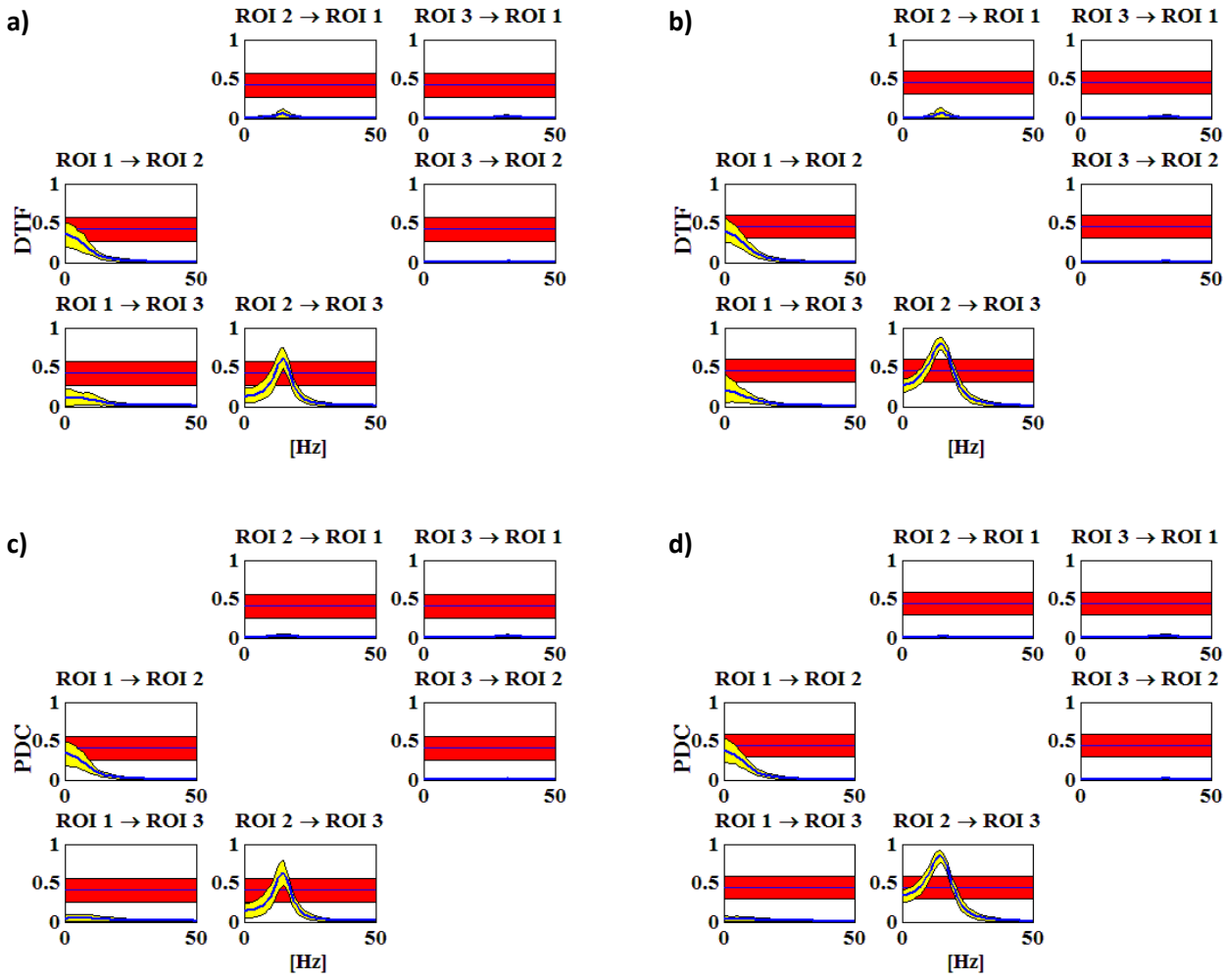

Fig. 4.1*: DTF and PDC index as function of frequency for open-loop network. Panels a) and c) show basal condition (A=B=1), while the other two panels, b) and d), are relative to the experiment with A=1 and B=2. Yellow and red bands represent 100 realizations and their threshold respectively, while blue line within yellow and red bands are their mean functions.*

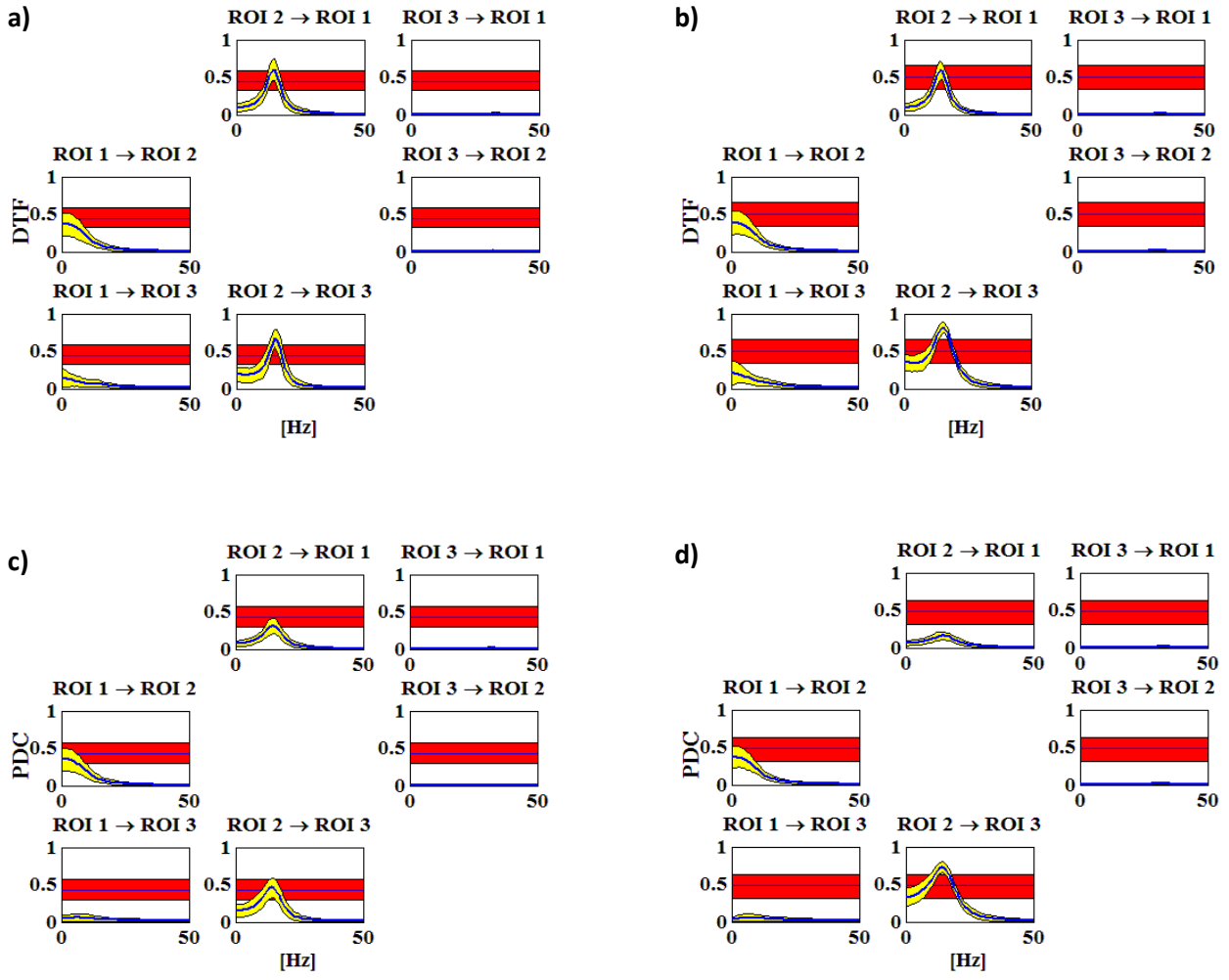

***Fig. 4.2**: DTF and PDC index as function of frequency for network with feed-back link. Panels a) and c) show basal condition (A=B=C=1), while the other two panels, b) and d), are relative to the experiment with A=C=1 and B=2. Yellow and red bands represent 100 realizations and their threshold respectively, while blue line within yellow and red bands are their mean functions.*

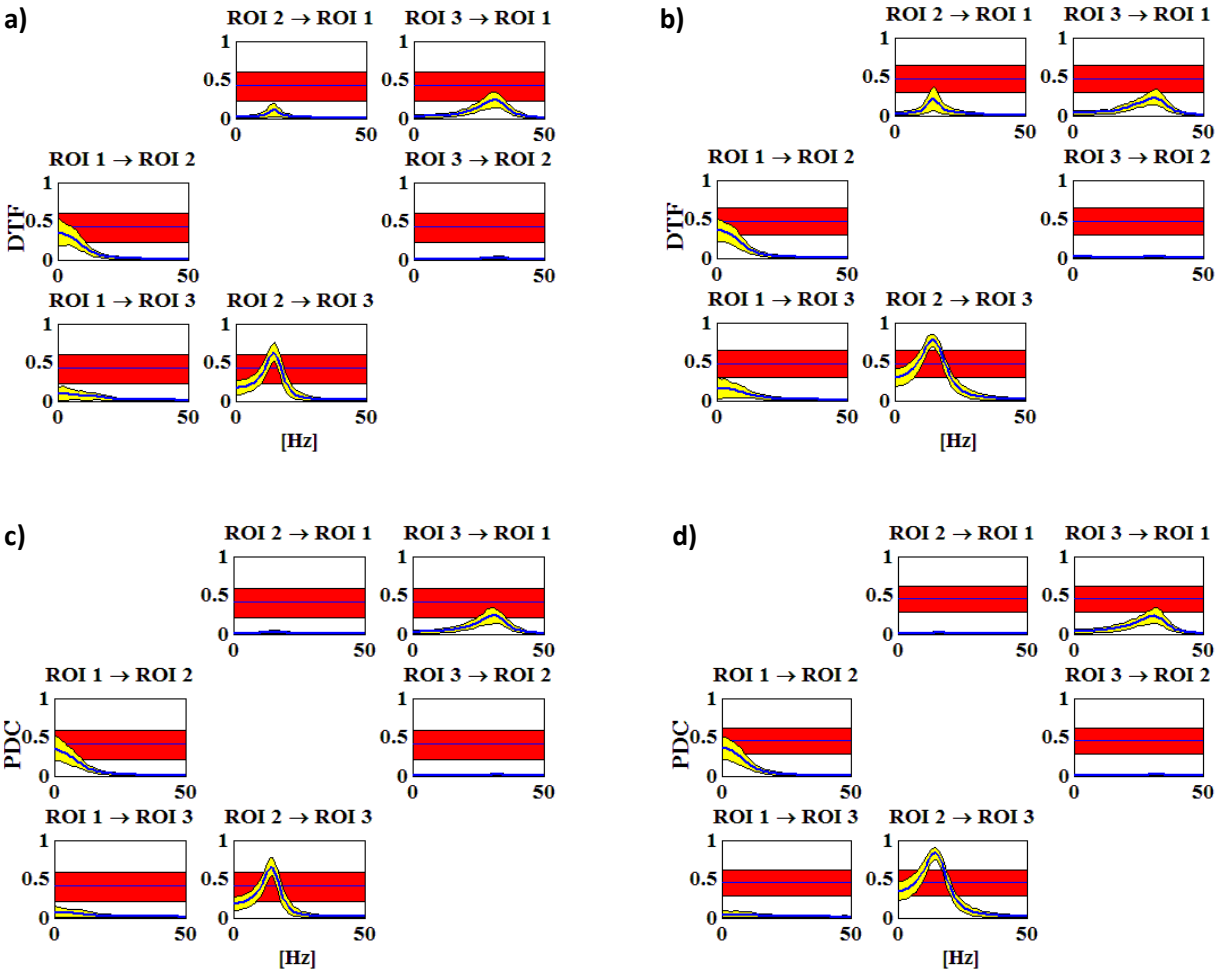

Fig. 4.3*: DTF and PDC index as function of frequency for cycle network. Panels a) and c) show basal condition (A=B=C=1), while the other two panels, b) and d), are relative to the experiment with A=C=1 and B=2. Yellow and red bands represent 100 realizations and their threshold respectively, while blue line within yellow and red bands are their mean functions.*

In Tables 4.18, 4.19, 4.20 and 4.21 are reported estimates of strength true connections for all experiments by each index (GC, DTF, PDC and SEM) for feed-forward network. In Tables 4.22, 4.23, 4.24 and 4.25 are reported estimates of strength true connections for all experiments by each index (GC, DTF, PDC and SEM) for open-loop network. In Tables 4.26, 4.27, 4.28 are reported estimates of strength true connections for all experiments by each index (GC, DTF, PDC) for network with feed-back link. In this case SEM method cannot be applied because it cannot define a model for this network. In Tables 4.29, 4.30, 4.31 and 4.32 are reported estimates of strength true connections for all experiments by each index (GC, DTF, PDC and SEM) for cycle network.

4.1.3.1 Feed-forward network

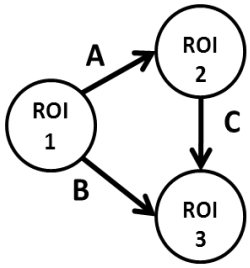

Links	DATASET 1 A=B=C=1	DATASET 2 A=B=C=1	DATASET 3 A=B=C=1
ROI 1 -> ROI 2	0,03	0,07	0,08
ROI 1 -> ROI 3	0,02	0,05	0,06
ROI 2 -> ROI 3	0,03	0,07	0,09

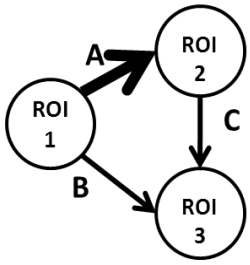

Links	DATASET 1			DATASET 2			DATASET 3		
	x2	x3	x4	x2	x3	x4	x2	x3	x4
ROI 1 -> ROI 2	0,10	0,15	0,24	0,16	0,27	0,36	0,20	0,31	0,40
ROI 1 -> ROI 3	0,01	0,01	0,01	0,03	0,03	0,02	0,05	0,04	0,03
ROI 2 -> ROI 3	0,03	0,03	0,03	0,03	0,04	0,04	0,10	0,11	0,12

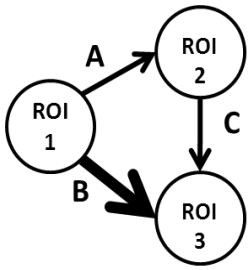

Links	DATASET 1			DATASET 2			DATASET 3		
	x2	x3	x4	x2	x3	x4	x2	x3	x4
ROI 1 -> ROI 2	0,03	0,02	0,02	0,05	0,04	0,04	0,07	0,05	0,04
ROI 1 -> ROI 3	0,05	0,11	0,16	0,12	0,20	0,27	0,17	0,26	0,33
ROI 2 -> ROI 3	0,02	0,02	0,02	0,06	0,06	0,06	0,08	0,09	0,07

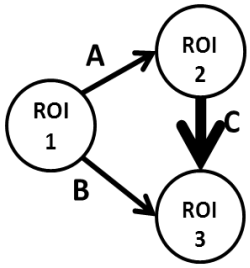

Links	DATASET 1			DATASET 2			DATASET 3		
	x2	x3	x4	x2	x3	x4	x2	x3	x4
ROI 1 -> ROI 2	0,03	0,03	0,03	0,06	0,06	0,06	0,08	0,07	0,07
ROI 1 -> ROI 3	0,01	0,01	0,01	0,04	0,04	0,04	0,06	0,06	0,06
ROI 2 -> ROI 3	0,08	0,14	0,22	0,17	0,28	0,37	0,22	0,34	0,42

***Table 4.18**: GC index: average strength estimates in each experiment. Bold arrow in network model indicates the link with true strength multiplied by factors 2, 3 and 4.*

	Links	DATASET 1 A=B=C=1	DATASET 2 A=B=C=1	DATASET 3 A=B=C=1
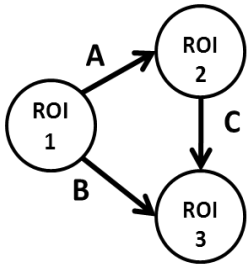	*ROI 1 -> ROI 2*	2,45	4,45	5,12
	ROI 1 -> ROI 3	3,18	6,28	8,16
	ROI 2 -> ROI 3	2,93	6,62	8,17

	Links	DATASET 1			DATASET 2			DATASET 3		
		x2	x3	x4	x2	x3	x4	x2	x3	x4
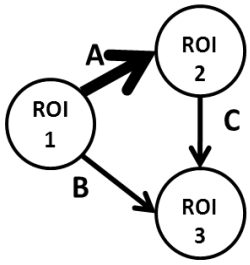	*ROI 1 -> ROI 2*	5,32	6,61	8,26	7,60	9,60	10,55	8,99	10,61	11,12
	ROI 1 -> ROI 3	3,44	3,68	4,47	7,08	7,88	8,66	9,66	10,00	9,98
	ROI 2 -> ROI 3	3,68	3,93	4,88	7,25	8,29	9,14	8,57	9,26	10,15

	Links	DATASET 1			DATASET 2			DATASET 3		
		x2	x3	x4	x2	x3	x4	x2	x3	x4
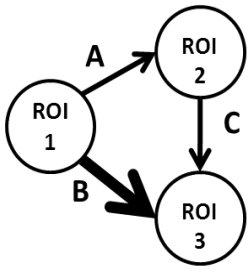	*ROI 1 -> ROI 2*	2,26	2,24	2,44	4,07	3,92	4,23	5,38	5,05	4,98
	ROI 1 -> ROI 3	4,82	7,70	9,53	9,52	11,94	13,87	11,75	14,19	15,98
	ROI 2 -> ROI 3	2,41	1,96	1,79	5,57	4,27	3,63	6,61	5,64	4,21

	Links	DATASET 1			DATASET 2			DATASET 3		
		x2	x3	x4	x2	x3	x4	x2	x3	x4
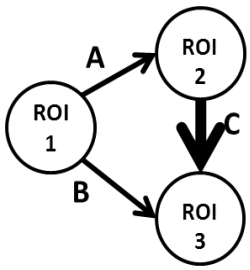	*ROI 1 -> ROI 2*	2,62	2,47	2,46	4,42	3,84	4,40	4,84	4,78	4,95
	ROI 1 -> ROI 3	2,74	2,53	2,43	5,76	4,70	4,97	7,30	6,47	6,01
	ROI 2 -> ROI 3	6,41	9,22	11,09	11,22	14,07	14,90	12,91	15,07	16,01

***Table 4.19**: DTF index: strength estimates computed via AUC of the mean function in the frequency domain for each experiment. Bold arrow in network model indicates the link with true strength multiplied by factors 2, 3 and 4.*

	Links	DATASET 1 A=B=C=1			DATASET 2 A=B=C=1			DATASET 3 A=B=C=1		
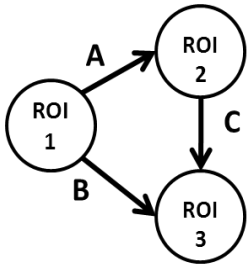	*ROI 1 -> ROI 2*	2,18			3,24			3,19		
	ROI 1 -> ROI 3	2,64			5,05			6,94		
	ROI 2 -> ROI 3	3,14			7,78			9,97		
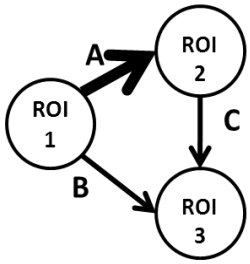	**Links**	**DATASET 1**			**DATASET 2**			**DATASET 3**		
		x2	x3	x4	x2	x3	x4	x2	x3	x4
	ROI 1 -> ROI 2	4,86	6,18	7,85	6,22	8,25	9,24	6,50	8,44	9,00
	ROI 1 -> ROI 3	2,08	1,62	1,50	3,86	3,39	3,26	6,10	4,82	4,54
	ROI 2 -> ROI 3	3,94	4,30	5,63	8,92	10,75	12,40	11,44	13,24	14,80
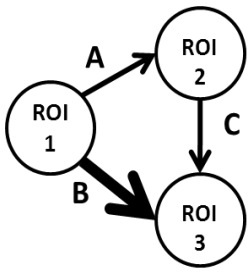	**Links**	**DATASET 1**			**DATASET 2**			**DATASET 3**		
		x2	x3	x4	x2	x3	x4	x2	x3	x4
	ROI 1 -> ROI 2	1,79	1,44	1,43	2,00	1,50	1,39	2,04	1,43	1,18
	ROI 1 -> ROI 3	4,40	7,56	9,56	9,83	12,68	14,79	12,46	15,78	17,47
	ROI 2 -> ROI 3	2,77	2,42	2,29	7,07	6,08	5,46	9,08	8,42	6,77
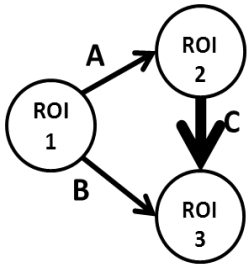	**Links**	**DATASET 1**			**DATASET 2**			**DATASET 3**		
		x2	x3	x4	x2	x3	x4	x2	x3	x4
	ROI 1 -> ROI 2	2,43	2,25	2,39	3,32	3,11	3,62	3,17	3,44	3,74
	ROI 1 -> ROI 3	2,00	1,75	1,35	4,35	3,16	2,82	6,18	4,74	3,76
	ROI 2 -> ROI 3	6,99	9,99	12,17	13,26	16,16	17,48	15,96	18,46	19,30

***Table 4.20**: PDC index: strength estimates computed via AUC of the mean function in the frequency domain for each experiment. Bold arrow in network model indicates the link with true strength multiplied by factors 2, 3 and 4.*

	Links	DATASET 1 A=B=C=1	DATASET 2 A=B=C=1	DATASET 3 A=B=C=1
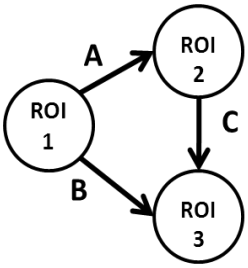	*ROI 1 -> ROI 2*	0,16	0,21	0,23
	ROI 1 -> ROI 3	0,10	0,15	0,18
	ROI 2 -> ROI 3	0,10	0,08	0,07

	Links	DATASET 1			DATASET 2			DATASET 3		
		x2	x3	x4	x2	x3	x4	x2	x3	x4
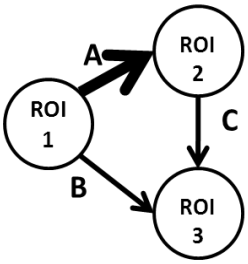	*ROI 1 -> ROI 2*	0,29	0,36	0,42	0,21	0,36	0,45	0,23	0,39	0,50
	ROI 1 -> ROI 3	0,09	0,07	0,05	0,15	0,14	0,12	0,18	0,18	0,17
	ROI 2 -> ROI 3	0,14	0,18	0,23	0,08	0,13	0,20	0,07	0,12	0,19

	Links	DATASET 1			DATASET 2			DATASET 3		
		x2	x3	x4	x2	x3	x4	x2	x3	x4
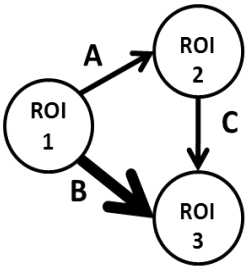	*ROI 1 -> ROI 2*	0,16	0,17	0,17	0,21	0,22	0,22	0,23	0,22	0,23
	ROI 1 -> ROI 3	0,18	0,26	0,32	0,15	0,26	0,35	0,18	0,31	0,42
	ROI 2 -> ROI 3	0,11	0,13	0,15	0,08	0,10	0,12	0,07	0,09	0,10

	Links	DATASET 1			DATASET 2			DATASET 3		
		x2	x3	x4	x2	x3	x4	x2	x3	x4
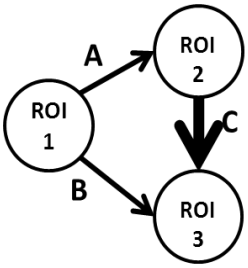	*ROI 1 -> ROI 2*	0,16	0,16	0,16	0,21	0,20	0,21	0,23	0,23	0,22
	ROI 1 -> ROI 3	0,09	0,09	0,08	0,15	0,15	0,15	0,18	0,19	0,19
	ROI 2 -> ROI 3	0,15	0,19	0,24	0,08	0,12	0,15	0,07	0,09	0,10

Table 4.21: *SEM index: average strength estimates in each experiment. Bold arrow in network model indicates the link with true strength multiplied by factors 2, 3 and 4.*

4.1.3.2 Open-loop network

	Links	DATASET 1			DATASET 2			DATASET 3		
		A=B=1			A=B=1			A=B=1		
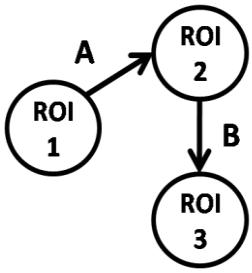	*ROI 1 -> ROI 2*	0,03			0,06			0,09		
	ROI 2 -> ROI 3	0,02			0,06			0,09		
	Links	**DATASET 1**			**DATASET 2**			**DATASET 3**		
		x2	x3	x4	x2	x3	x4	x2	x3	x4
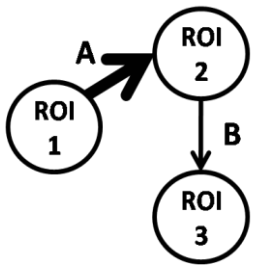	*ROI 1 -> ROI 2*	0,08	0,16	0,24	0,17	0,27	0,36	0,22	0,32	0,40
	ROI 2 -> ROI 3	0,02	0,03	0,04	0,07	0,08	0,09	0,10	0,10	0,12
	Links	**DATASET 1**			**DATASET 2**			**DATASET 3**		
		x2	x3	x4	x2	x3	x4	x2	x3	x4
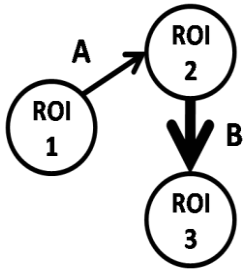	*ROI 1 -> ROI 2*	0,03	0,03	0,03	0,07	0,06	0,07	0,09	0,09	0,09
	ROI 2 -> ROI 3	0,08	0,15	0,22	0,17	0,28	0,37	0,23	0,34	0,43

***Table 4.22**: GC index: average strength estimates in each experiment. Bold arrow in network model indicates the link with true strength multiplied by factors 2, 3 and 4.*

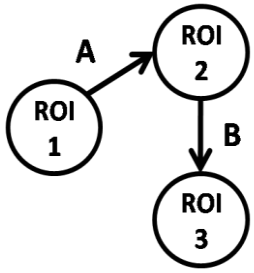

Links	DATASET 1 A=B=1	DATASET 2 A=B=1	DATASET 3 A=B=1
ROI 1 -> ROI 2	2,28	4,00	5,09
ROI 2 -> ROI 3	3,22	7,45	9,90

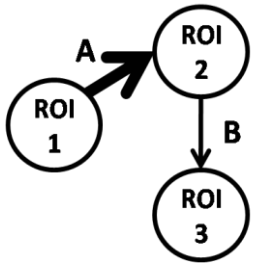

Links	DATASET 1			DATASET 2			DATASET 3		
	x2	x3	x4	x2	x3	x4	x2	x3	x4
ROI 1 -> ROI 2	4,51	6,90	8,21	7,85	9,43	10,37	8,99	10,84	11,22
ROI 2 -> ROI 3	3,41	4,50	5,52	8,21	9,07	9,53	10,27	10,45	11,59

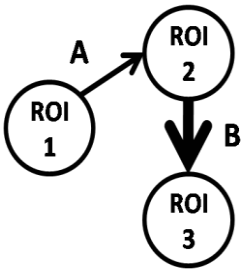

Links	DATASET 1			DATASET 2			DATASET 3		
	x2	x3	x4	x2	x3	x4	x2	x3	x4
ROI 1 -> ROI 2	2,50	2,48	2,56	4,28	4,16	4,03	5,12	5,20	5,10
ROI 2 -> ROI 3	6,99	9,91	11,54	12,55	15,07	16,60	15,03	16,95	17,80

***Table 4.23**: DTF index: strength estimates computed via AUC of the mean function in the frequency domain for each experiment. Bold arrow in network model indicates the link with true strength multiplied by factors 2, 3 and 4.*

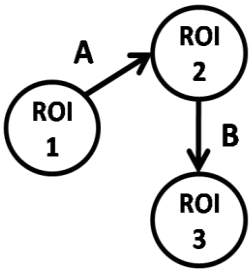

Links	DATASET 1 A=B=1	DATASET 2 A=B=1	DATASET 3 A=B=1
ROI 1 -> ROI 2	2,24	3,85	4,82
ROI 2 -> ROI 3	3,27	7,79	10,61

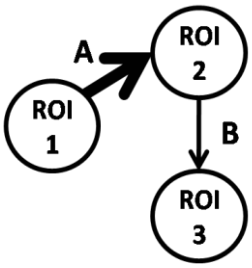

Links	DATASET 1			DATASET 2			DATASET 3		
	x2	x3	x4	x2	x3	x4	x2	x3	x4
ROI 1 -> ROI 2	4,43	6,72	8,07	7,55	9,10	9,99	8,57	10,45	10,67
ROI 2 -> ROI 3	3,50	4,85	6,08	9,31	10,93	12,13	12,00	13,58	15,75

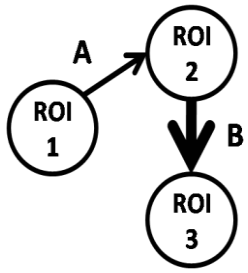

Links	DATASET 1			DATASET 2			DATASET 3		
	x2	x3	x4	x2	x3	x4	x2	x3	x4
ROI 1 -> ROI 2	2,45	2,43	2,52	4,13	4,07	3,97	4,88	5,03	4,95
ROI 2 -> ROI 3	7,17	10,41	12,19	13,54	16,51	18,15	16,72	19,11	20,11

***Table 4.24**: PDC index: strength estimates computed via AUC of the mean function in the frequency domain for each experiment. Bold arrow in network model indicates the link with true strength multiplied by factors 2, 3 and 4.*

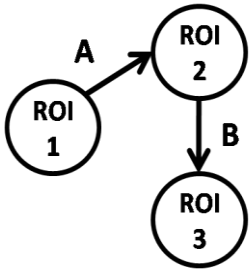

Links	DATASET 1 A=B=1	DATASET 2 A=B=1	DATASET 3 A=B=1
ROI 1 -> ROI 2	0,15	0,20	0,23
ROI 2 -> ROI 3	0,07	0,06	0,05

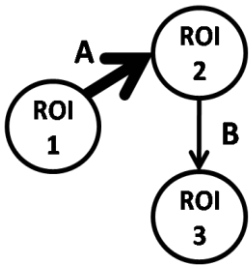

Links	DATASET 1			DATASET 2			DATASET 3		
	x2	x3	x4	x2	x3	x4	x2	x3	x4
ROI 1 -> ROI 2	0,28	0,37	0,41	0,36	0,45	0,50	0,39	0,50	0,56
ROI 2 -> ROI 3	0,09	0,12	0,15	0,09	0,14	0,18	0,10	0,15	0,20

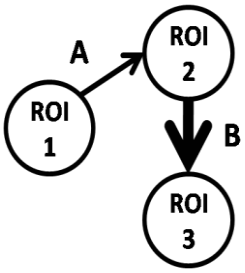

Links	DATASET 1			DATASET 2			DATASET 3		
	x2	x3	x4	x2	x3	x4	x2	x3	x4
ROI 1 -> ROI 2	0,15	0,16	0,16	0,21	0,21	0,21	0,22	0,22	0,22
ROI 2 -> ROI 3	0,12	0,18	0,22	0,11	0,14	0,15	0,08	0,10	0,09

Table 4.25: *SEM index: average strength estimates in each experiment. Bold arrow in network model indicates the link with true strength multiplied by factors 2, 3 and 4.*

4.1.3.3 Network with feed-back link

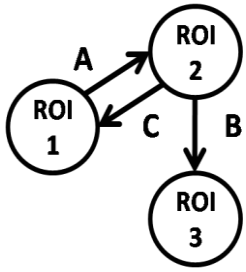

Links	DATASET 1 A=B=1	DATASET 2 A=B=1	DATASET 3 A=B=1
ROI 1 -> ROI 2	0,03	0,08	0,12
ROI 2 -> ROI 3	0,02	0,06	0,08
ROI 2 -> ROI 1	0,04	0,11	0,16

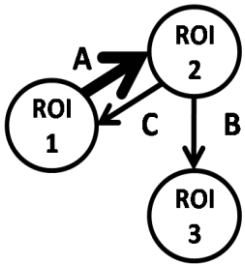

Links	DATASET 1			DATASET 2			DATASET 3		
	x2	x3	x4	x2	x3	x4	x2	x3	x4
ROI 1 -> ROI 2	0,09	0,19	0,26	0,22	0,33	0,39	0,28	0,37	0,41
ROI 2 -> ROI 3	0,03	0,03	0,03	0,07	0,07	0,08	0,09	0,09	0,07
ROI 2 -> ROI 1	0,04	0,05	0,06	0,13	0,15	0,16	0,19	0,20	0,19

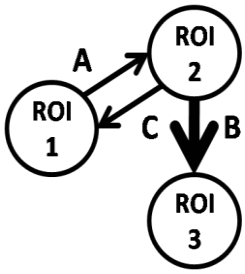

Links	DATASET 1			DATASET 2			DATASET 3		
	x2	x3	x4	x2	x3	x4	x2	x3	x4
ROI 1 -> ROI 2	0,02	0,03	0,03	0,08	0,07	0,08	0,11	0,11	0,10
ROI 2 -> ROI 3	0,07	0,14	0,20	0,17	0,27	0,36	0,21	0,33	0,41
ROI 2 -> ROI 1	0,04	0,03	0,03	0,10	0,08	0,06	0,13	0,10	0,09

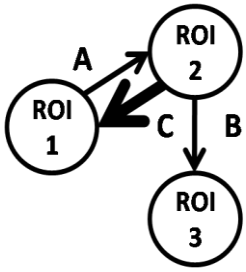

Links	DATASET 1			DATASET 2			DATASET 3		
	x2	x3	x4	x2	x3	x4	x2	x3	x4
ROI 1 -> ROI 2	0,04	0,06	0,07	0,12	0,16	0,18	0,16	0,19	0,21
ROI 2 -> ROI 3	0,01	0,01	0,01	0,05	0,04	0,02	0,06	0,04	0,03
ROI 2 -> ROI 1	0,13	0,23	0,32	0,29	0,42	0,53	0,37	0,51	0,59

***Table 4.26**: GC index: average strength estimates in each experiment. Bold arrow in network model indicates the link with true strength multiplied by factors 2, 3 and 4.*

	Links	DATASET 1 A=B=1	DATASET 2 A=B=1	DATASET 3 A=B=1
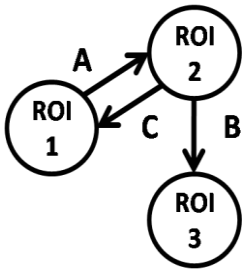	*ROI 1 -> ROI 2*	2,96	4,79	6,33
	ROI 2 -> ROI 3	3,32	7,80	10,28
	ROI 2 -> ROI 1	3,41	6,40	7,99

	Links	DATASET 1			DATASET 2			DATASET 3		
		x2	x3	x4	x2	x3	x4	x2	x3	x4
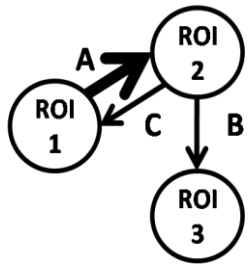	*ROI 1 -> ROI 2*	5,43	8,68	9,93	9,74	13,00	14,12	11,97	14,87	14,54
	ROI 2 -> ROI 3	3,63	4,35	5,21	8,00	9,17	10,55	10,08	10,81	12,99
	ROI 2 -> ROI 1	3,19	4,27	5,35	7,24	7,96	9,29	8,32	9,01	10,72

	Links	DATASET 1			DATASET 2			DATASET 3		
		x2	x3	x4	x2	x3	x4	x2	x3	x4
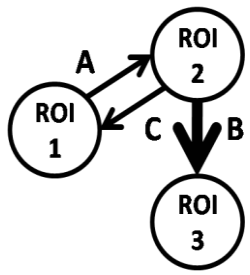	*ROI 1 -> ROI 2*	2,11	2,59	2,95	5,15	4,90	5,42	5,96	6,31	6,31
	ROI 2 -> ROI 3	6,68	9,57	11,29	12,74	15,15	16,04	15,16	16,72	17,33
	ROI 2 -> ROI 1	3,22	3,27	3,11	6,39	6,21	5,92	8,15	7,81	8,00

	Links	DATASET 1			DATASET 2			DATASET 3		
		x2	x3	x4	x2	x3	x4	x2	x3	x4
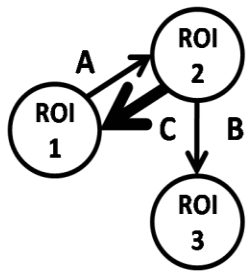	*ROI 1 -> ROI 2*	3,66	5,36	6,34	7,31	9,63	11,06	8,38	9,77	11,30
	ROI 2 -> ROI 3	3,00	2,95	3,15	7,79	7,86	7,93	10,46	11,30	10,80
	ROI 2 -> ROI 1	6,31	7,91	8,53	10,08	11,16	11,86	11,83	13,97	13,90

***Table 4.27**: DTF index: strength estimates computed via AUC of the mean function in the frequency domain for each experiment. Bold arrow in network model indicates the link with true strength multiplied by factors 2, 3 and 4.*

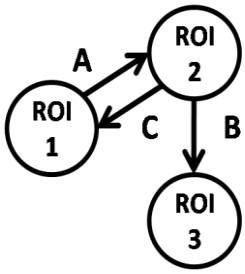

Links	DATASET 1 A=B=1	DATASET 2 A=B=1	DATASET 3 A=B=1
ROI 1 -> ROI 2	2,87	4,57	5,96
ROI 2 -> ROI 3	3,04	6,75	9,13
ROI 2 -> ROI 1	2,96	4,43	4,79

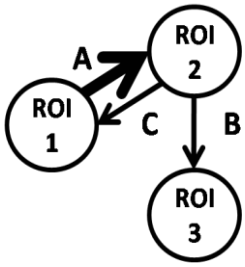

Links	DATASET 1			DATASET 2			DATASET 3		
	x2	x3	x4	x2	x3	x4	x2	x3	x4
ROI 1 -> ROI 2	5,34	8,52	9,64	9,31	12,16	12,54	11,10	12,76	10,94
ROI 2 -> ROI 3	3,43	4,35	5,25	7,63	10,21	12,86	11,36	14,26	16,53
ROI 2 -> ROI 1	2,74	3,57	4,24	4,80	4,64	4,67	4,30	4,03	4,50

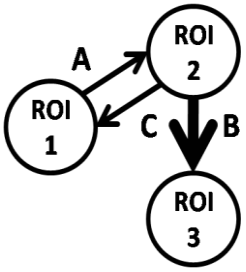

Links	DATASET 1			DATASET 2			DATASET 3		
	x2	x3	x4	x2	x3	x4	x2	x3	x4
ROI 1 -> ROI 2	2,06	2,52	2,92	4,92	4,75	5,23	5,61	5,92	6,01
ROI 2 -> ROI 3	6,28	9,33	11,25	12,60	15,65	17,01	15,52	18,06	19,04
ROI 2 -> ROI 1	2,39	1,91	1,64	2,96	2,15	1,82	3,13	2,38	2,21

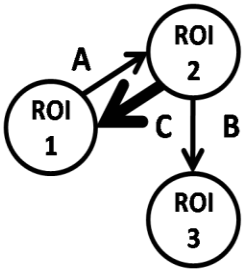

Links	DATASET 1			DATASET 2			DATASET 3		
	x2	x3	x4	x2	x3	x4	x2	x3	x4
ROI 1 -> ROI 2	3,58	5,10	6,05	6,91	8,96	10,19	7,80	8,62	9,71
ROI 2 -> ROI 3	2,34	2,31	2,50	5,73	6,23	5,90	8,53	9,23	9,44
ROI 2 -> ROI 1	5,80	7,21	7,71	7,65	8,48	9,17	8,03	9,57	9,40

***Table 4.28**: PDC index: strength estimates computed via AUC of the mean function in the frequency domain for each experiment. Bold arrow in network model indicates the link with true strength multiplied by factors 2, 3 and 4.*

4.1.3.4 Cycle network

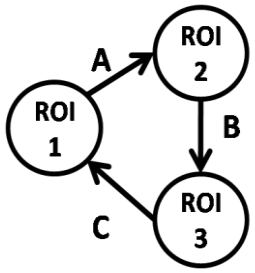

Links	DATASET 1 A=B=1	DATASET 2 A=B=1	DATASET 3 A=B=1
ROI 1 -> ROI 2	0,03	0,07	0,10
ROI 2 -> ROI 3	0,03	0,07	0,09
ROI 3 -> ROI 1	0,04	0,10	0,13

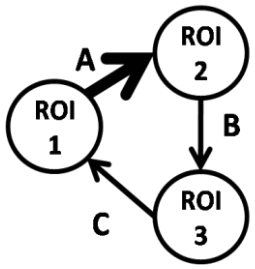

Links	DATASET 1			DATASET 2			DATASET 3		
	x2	x3	x4	x2	x3	x4	x2	x3	x4
ROI 1 -> ROI 2	0,09	0,16	0,24	0,19	0,29	0,38	0,24	0,35	0,43
ROI 2 -> ROI 3	0,03	0,03	0,03	0,08	0,09	0,10	0,10	0,12	0,13
ROI 3 -> ROI 1	0,04	0,05	0,05	0,10	0,10	0,11	0,13	0,13	0,14

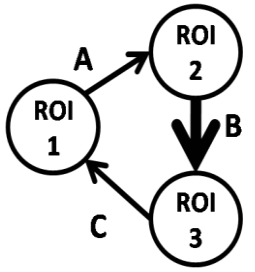

Links	DATASET 1			DATASET 2			DATASET 3		
	x2	x3	x4	x2	x3	x4	x2	x3	x4
ROI 1 -> ROI 2	0,03	0,03	0,03	0,07	0,07	0,07	0,09	0,10	0,10
ROI 2 -> ROI 3	0,08	0,15	0,21	0,18	0,30	0,38	0,24	0,34	0,43
ROI 3 -> ROI 1	0,05	0,05	0,05	0,10	0,11	0,11	0,13	0,14	0,13

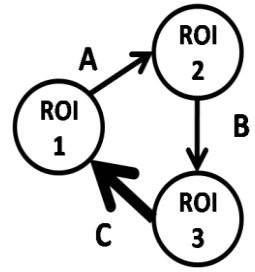

Links	DATASET 1			DATASET 2			DATASET 3		
	x2	x3	x4	x2	x3	x4	x2	x3	x4
ROI 1 -> ROI 2	0,04	0,04	0,05	0,08	0,10	0,11	0,11	0,12	0,15
ROI 2 -> ROI 3	0,02	0,02	0,02	0,07	0,07	0,07	0,10	0,10	0,11
ROI 3 -> ROI 1	0,15	0,26	0,39	0,28	0,48	0,65	0,35	0,57	0,75

***Table 4.29**: GC index: average strength estimates in each experiment. Bold arrow in network model indicates the link with true strength multiplied by factors 2, 3 and 4.*

	Links	DATASET 1			DATASET 2			DATASET 3		
		A=B=1			A=B=1			A=B=1		
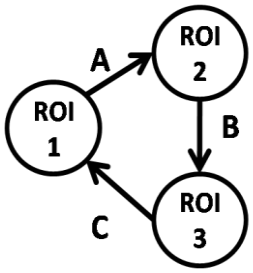	*ROI 1 -> ROI 2*	2,37			4,17			5,12		
	ROI 2 -> ROI 3	3,35			7,94			10,35		
	ROI 3 -> ROI 1	2,63			4,28			4,34		
	Links	**DATASET 1**			**DATASET 2**			**DATASET 3**		
		x2	x3	x4	x2	x3	x4	x2	x3	x4
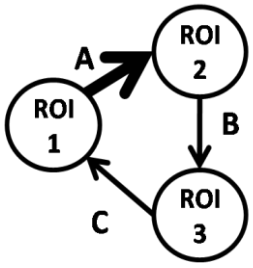	*ROI 1 -> ROI 2*	4,99	6,48	7,87	7,62	9,42	10,19	9,25	10,63	11,01
	ROI 2 -> ROI 3	3,77	4,34	4,96	8,67	9,13	10,39	10,56	11,59	12,14
	ROI 3 -> ROI 1	2,56	3,03	3,04	4,16	4,36	4,47	4,30	4,49	4,51
	Links	**DATASET 1**			**DATASET 2**			**DATASET 3**		
		x2	x3	x4	x2	x3	x4	x2	x3	x4
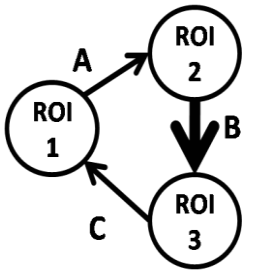	*ROI 1 -> ROI 2*	2,35	2,74	2,55	4,24	4,07	4,14	4,78	5,09	5,00
	ROI 2 -> ROI 3	7,03	9,8	11,84	12,84	16,03	17,19	15,95	17,96	18,74
	ROI 3 -> ROI 1	3,14	3,53	3,72	4,44	5,27	5,83	4,79	5,60	6,18
	Links	**DATASET 1**			**DATASET 2**			**DATASET 3**		
		x2	x3	x4	x2	x3	x4	x2	x3	x4
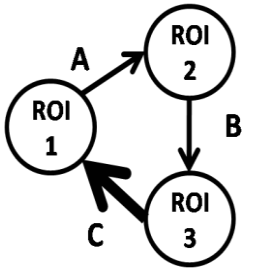	*ROI 1 -> ROI 2*	2,72	2,76	3,20	4,59	5,15	5,53	5,30	5,56	6,46
	ROI 2 -> ROI 3	3,02	2,99	2,99	8,07	8,20	8,53	10,64	11,39	11,71
	ROI 3 -> ROI 1	6,83	9,80	12,5	9,39	12,92	14,84	9,79	13,36	14,78

***Table 4.30**: DTF index: strength estimates computed via AUC of the mean function in the frequency domain for each experiment. Bold arrow in network model indicates the link with true strength multiplied by factors 2, 3 and 4.*

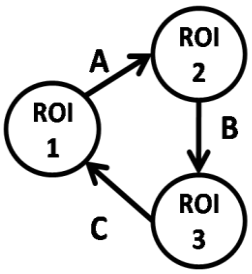

Links	DATASET 1 A=B=1	DATASET 2 A=B=1	DATASET 3 A=B=1
ROI 1 -> ROI 2	2,33	3,98	4,84
ROI 2 -> ROI 3	3,39	8,25	10,98
ROI 3 -> ROI 1	2,65	4,33	4,43

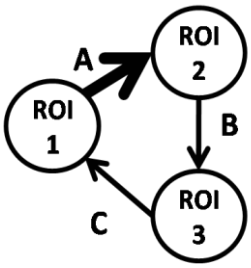

Links	DATASET 1			DATASET 2			DATASET 3		
	x2	x3	x4	x2	x3	x4	x2	x3	x4
ROI 1 -> ROI 2	4,96	6,43	7,79	7,38	9,21	9,79	8,83	10,07	10,17
ROI 2 -> ROI 3	3,96	4,68	5,45	9,74	10,94	13,13	12,52	14,71	16,25
ROI 3 -> ROI 1	2,59	3,08	3,10	4,25	4,50	4,65	4,40	4,71	4,78

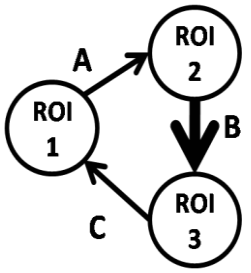

Links	DATASET 1			DATASET 2			DATASET 3		
	x2	x3	x4	x2	x3	x4	x2	x3	x4
ROI 1 -> ROI 2	2,29	2,70	2,53	4,14	3,95	4,06	4,52	4,80	4,78
ROI 2 -> ROI 3	7,23	10,25	12,32	13,77	17,31	18,69	17,36	19,89	20,89
ROI 3 -> ROI 1	3,17	3,64	3,89	4,60	5,66	6,46	5,08	6,18	6,99

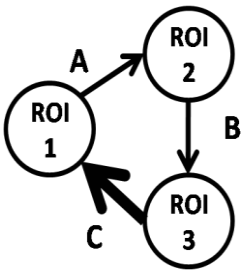

Links	DATASET 1			DATASET 2			DATASET 3		
	x2	x3	x4	x2	x3	x4	x2	x3	x4
ROI 1 -> ROI 2	2,63	2,70	3,12	4,38	4,99	5,31	5,04	5,17	5,88
ROI 2 -> ROI 3	3,14	3,16	3,22	8,39	8,63	9,14	11,29	12,17	12,77
ROI 3 -> ROI 1	6,89	9,96	12,76	9,78	13,56	15,77	10,31	14,4	16,09

***Table 4.31**: PDC index: strength estimates computed via AUC of the mean function in the frequency domain for each experiment. Bold arrow in network model indicates the link with true strength multiplied by factors 2, 3 and 4.*

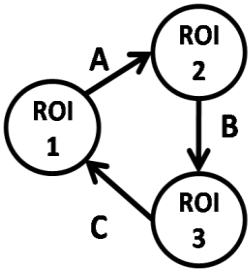

Links	DATASET 1 A=B=1	DATASET 2 A=B=1	DATASET 3 A=B=1
ROI 1 -> ROI 2	0,15	0,18	0,20
ROI 2 -> ROI 3	0,08	0,06	0,05
ROI 3 -> ROI 1	-0,09	-0,06	-0,03

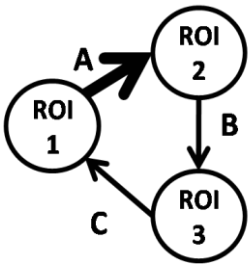

Links	DATASET 1			DATASET 2			DATASET 3		
	x2	x3	x4	x2	x3	x4	x2	x3	x4
ROI 1 -> ROI 2	0,27	0,34	0,40	0,32	0,41	0,47	0,36	0,46	0,53
ROI 2 -> ROI 3	0,11	0,15	0,19	0,10	0,15	0,20	0,09	0,15	0,20
ROI 3 -> ROI 1	-0,10	-0,10	-0,12	-0,05	-0,05	-0,06	-0,01	-0,01	-0,01

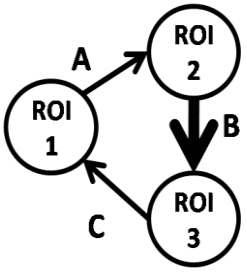

Links	DATASET 1			DATASET 2			DATASET 3		
	x2	x3	x4	x2	x3	x4	x2	x3	x4
ROI 1 -> ROI 2	0,13	0,11	0,09	0,15	0,12	0,10	0,18	0,16	0,14
ROI 2 -> ROI 3	0,14	0,18	0,21	0,11	0,15	0,16	0,10	0,12	0,12
ROI 3 -> ROI 1	-0,09	-0,10	-0,10	-0,08	-0,11	-0,16	-0,06	-0,12	-0,19

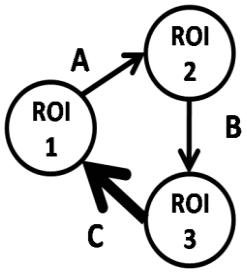

Links	DATASET 1			DATASET 2			DATASET 3		
	x2	x3	x4	x2	x3	x4	x2	x3	x4
ROI 1 -> ROI 2	0,13	0,13	0,12	0,15	0,15	0,13	0,18	0,17	0,15
ROI 2 -> ROI 3	0,09	0,10	0,10	0,07	0,07	0,08	0,06	0,06	0,07
ROI 3 -> ROI 1	-0,16	-0,22	-0,26	-0,12	-0,16	-0,19	-0,08	-0,12	-0,14

Table 4.32: *SEM index: average strength estimates in each experiment. Bold arrow in network model indicates the link with true strength multiplied by factors 2, 3 and 4.*

Results of strength estimates reported above, suggest some considerations about each index. Let us start from GC index. In feed-forward network (Table 4.18), characterized by three direct coupling (ROI 1 → ROI 2, ROI 2 → ROI 3, ROI 1 → ROI 3) and an indirect link (ROI 1 → ROI 3), the causality increases only between signals involved in the connection with increasing weight. Also for the open-loop network (Table 4.22) characterized by two direct coupling (ROI 1 → ROI 2, ROI 2 → ROI 3) and an indirect link (ROI 1 → ROI 3) we can observe a causality increase only between signals involved in the connection with increasing weight. In presence of reciprocal links, as in network with feed-back link (Table 4.26), characterized by direct connection between ROI 1 and ROI 2 in both ways, direct link between ROI 2 and ROI 3 and indirect connection from ROI 1 to ROI 3, GC index records again a causality increase in the link ROI 1 → ROI 2 when increases the corresponding true weight A, a causality increase in the link ROI 2 → ROI 3 when increases B and a causality increase in the link ROI 2 → ROI 1 when increases C. Finally, observing results obtained with cycle network (Table 4.29), also in this case the increase of a weight influences the strength only in the corresponding link. Indeed, other significant links remain almost unvaried (as also it occurs in the other previous networks), despite the cyclic topology of network.

As regard DTF and PDC indices, reported in Tables 4.19, 4.23, 4.27 and 4.30 for DTF and 4.20, 4.24, 4.28 and 4.31 for PDC, we can notice that when connection weight increases, DTF value reflects an increase in signal connectivity related to that connection both in direct and indirect way. This limit can be noticed observing panels a) and b) in Figs. 4.1, 4.2 and 4.3: even if not recognized as significant, DTF index shows the influence of signal from ROI 1 to ROI 3 due to the presence of an indirect connection. At last, we can say that sometimes it occurs that increase in signal connectivity related to increase of corresponding connection weight is not very significant. Approximately the same considerations are also valid for PDC with the only difference that connectivity analysis using PDC allows to distinguish direct connections from indirect ones. Indeed, with reference to panels c) and d) of Figs. 4.1, 4.2 and 4.3, the contribution due to indirect connection from ROI 1 to ROI 3 results heavily weakened.

Finally, as regard SEM, we can say that its results underline the difficulty in estimating connection series. Considering values of open-loop network (Table 4.25), we observe that SEM is able to recognize strength increasing from ROI 1 to ROI 2 when A increases and strength increasing from ROI 2 to ROI 3 when B increases but in the basal condition, where weights are equal, it is not in agreement with true network. Besides the problem of SEM, not only in this network but also in feed-forward and cycle network, concerns the connection from ROI 2 to ROI 3; indeed, when the weights of the other connections increase and the weight related to connection ROI 2 → ROI 3 is equal to basal condition, values of strength related to this connection are not in line with basal

condition values because they also increase. Performances get worse in the cycle network (Table 4.32) estimation where SEM confuses the direction of one link and finally fall down in estimating network with reciprocal connection.

Figs. 4.4, 4.5, 4.6 and 4.7 displays, for each network, scatter-plots showing regression between estimates and true weights, pooling together results over experimental conditions for all methods and datasets. Following tables report the correlation coefficient R for each regression line relative to scatter-plots in Figs. 4.4, 4.5, 4.6 and 4.7 for each index and dataset:

Link from ROI 1 to ROI 2			
	DATASET 1	DATASET 2	DATASET 3
GC	0,99	0,99	0,98
DTF	0,97	0,95	0,92
PDC	0,95	0,85	0,84
SEM	0,98	0,98	0,97
Link from ROI 1 to ROI 3			
	DATASET 1	DATASET 2	DATASET 3
GC	0,99	0,99	0,98
DTF	0,92	0,82	0,80
PDC	0,99	0,95	0,93
SEM	0,97	0,97	0,97
Link from ROI 2 to ROI 3			
	DATASET 1	DATASET 2	DATASET 3
GC	0,99	0,98	0,98
DTF	0,90	0,77	0,75
PDC	0,90	0,72	0,66
SEM	< 0,5	< 0,5	< 0,5

a)

Link from ROI 1 to ROI 2			
	DATASET 1	DATASET 2	DATASET 3
GC	0,9960	0,9996	0,9963
DTF	0,9959	0,9716	0,9605
PDC	0,9965	0,9721	0,9584
SEM	0,9858	0,9826	0,9850
Link from ROI 2 to ROI 3			
	DATASET 1	DATASET 2	DATASET 3
GC	0,9951	0,9972	0,9957
DTF	0,9680	0,9703	0,9557
PDC	0,9594	0,9268	0,8811
SEM	0,8752	0,2894	-0,2959

b)

Link from ROI 1 to ROI 2			
	DATASET 1	DATASET 2	DATASET 3
GC	0,9824	0,9441	0,9336
DTF	0,8728	0,7990	0,8326
PDC	0,8815	0,7865	0,7487
SEM	-	-	-
Link from ROI 2 to ROI 3			
	DATASET 1	DATASET 2	DATASET 3
GC	0,9937	0,9876	0,9835
DTF	0,9693	0,9426	0,9245
PDC	0,9532	0,8444	0,9089
SEM	-	-	-
Link from ROI 2 to ROI 1			
	DATASET 1	DATASET 2	DATASET 3
GC	0,9953	0,9795	0,9654
DTF	0,9272	0,8684	0,9061
PDC	0,9128	0,8712	0,8961
SEM	-	-	-

c)

Link from ROI 1 to ROI 2			
	DATASET 1	DATASET 2	DATASET 3
GC	0,9958	0,9930	0,9882
DTF	0,9878	0,9611	0,9428
PDC	0,9879	0,9596	0,9372
SEM	0,9774	0,9716	0,9789
Link from ROI 2 to ROI 3			
	DATASET 1	DATASET 2	DATASET 3
GC	0,9979	0,9953	0,9933
DTF	0,9764	0,9663	0,9545
PDC	0,9713	0,9164	0,8833
SEM	0,7079	0,4215	0,2212
Link from ROI 3 to ROI 1			
	DATASET 1	DATASET 2	DATASET 3
GC	0,9985	0,9995	0,9993
DTF	0,9933	0,9830	0,9752
PDC	0,9927	0,9802	0,9718
SEM	-0,9878	-0,7514	-0,4522

d)

Tables 4.33*: correlation coefficient R relative to scatter plots in Figs. 4.4, 4.5, 4.6 and 4.7 for each index and dataset for: a) feed-forward network, b) open-loop network, c) network with feed-back link, d) cycle network.*

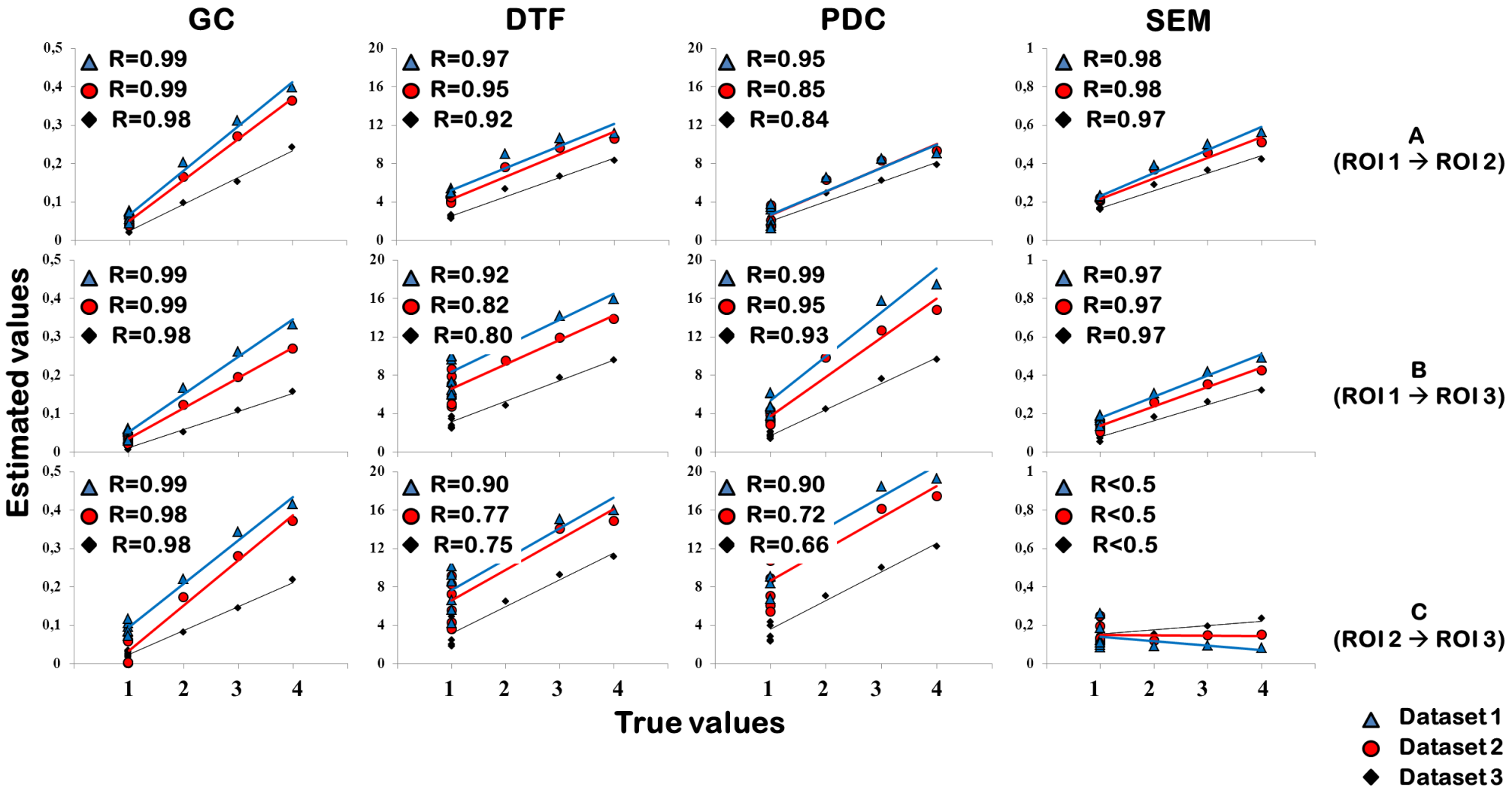

Fig. 4.4: *Linear regression and R correlation coefficients between GC, DTF, PDC and SEM estimated connectivity values and true connections weights for feed-forward network. Values [1, 2, 3, 4] are weight values assumed by parameters A, B and C, corresponding to connection ROI1→ ROI2, ROI1→ ROI3 and ROI2→ ROI3 respectively. For each dataset, four conditions were performed, comprehending a basal one with unit value in A, B and C, and three obtained by varying one parameter at a time from 2 to 4. High correlations (R>0.9, P<0.05) are evident in direct links - ROI1→ ROI2, ROI1→ ROI3 – for all indexes, while only GC shows the same performances also in link ROI2→ ROI3, demonstrating its robustness.*

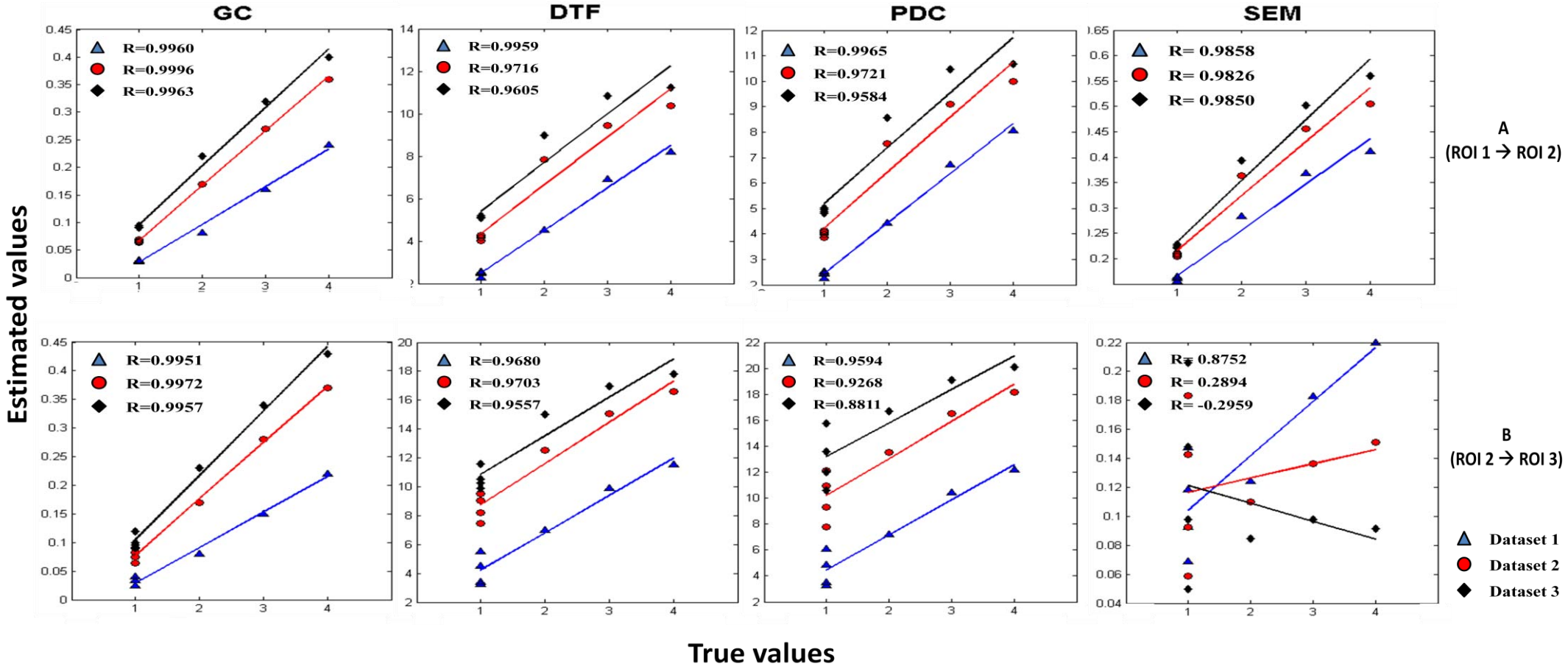

***Fig. 4.5**: Linear regression and R correlation coefficients between GC, DTF, PDC and SEM estimated connectivity values and true connections weights for open-loop network . Values [1, 2, 3, 4] are weight values assumed by parameters A and B, corresponding to connection ROI1 → ROI2 and ROI2 → ROI3 respectively. For each dataset, four conditions were performed, comprehending a basal one with unit value in A and B, and three obtained by varying one parameter at a time from 2 to 4.*

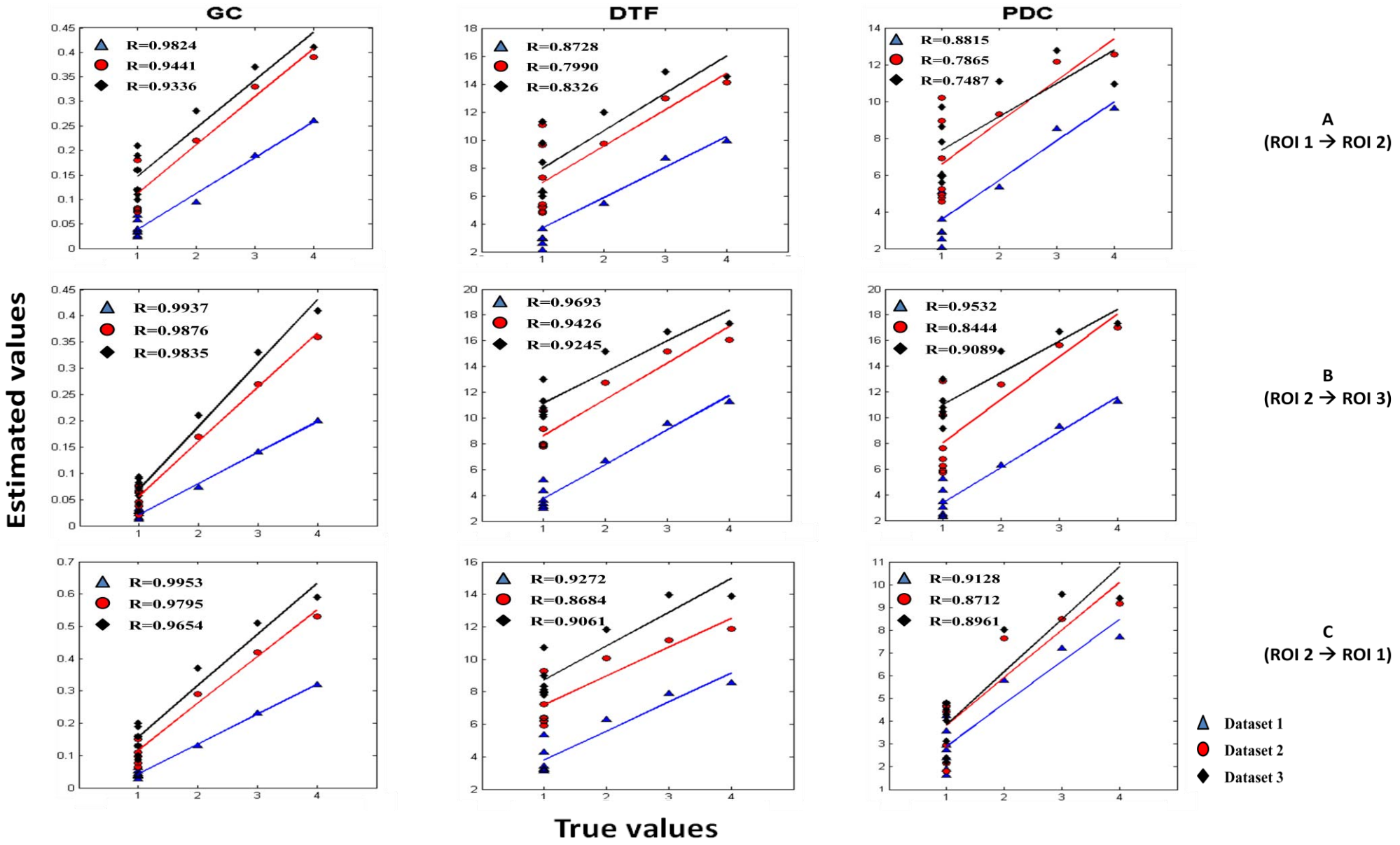

***Fig. 4.6**: Linear regression and R correlation coefficients between GC, DTF and PDC estimated connectivity values and true connections weights for network with feed-back link. Values [1, 2, 3, 4] are weight values assumed by parameters A, B and C, corresponding to connection ROI1→ ROI2, ROI2→ ROI3 and ROI2→ ROI1 respectively. For each dataset, four conditions were performed, comprehending a basal one with unit value in A, B and C, and three obtained by varying one parameter at a time from 2 to 4.*

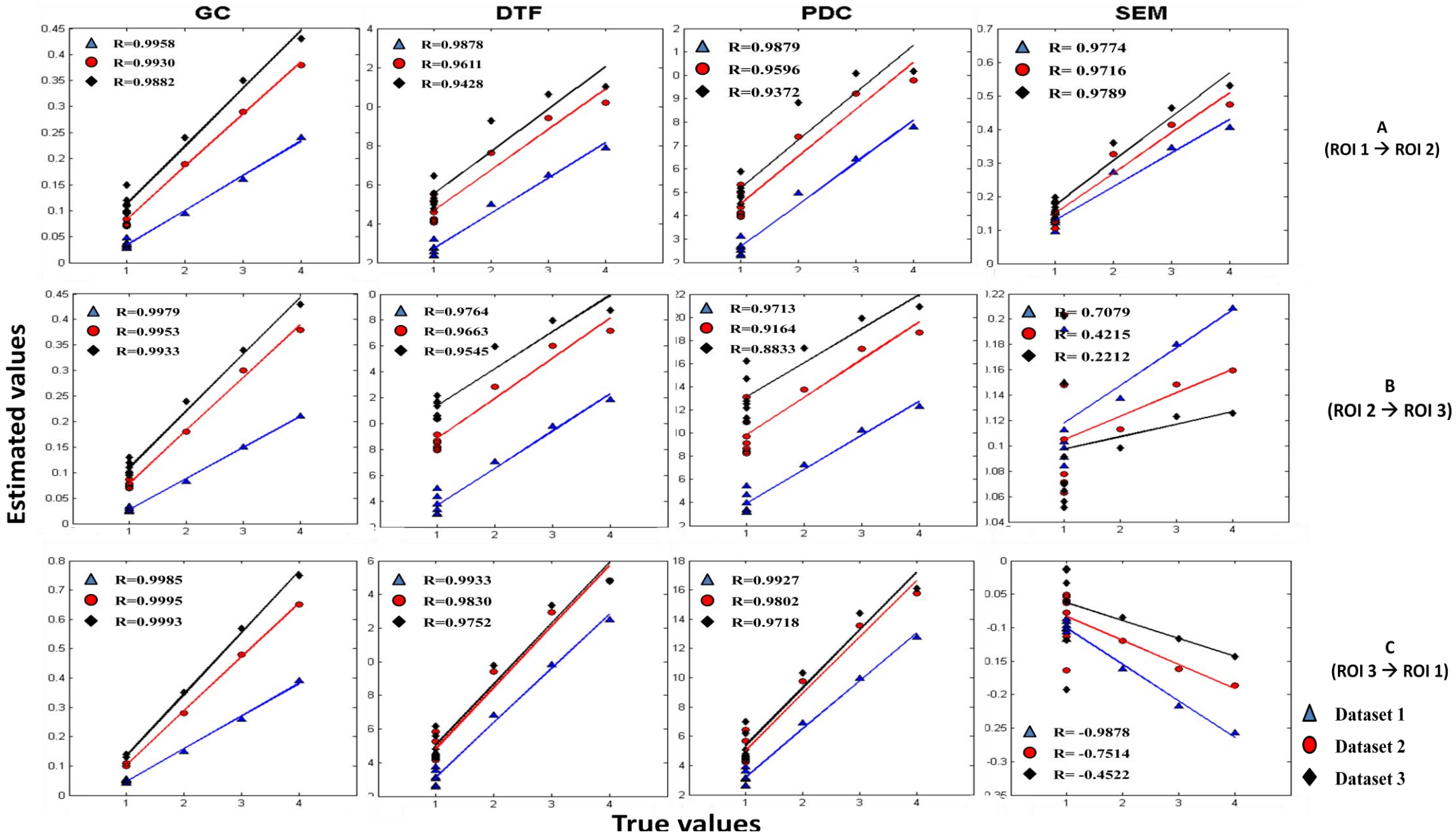

***Fig. 4.7**: Linear regression and R correlation coefficients between GC, DTF, PDC and SEM estimated connectivity values and true connections weights for cycle network. Values [1, 2, 3, 4] are weight values assumed by parameters A, B and C, corresponding to connection ROI1 → ROI2, ROI2 → ROI3 and ROI3 → ROI1 respectively. For each dataset, four conditions were performed, comprehending a basal one with unit value in A, B and C, and three obtained by varying one parameter at a time from 2 to 4.*

Observing Tables 4.33 a), 4.33 b), 4.33 c) and 4.33 d) and Figs. 4.4, 4.5, 4.6 and 4.7 we can notice that correlation proves that exists an high significant linear relationship with $R > 0.9$ for all GC estimates in all networks.

As regard DTF and PDC there are different situations depending on the network type. For open-loop network and cycle network what has been said for the GC estimates is still true, i.e. also for DTF and PDC estimates exists an high significant linear relationship with $R > 0.9$. Instead, for network with feed-back link, correlation slightly decreases for DTF and PDC with $R \sim 0.8$, particularly in link from ROI 1 to ROI 2. For feed-forward network correlation decreases, $R \sim 0.8$ and $R \sim 0.7$, in links connecting ROI 3.

As regard SEM, for open-loop network, for cycle network and for feed-forward network, estimates are well correlated with true weights in direct link from ROI 1 to ROI 2, while it fails in estimating the link from ROI 2 to ROI 3 and in the cycle network provides negative values of correlation in link from ROI 3 to ROI 1. In this regard, it is interesting to note that the coefficient sign reveals what kind of covariance relationship exists between network components. A positive coefficient means a synergic connection, conversely, a negative one implies that the increasing activity in one variable leads to a decrease in the activity of the variable it projects to.

Chapter 5

Discussion

The purpose of this study was to assess the effectiveness of commonly used measures for brain connectivity estimate using in silico data. The strategy used was to reproduce plausible neurophysiological processes in which we could manipulate coupling among ROIs. These ROIs were simulated by a neural mass model generating real power spectra very similar to the empirical ones.

Two connectivity methods were tested, both based on linear regression equations but different in describing data dynamics: MVAR indices and SEM. MVAR models consider past data information, while SEM describes variables interaction using only present instants. Considering connectivity estimate we can say that in the first approach topology, causality and strength are all inferred from data, while in the second one the model topology is postulated from a priori knowledge and only connections strength is estimated from the data. The aim of this work was to compare their performances underlining their strengths and weaknesses in order to provide a validated protocol to support both cognitive research and clinical activity.

5.1 Network connectivity estimation

In chapter 4, the results of connectivity estimation were presented for all networks analyzed: feed-forward network, open-loop network, network with feed-back link and cycle network. In this paragraph will be commented the results obtained and reported in tables of previous chapter.

Main results regarding both topology and strength are summarized in Fig. 5.1. For each network continuous lines indicate true connections and the associated numbers quantify the percentage of true positives, averaged throughout all experiments, while dashed lines indicate absent connections, thus the associated numbers quantify the percentage of false positives, averaged throughout all experiments. Blue numbers associated with continuous lines indicate the correlation coefficient between true and estimated values, i.e. the correlation coefficient R for each regression line shown in Figs. 4.4, 4.5, 4.6 and 4.7 of chapter 4. Results obtained by means of SEM show only the correlation coefficient R since SEM assumes known topology. Finally, we can note that SEM is applied to three networks only since it cannot define a model for network with feed-back link.

While numbers in Fig. 5.1 pool together all results from the three experiments, in the Appendix results for each individual experiment are reported.

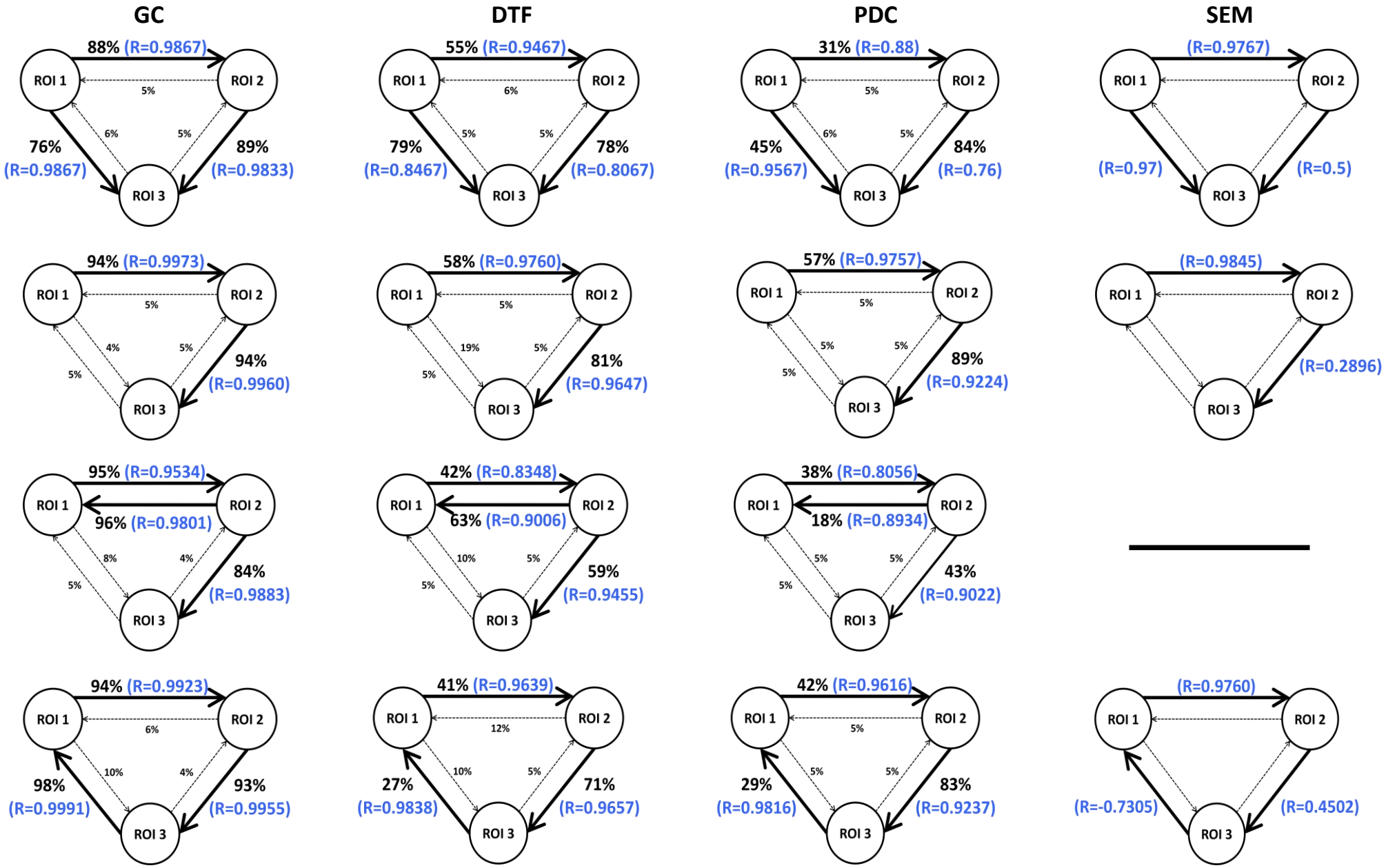

***Fig. 5.1**: Network topology and strength connection: continuous lines indicate true connections and the associated numbers quantify the percentage of true positives, averaged throughout all experiments. Dashed lines indicate absent connections, thus the associated numbers quantify the percentage of false positives, averaged throughout all experiments. The blue numbers associated with continuous lines indicate the correlation coefficient between true and estimated values.*

Figure 5.1 indicates that as regard topology, all methods are able to suggest the absence of causal influence where effectively no connection exists, i.e. ROI 2 → ROI 1, ROI 3 → ROI 1 and ROI 3 → ROI 2 for feed-forward network, ROI 2 → ROI 1, ROI 3 → ROI 2, ROI 3 → ROI 1 and ROI 1 → ROI 3 for open-loop network, ROI 3 → ROI 2, ROI 3 → ROI 1 and ROI 1 → ROI 3 for network with feed-back link and ROI 2 → ROI 1, ROI 1 → ROI 3 and ROI 3 → ROI 2 for cycle network, since the percentages of revealed connections by all methods are much lower than those of real direct connections, i.e. ROI 1 → ROI 2, ROI 1 → ROI 3 and ROI 2 → ROI 3 for feed-forward network, ROI 1 → ROI 2 and ROI 2 → ROI 3 for open-loop network, ROI 1 → ROI 2, ROI 2 → ROI 1 and ROI 2 → ROI 3 for network with feed-back link and ROI 1 → ROI 2, ROI 2 → ROI 3 and ROI 3 → ROI 1 for cycle network. Overall results of topology estimation, averaged by pooling together datasets and conditions, show that for each index the percentage associated with false positives is nearly always about 5% (except for few cases where there are values, mostly in DTF and referring to indirect connections, around 10%, 12% and 19%), while that one associated with true positives is approximately greater than 50%. Analyzing statistical performances (Tables 4.14 4.15, 4.16, 4.17) for each network, all methods provide high values of specificity, meaning they clearly recognize where connection does not exist, as said above. As regard value of sensitivity, instead, it is greater than 90% only for GC index, while DTF and PDC provide less powerful performances and hence this means that these two indices have greater difficulty in identifying true connections. In fact, as regard False Positive Rate (α) and False Negative Rate (β) we can say that first one assumes a rather low value in all indices and for all networks, while the second one assumes low values for GC index in all networks but assumes high values for DTF and PDC indices. Observing Fig. 5.1, indeed, we can note easily that for all networks GC index provides the highest percentages of true positives. This allows to say that GC can be considered a good network estimator; it is able to recognize not only coupling direction but also to locate direct connection contributions in case of reciprocal and cycle links.

Furthermore, previous works ([19] and [24]) have shown that results according to DTF and PDC greatly vary depending on the statistical testing strategy used. Unlike GC, for which statistical test is based on evaluation of the F-statistic and results depend on p-value only, for DTF and PDC exist different ways to assess connectivity significance. Alongside well-known methods based on phase-randomization, adopted in this work, surrogate data can be generated shuffling time series samples or using multivariate ARMA processes. Other innovative approaches are proposed in literature for PDC analysis, such as those based on asymptotic statistic ([27]) and anti-symmetrisation testing ([28]).

In ([19]) and ([24]) an ad hoc analysis to understand the optimal strategy was performed comparing permutation methods, both time samples and phase, and those based on simulation with multivariate ARMA processes ([24]). Results obtained in these works evidenced that, unlike phase-randomization, thresholds obtained with sample-shuffling and ARMA simulation provided smaller false negative rate but much more false positives. For this reason also in this work was used phase-randomization strategy with disadvantage of having smaller sensitivity values. Moreover, the average value of the threshold distribution that comes out from the four networks is always around 0.5, a well-established threshold value in literature to determine the coherence significance ([29]).
As regard strength, since true networks and estimates are measured with different scales, linear regression analysis is used to understand if they are sensitive to strength modulation (Fig. 5.1 and Figs. 4.4, 4.5, 4.6, 4.7). Examining Fig. 5.1 we can note that for GC index the correlation coefficient is always $R > 0.95$ in all networks, meaning that increasing true weights of one connection estimates increase nearly proportionally with them. Similar considerations are also valid for DTF and PDC even if sometimes their correlation coefficients slightly decrease. Hence, correlation evidences the ability of MVAR indices to quite well reproduce connection intensity for all networks. Unfortunately we cannot say the same for the SEM. Observing Fig. 5.1, SEM reveals considerable difficulty in estimating connection between ROI 2 and ROI 3 for all considered networks; in fact, for this connection the value of correlation coefficient is low and relationship between true networks and estimates is little linear. Besides, for cycle network SEM confuses the direction of link from ROI 3 to ROI 1 and hence appears a negative correlation. SEM weakness to describe simple connectivity patterns is probably due to the over-simplified model underlying SEM equations. Indeed, unlike MVAR approach, including past information of each time series, SEM computes connections taking into account only present information. This is an unreliable assumption causing troubles in particular in case of cycle network (as said above) and reciprocal network for which SEM is not even able to define a model.

Even if the networks explored in this work and in ([19]) are simple, some useful conclusions emerged and they will be presented in the next paragraph.

5.2 Conclusion

Results obtained for all networks, widely discussed in the previous paragraph, demonstrate that Granger causality is the best method among those considered for the estimation of cortical connectivity. As regard topology, GC index can be used as a good estimator supported by its high values of specificity and sensitivity. As regard strength, even if GC index isn't a directed measure of intensity connectivity, its regression analysis confirms the existence of a linear relationship between true and estimated strength. Also frequency indices, DTF and PDC, show to be able to provide information about network topology and connection intensity but their results are less accurate than GC performances. Neither these two indices are a direct measure of strength connectivity, nevertheless also for them regression analysis confirms the existence of a linear relationship between true and estimated intensity.

The method that, instead, proves to be really limited is SEM. Results show the difficulty of its approach to describe simple connections. Considering only the present information and not the past makes SEM limited and not sufficiently robust to characterize neuronal dynamic activity, as if brain connectivity could describe time series relationships by the instant we observe it.

Finally, this work suggests that GC is a stand-alone estimator and can be used as a explorative instrument to define both network topology and intensity connections. As regards DTF, it is not able to discriminate contribution coming from indirect rather than direct relation. PDC, instead, is able to distinguish direct connections. For this reason this work suggests that DTF and PDC should be used together to obtain a more robust network characterization.

The goodness of results obtained in this work for MVAR indices opens new possibility of research that go further simulation study. Next stage, indeed, can be testing these methods on real EEG in order to study true connections among brain areas.

A. Individual networks topology estimation

In this appendix are shown, for each individual network, figures of results of topology estimation averaged throughout each dataset, reporting for each link between two ROIs the mean percentage of statistical significant connections for each index. Continuous lines indicate true connections and the dashed ones represent links where connection is absent. The blue numbers associated with continuous lines indicate the correlation coefficient between true and estimated values; this coefficient is useful for strength connections analysis but not for topology analysis.
Besides in addition to topology figures, are also reported tables of performances, one for each dataset for all networks, in order to compare the ability of each index to estimate topology in different situations, i.e. when slope is 0.36, 0.56 and 0.66.

Fig. A.1 and Tables A.1, A.2 and A.3 report, respectively, estimated topology and performances for the open-loop network. Observing the performances we can note that value of specificity is always greater or equal than 90%, except for a case in which it is 89%, for all datasets and indices. This means that, independently of the dataset, all indices have a great ability of identifying absence of connections. As regard sensitivity, instead, in all datasets the highest value is given by the GC index. In dataset 3 (r = 0.66), for example, value of sensitivity for GC index is even equal to 100%. Hence, GC is index that has greater ability of identifying true connections than DTF and PDC. For False Positive Rate and False Negative Rate we can say that the first one assumes, as expected, rather low values for all indices and in all datasets (mean value of False Positive Rate is around 6%), while the second one always assumes low values for GC index and high values for DTF and PDC indices.

Summarizing we can say that as regard GC index the best performances in terms of topology are given by dataset 3, while as regard DTF and PDC indices the best performances are given by dataset 2.

Fig. A.2 and Tables A.4, A.5 and A.6 report, respectively, estimated topology and performances for network with feed-back link, while Fig. A.3 and Tables A.7, A.8 and A.9 report, respectively, estimated topology and performances for cycle network. Also for these two networks it occurs that specificity is greater than 90% and sensitivity is highest for GC index (there is also here value of sensitivity equal to 100% in dataset 3 of cycle network for example) and lowest for DTF and PDC. Hence, once again GC is the index that has greater ability of identifying true connections than DTF and PDC. Remains true also what has been said for False Positive Rate and False Negative Rate.

Concluding for these two networks we can say that as regard GC index the best performances in terms of topology are given once again by dataset 3 both in network with feed-back link and cycle network, while as regard DTF index the best performances in terms of topology are given by dataset 2 for network with feed-back link and by dataset 1 for cycle network. Finally, as regard PDC index the best performances in terms of topology are given by dataset 1 for both networks.

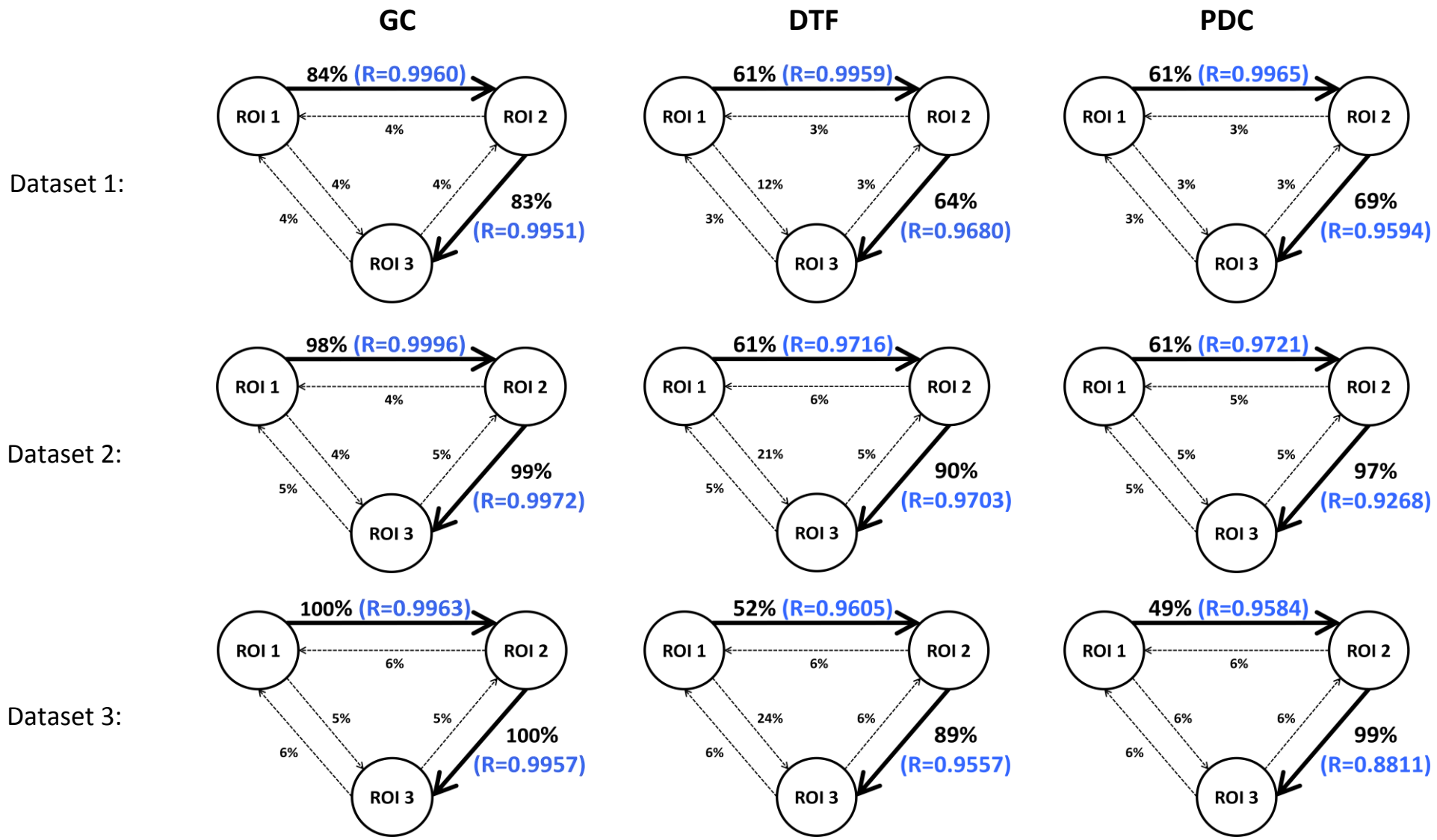

***Figure A.1**: Estimated topology for the open-loop network: continuous lines indicate true connections and the associated numbers quantify the percentage of true positives, averaged throughout each dataset. Dashed lines indicate absent connections, thus the associated numbers quantify the percentage of false positives averaged throughout each dataset. The blue numbers associated with continuous lines indicate the correlation coefficient between true and estimated values.*

(a) GC outcomes

	Positive Condition	Negative Condition		
Positive Outcomes	1168	113	**False Positive Rate (α)**	4%
Negative Outcomes	232	2687	**False Negative Rate (β)**	16%
	Sensitivity	**Specificity**		
	83%	96%		

(b) DTF outcomes

	Positive Condition	Negative Condition		
Positive Outcomes	877	161	**False Positive Rate (α)**	6%
Negative Outcomes	523	2639	**False Negative Rate (β)**	37%
	Sensitivity	**Specificity**		
	63%	94%		

(c) PDC outcomes

	Positive Condition	Negative Condition		
Positive Outcomes	911	97	**False Positive Rate (α)**	3%
Negative Outcomes	489	2703	**False Negative Rate (β)**	35%
	Sensitivity	**Specificity**		
	65%	96%		

Table A.1*: Statistical measures of performances of GC (a), DTF (b) and PDC (c) throughout experimental conditions for dataset with r=0.36 of open-loop network.*

(a) GC outcomes

	Positive Condition	Negative Condition		
Positive Outcomes	1378	130	**False Positive Rate (α)**	5%
Negative Outcomes	22	2670	**False Negative Rate (β)**	1%
	Sensitivity	**Specificity**		
	98%	95%		

(b) DTF outcomes

	Positive Condition	Negative Condition		
Positive Outcomes	1065	271	**False Positive Rate (α)**	10%
Negative Outcomes	335	2529	**False Negative Rate (β)**	24%
	Sensitivity	**Specificity**		
	76%	90%		

(c) PDC outcomes

	Positive Condition	Negative Condition		
Positive Outcomes	1109	156	**False Positive Rate (α)**	5%
Negative Outcomes	291	2644	**False Negative Rate (β)**	21%
	Sensitivity	**Specificity**		
	79%	94%		

Table A.2*: Statistical measures of performances of GC (a), DTF (b) and PDC (c) throughout experimental conditions for dataset with r=0.56 of open-loop network.*

(a) GC outcomes

	Positive Condition	Negative Condition		
Positive Outcomes	1398	162	**False Positive Rate (α)**	6%
Negative Outcomes	2	2638	**False Negative Rate (β)**	0%
	Sensitivity	**Specificity**		
	100%	94%		

(b) DTF outcomes

	Positive Condition	Negative Condition		
Positive Outcomes	984	292	**False Positive Rate (α)**	10%
Negative Outcomes	416	2508	**False Negative Rate (β)**	30%
	Sensitivity	**Specificity**		
	70%	89%		

(c) PDC outcomes

	Positive Condition	Negative Condition		
Positive Outcomes	1043	160	**False Positive Rate (α)**	6%
Negative Outcomes	357	2640	**False Negative Rate (β)**	25%
	Sensitivity	**Specificity**		
	74%	94%		

Table A.3*: Statistical measures of performances of GC (a), DTF (b) and PDC (c) throughout experimental conditions for dataset with r=0.66 of open-loop network.*

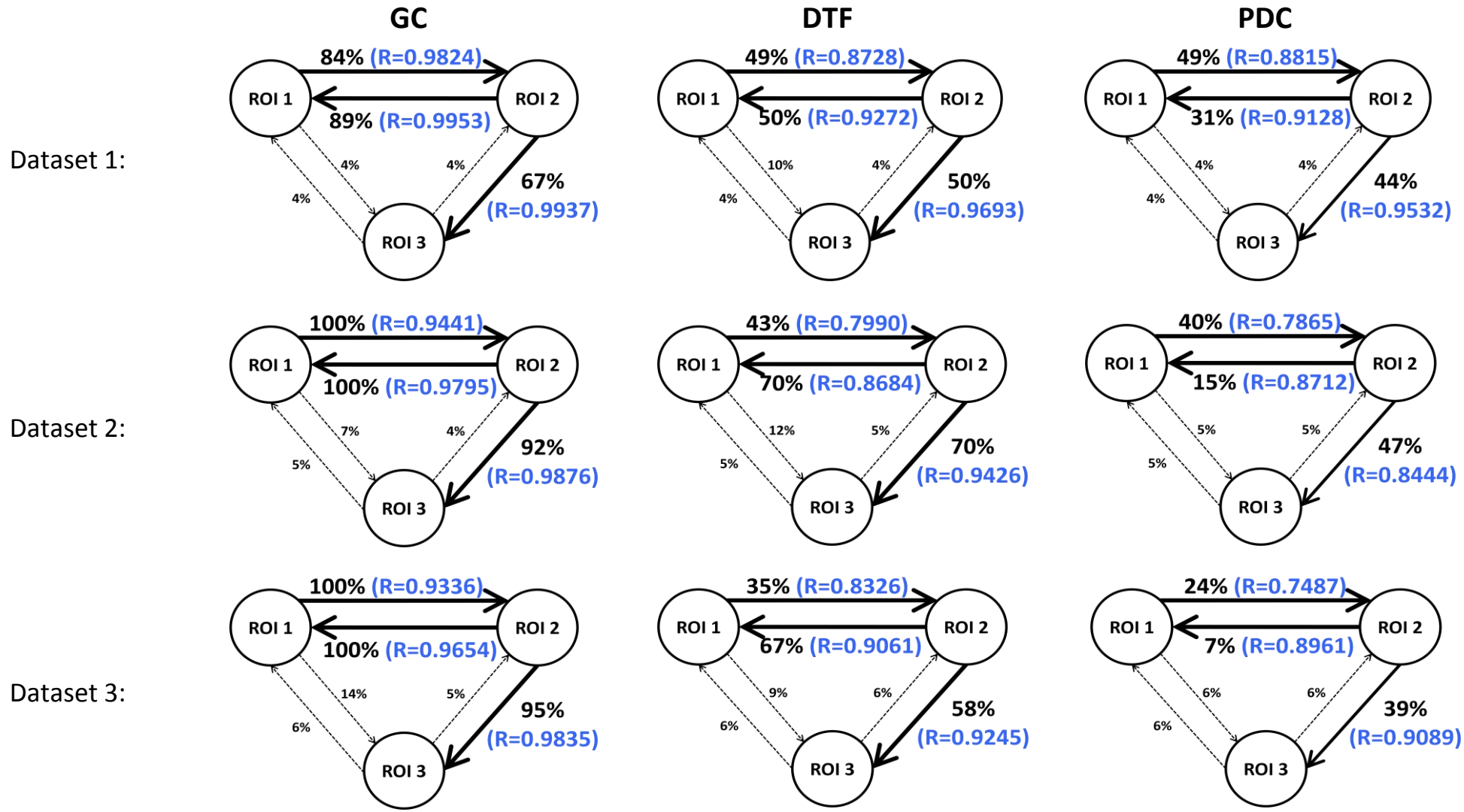

***Fig. A.2**: Estimated topology for the network with feed-back link: continuous lines indicate true connections and the associated numbers quantify the percentage of true positives, averaged throughout each dataset. Dashed lines indicate absent connections, thus the associated numbers quantify the percentage of false positives averaged throughout each dataset. The blue numbers associated with continuous lines indicate the correlation coefficient between true and estimated values.*

(a) GC outcomes

	Positive Condition	Negative Condition		
Positive Outcomes	2401	121	**False Positive Rate (α)**	4%
Negative Outcomes	599	2879	**False Negative Rate (β)**	20%
	Sensitivity	**Specificity**		
	80%	96%		

(b) DTF outcomes

	Positive Condition	Negative Condition		
Positive Outcomes	1499	189	**False Positive Rate (α)**	6%
Negative Outcomes	1501	2811	**False Negative Rate (β)**	50%
	Sensitivity	**Specificity**		
	50%	94%		

(c) PDC outcomes

	Positive Condition	Negative Condition		
Positive Outcomes	1240	126	**False Positive Rate (α)**	4%
Negative Outcomes	1760	2874	**False Negative Rate (β)**	59%
	Sensitivity	**Specificity**		
	41%	96%		

Table A.4*: Statistical measures of performances of GC (a), DTF (b) and PDC (c) throughout experimental conditions for dataset with r=0.36 of network with feed-back link.*

(a) GC outcomes

	Positive Condition	Negative Condition		
Positive Outcomes	2912	156	**False Positive Rate (α)**	5%
Negative Outcomes	88	2844	**False Negative Rate (β)**	3%
	Sensitivity	**Specificity**		
	97%	95%		

(b) DTF outcomes

	Positive Condition	Negative Condition		
Positive Outcomes	1834	221	**False Positive Rate (α)**	7%
Negative Outcomes	1166	2779	**False Negative Rate (β)**	39%
	Sensitivity	**Specificity**		
	61%	93%		

(c) PDC outcomes

	Positive Condition	Negative Condition		
Positive Outcomes	1026	156	**False Positive Rate (α)**	5%
Negative Outcomes	1974	2844	**False Negative Rate (β)**	66%
	Sensitivity	**Specificity**		
	34%	95%		

Table A.5*: Statistical measures of performances of GC (a), DTF (b) and PDC (c) throughout experimental conditions for dataset with r=0.56 of network with feed-back link.*

(a) GC outcomes

	Positive Condition	Negative Condition		
Positive Outcomes	2946	250	**False Positive Rate (α)**	8%
Negative Outcomes	54	2750	**False Negative Rate (β)**	2%
	Sensitivity	**Specificity**		
	98%	92%		

(b) DTF outcomes

	Positive Condition	Negative Condition		
Positive Outcomes	1605	210	**False Positive Rate (α)**	7%
Negative Outcomes	1395	2790	**False Negative Rate (β)**	46%
	Sensitivity	**Specificity**		
	53%	93%		

(c) PDC outcomes

	Positive Condition	Negative Condition		
Positive Outcomes	700	186	**False Positive Rate (α)**	6%
Negative Outcomes	2300	2814	**False Negative Rate (β)**	77%
	Sensitivity	**Specificity**		
	23%	94%		

***Table A.6**: Statistical measures of performances of GC (a), DTF (b) and PDC (c) throughout experimental conditions for dataset with r=0.66 of network with feed-back link.*

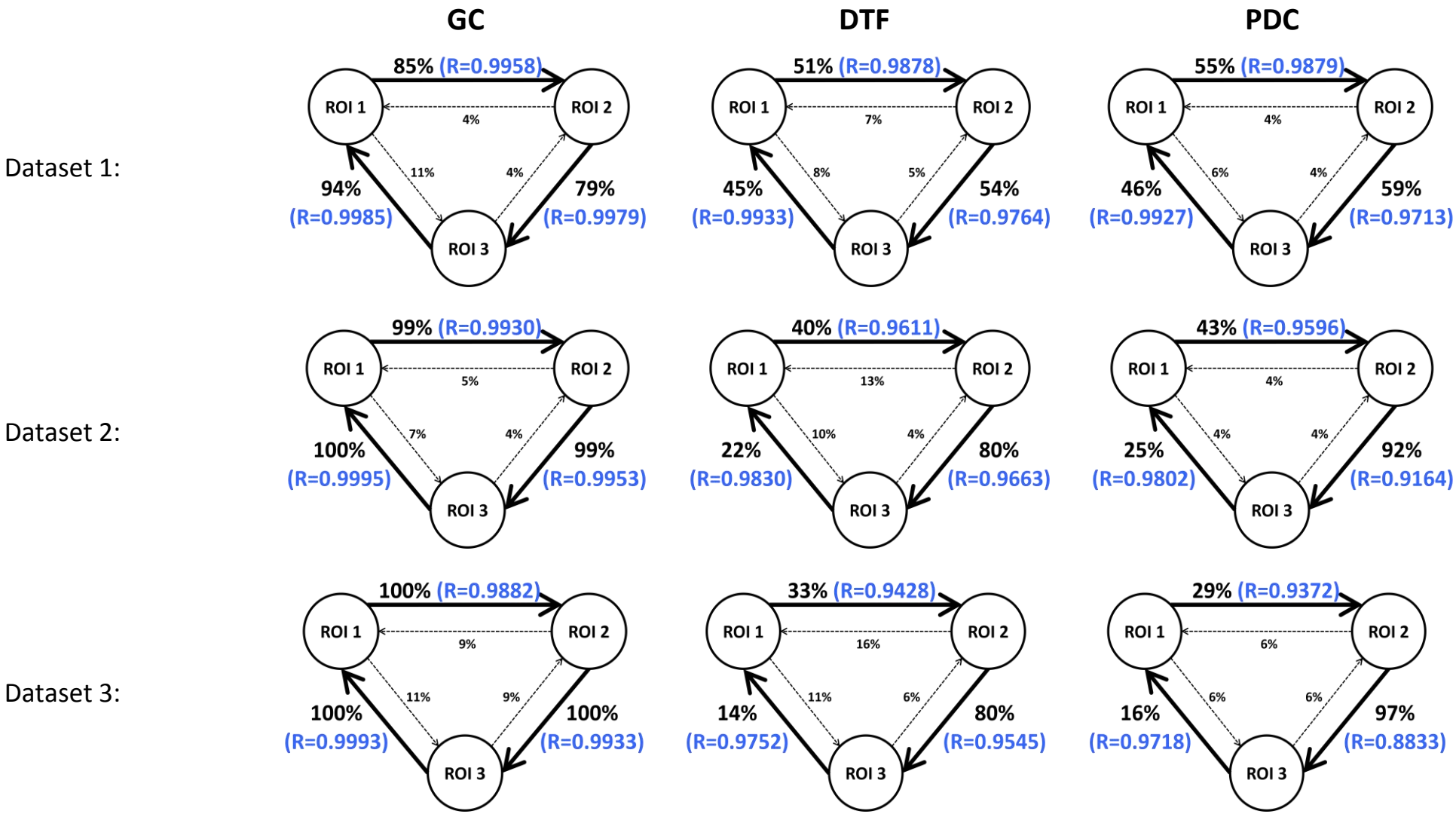

***Fig. A.3**: Estimated topology for the cycle network: continuous lines indicate true connections and the associated numbers quantify the percentage of true positives, averaged throughout each dataset. Dashed lines indicate absent connections, thus the associated numbers quantify the percentage of false positives averaged throughout each dataset. The blue numbers associated with continuous lines indicate the correlation coefficient between true and estimated values.*

(a) GC outcomes

	Positive Condition	Negative Condition		
Positive Outcomes	2583	187	**False Positive Rate (α)**	6%
Negative Outcomes	417	2813	**False Negative Rate (β)**	14%
	Sensitivity	**Specificity**		
	86%	94%		

(b) DTF outcomes

	Positive Condition	Negative Condition		
Positive Outcomes	1496	206	**False Positive Rate (α)**	7%
Negative Outcomes	1504	2794	**False Negative Rate (β)**	50%
	Sensitivity	**Specificity**		
	50%	93%		

(c) PDC outcomes

	Positive Condition	Negative Condition		
Positive Outcomes	1610	144	**False Positive Rate (α)**	5%
Negative Outcomes	1390	2856	**False Negative Rate (β)**	46%
	Sensitivity	**Specificity**		
	54%	95%		

Table A.7*: Statistical measures of performances of GC (a), DTF (b) and PDC (c) throughout experimental conditions for dataset with r=0.36 of cycle network.*

(a) GC outcomes

	Positive Condition	Negative Condition		
Positive Outcomes	2974	162	**False Positive Rate (α)**	5%
Negative Outcomes	26	2838	**False Negative Rate (β)**	1%
	Sensitivity	**Specificity**		
	99%	95%		

(b) DTF outcomes

	Positive Condition	Negative Condition		
Positive Outcomes	1421	270	**False Positive Rate (α)**	9%
Negative Outcomes	1579	2730	**False Negative Rate (β)**	53%
	Sensitivity	**Specificity**		
	47%	91%		

(c) PDC outcomes

	Positive Condition	Negative Condition		
Positive Outcomes	1605	130	**False Positive Rate (α)**	4%
Negative Outcomes	1395	2870	**False Negative Rate (β)**	46%
	Sensitivity	**Specificity**		
	53%	96%		

Table A.8*: Statistical measures of performances of GC (a), DTF (b) and PDC (c) throughout experimental conditions for dataset with r=0.56 of cycle network.*

(a) GC outcomes

	Positive Condition	Negative Condition		
Positive Outcomes	2999	259	**False Positive Rate (α)**	9%
Negative Outcomes	1	2741	**False Negative Rate (β)**	0%
	Sensitivity	**Specificity**		
	100%	91%		

(b) DTF outcomes

	Positive Condition	Negative Condition		
Positive Outcomes	1261	333	**False Positive Rate (α)**	11%
Negative Outcomes	1739	2667	**False Negative Rate (β)**	58%
	Sensitivity	**Specificity**		
	42%	89%		

(c) PDC outcomes

	Positive Condition	Negative Condition		
Positive Outcomes	1418	178	**False Positive Rate (α)**	6%
Negative Outcomes	1582	2822	**False Negative Rate (β)**	53%
	Sensitivity	**Specificity**		
	47%	94%		

Table A.9*: Statistical measures of performances of GC (a), DTF (b) and PDC (c) throughout experimental conditions for dataset with r=0.66 of cycle network.*

Bibliography

[1] L. Lemieux, J. Daunizeau, and M. C. Walker. Concepts of connectivity and human epileptic activity. *Front Syst Neurosci*, 5:12, 2011.

[2] P. A. Valdes-Sosa, A. Roebroeck, J. Daunizeau, and K. Friston. Effective connectivity: influence, causality and biophysical modeling. *Neuroimage*, 58(2):339–361, Sep 2011.

[3] C.W.J. Granger. Investigating causal relations by econometric models and crossspectral methods. *Econometrica*, 37(3):768–778, 1969.

[4] K. J. Friston, L. Harrison, and W. Penny. Dynamic causal modelling. *Neuroimage*, 19(4):1273–1302, Aug 2003.

[5] A. R. McIntosh and F. Gonzalez-Lima. Structural equation modeling and its application to network analysis in functional brain imaging. *Hum. Brain Mapp*, 2(22), 1994.

[6] K. J. Friston. Functional and effective connectivity: a review. *Brain Connect*, 1(1):13–36, 2011.

[7] L. Astolfi, F. Cincotti, D. Mattia, S. Salinari, C. Babiloni, A. Basilisco, P. M. Rossini, L. Ding, Y. Ni, B. He, M. G. Marciani, and F. Babiloni. Estimation of the effective and functional human cortical connectivity with structural equation modeling and directed transfer function applied to high-resolution EEG. *Magn Reson Imaging*, 22(10):1457–1470, Dec 2004.

[8] A. Boucard, A. Marchand, and X. Nogues. Reliability and validity of structural equation modeling applied to neuroimaging data: a simulation study. *J. Neurosci. Methods*, 166(2):278–292, Nov 2007.

[9] M. Ursino, F. Cona, and M. Zavaglia. The generation of rhythms within a cortical region: analysis of a neural mass model. *Neuroimage*, 52(3):1080–1094, Sep 2010.

[10] N. Wiener. *The Theory of Prediction*. McGraw-Hill New York, 1956.

[11] J. Geweke. Measurement of linear dependence and feedback between multiple time series. *Journal of the American Statistical Association*, 77:304–313, 1982.

[12] J. Geweke. *Inference and causality in economic time series models. in: Handbook of Econometrics*. Elsevier, 1984.

[13] S. L. Bressler and A. K. Seth. Wiener-Granger causality: a well established methodology. *Neuroimage*, 58(2):323–329, Sep 2011.

[14] A. Schlogl and G. Supp. Analyzing event-related EEG data with multivariate autoregressive parameters. *Prog. Brain Res.*, 159:135–147, 2006.

[15] M. J. Kaminski and K. J. Blinowska. A new method of the description of the information flow in the brain structures. *Biol Cybern*, 65(3):203–210, 1991.

[16] L. A. Baccala and K. Sameshima. Partial directed coherence: a new concept in neural structure determination. *Biol Cybern*, 84(6):463–474, Jun 2001.

[17] A. R. McIntosh, C. L. Grady, L. G. Ungerleider, J. V. Haxby, S. I. Rapoport, and B. Horwitz. Network analysis of cortical visual pathways mapped with PET. *J. Neurosci.*, 14(2):655–666, Feb 1994.

[18] C. Buchel and K. J. Friston. Modulation of connectivity in visual pathways by attention: cortical interactions evaluated with structural equation modelling and fMRI. *Cereb. Cortex*, 7(8):768–778, Dec 1997.

[19] E. Sartori, Parametric connectivity analysis in time and frequency domain from in silico and EEG data. Università degli Studi di Padova, Dipartimento di Ingegneria dell'Informazione, 28 marzo 2013

[20] Freeman, W.J., 1978. Models of the dynamics of neural populations. Electroencephalogr. Clin. Neurophysiol. 34,9-18

[21] M. Zavaglia, F. Cona, and M. Ursino. A neural mass model to simulate different rhythms in a cortical region. *Comput Intell Neurosci*, page 456140, 2010.

[22] Arnold Neumaier and Tapio Schneider. Estimation of parameters and eigenmodes of multivariate autoregressive models. *ACM Trans. Math. Softw.*, 27(1):27–57, 2001.

[23] A. K. Seth. A MATLAB toolbox for Granger causal connectivity analysis. *J. Neurosci. Methods*, 186(2):262–273, Feb 2010.

[24] F. Piccolo. Analisi parametrica multivariata del segnale EEG per la stima della connettivit`a corticale. Master's thesis, Universit`a degli Studi di Padova, Dipartimento di Ingegneria dell'Informazione, 2011.

[25] John Fox. TEACHER'S CORNER: Structural Equation Modeling With the sem Package in R. *Structural Equation Modeling: A Multidisciplinary Journal*, 13(3):465–486, June 2006.

[26] M. Kaminski, M. Ding, W. A. Truccolo, and S. L. Bressler. Evaluating causal relations in neural systems: granger causality, directed transfer function and statistical assessment of significance. *Biol Cybern*, 85(2):145–157, Aug 2001.

[27] J. Toppi, F. Babiloni, G. Vecchiato, F. Cincotti, F. De Vico Fallani, D. Mattia, S. Salinari, and L. Astolfi. Testing the asymptotic statistic for the assessment of the significance of Partial Directed Coherence connectivity patterns. *Conf Proc IEEE Eng Med Biol Soc*, 2011:5016–5019, 2011.

[28] S. Haufe, V. V. Nikulin, K. R. Muller, and G. Nolte. A critical assessment of connectivity measures for EEG data: a simulation study. *Neuroimage*, 64:120–133, Jan 2013.

[29] Julius S. Bendat and Allan G. Piersol. *Random Data: Analysis & Measurement Procedures*. Wiley-Interscience, 2000.

[30] H. R. Wilson and J. D. Cowan. Excitatory and inhibitory interactions in localized populations of model neurons. *Biophys. J.*, 12(1):1–24, Jan 1972.

[31] F. H. Lopes da Silva, A. Hoeks, H. Smits, and L. H. Zetterberg. Model of brain rhythmic activity. The alpha-rhythm of the thalamus. *Kybernetik*, 15(1):27–37, May 1974.

[32] B. H. Jansen, G. Zouridakis, and M. E. Brandt. A neurophysiologically-based mathematical model of flash visual evoked potentials. *Biol Cybern*, 68(3):275–283, 1993.

[33] O. David and K. J. Friston. A neural mass model for MEG/EEG: coupling and neuronal dynamics. *Neuroimage*, 20(3):1743–1755, Nov 2003.

[34] O. David, L. Harrison, and K. J. Friston. Modelling event-related responses in the brain. *Neuroimage*, 25(3):756–770, Apr 2005.

[35] A. Babajani and H. Soltanian-Zadeh. Integrated MEG/EEG and fMRI model based on neural masses. *IEEE Trans Biomed Eng*, 53(9):1794–1801, Sep 2006.

[36] M. Zavaglia, L. Astolfi, F. Babiloni, and M. Ursino. The effect of connectivity on EEG rhythms, power spectral density and coherence among coupled neural populations: analysis with a neural mass model. *IEEE Trans Biomed Eng*, 55(1):69–77, Jan 2008.

[37] F. Wendling, F. Bartolomei, J. J. Bellanger, and P. Chauvel. Epileptic fast activity can be explained by a model of impaired GABAergic dendritic inhibition. *Eur. J. Neurosci.*, 15(9):1499–1508, May 2002.

[38] M. Zavaglia, L. Astolfi, F. Babiloni, and M. Ursino. A neural mass model for the simulation of cortical activity estimated from high resolution EEG during cognitive or motor tasks. *J. Neurosci. Methods*, 157(2):317–329, Oct 2006.

[39] R. J. Moran, S. J. Kiebel, K. E. Stephan, R. B. Reilly, J. Daunizeau, and K. J. Friston. A neural mass model of spectral responses in electrophysiology. *Neuroimage*, 37(3):706–720, Sep 2007.